



Smart Grid Energy Management Staff Exchange



SMARTGEMS
energy network

D4.1 Optimised Renewables' Operation for Smart Grids: Monitoring and Control Strategies - public version -

**Marie Skłodowska-Curie Actions (MSCA)
Research and Innovation Staff Exchange (RISE)
H2020-MSCA-RISE-2014**



Revision History

Revision date	Previous revision date	Summary of Changes	Changes marked
29/09/17		First issue	

Approvals

This document requires the following approvals.

Name	Partner	Date	Approval (y/n)
Prof. Denia Kolokotsa (Project Coordinator)	TUC	29/09/17	y
Prof. Margarita Assimakopoulos	UOA	29/09/17	y
Prof. Diofantos Chatzimitsis	CUT	29/09/17	y
Prof. Costas Papanicolas	Cyl	29/09/17	y
Prof. Maria Kolokotroni	UBRUN	29/09/17	y
Dr. Cristina Cristalli	AEA	29/09/17	y
Dr. Nerijus Kruopis	EGM	29/09/17	y
Fabio Montagnino	IDEA	29/09/17	y
Federica Fuligni	EXERGY	29/09/17	y
Prof. Siew Eang	NUS	29/09/17	y

Distribution

This document has been distributed to:

Name	Partner	Date
Prof. Denia Kolokotsa (Project Coordinator)	TUC	29/09/17
Prof. Kostas Kalaitzakis	TUC	29/09/17
Prof. Georgios Chalkiadakis	TUC	29/09/17
Kostas Gobakis	TUC	29/09/17

Nikos Kampelis	TUC	29/09/17
Prof. Margarita Assimakopoulos	UOA	29/09/17
Theoni Karlesi	UOA	29/09/17
Prof. Costas Papanicolas	Cyl	29/09/17
Marina Kyprianou	Cyl	29/09/17
Georgios Kirkos	Cyl	29/09/17
Dr. Cristina Cristalli	AEA	29/09/17
Riccardo Paci	AEA	29/09/17
Dr. Laura Standardi	AEA	29/09/17
Dr. Nerijus Kruopis	EGM	29/09/17
Karolis Koreiva	EGM	29/09/17
Fabio Montagnino	IDEA	29/09/17
Filippo Paredes	IDEA	29/09/17
Luca Venezia	IDEA	29/09/17
Pietro Muratore	IDEA	29/09/17
Federica Fuligni	EXERGY	29/09/17
Prof. Siew Eang	NUS	29/09/17
Prof. Maria Kolokotroni	UBRUN	29/09/17
Emmanuel Shittu	UBRUN	29/09/17
Thiago Santos	UBRUN	29/09/17

Table of Contents

Table of Contents.....	3
List of Tables	7
Summary	8
1. Introduction.....	9
2. Methodology.....	12
2.1 Energy management systems as a key component of micro-grids	12
2.2 Building modelling	13
2.3 Battery Energy Storage Systems (BESS)	15
2.3.1 UK scenario	15
2.3.2 Worldwide scenario	16
2.3.3 The Success of Lithium Technology	19
2.3.4 Integration of BESS in built environments.....	19
2.4 Combined geothermal and solar thermal energy storage systems.....	23
2.5 Design of a platform for monitoring and controlling building integrated solar polygeneration systems	25
3. Optimised Operation of Renewables for Smart Grids.....	27
3.1 Energy forecast at the Brunel University London	27
3.1.1 Data preparation	28
3.1.2 Forecast.....	30
3.1 Athalassa Campus and NTL building.....	32
3.2.1 Correlation with weather data.....	35
3.2.2 Novel Technology case study description	36
3.2.3 Data exploration	40
3.2.4 Correlation Matrix	40
3.2.5 Regression model	42
3.2.6 Explained variance score	43
3.2.7 Mean absolute percentage error	43
3.2.8 Mean absolute error	43
3.2.9 Mean squared error and Root mean squared error	44
3.2.10 Median absolute error	44
3.2.11 R ² score function	44
3.2.12 Linear regression model.....	45
3.2.13 Multiple regression model	46
3.2.14 Two variables linear regression.....	46
3.2.15 Three variables linear regression	47
3.2.16 Ridge regression	48
3.2.17 Single variable linear regression	49
3.2.18 Two variables linear regression.....	50
3.2.19 Three variables linear regression	51
3.2 The Geosolar integration at TUC	52
3.3.1 Energy consumption	53
3.3.2 Heat consumption.....	53
3.3.3 Cooling consumption	55
4. Research activities in the Smart GEMS Project.....	57
4.1 Neural Network toolbox integration through a DLL.....	57
4.1.1 Neural Network toolbox and Nonlinear autoregressive neural network with external input	58
4.1.2 Case study	60

4.1.3	Case study	60
4.1.4	Prepare the data for training.....	61
4.1.5	Set up Division of Data for Training, Validation, Testing	62
4.2	Study of TUC experiences in NN prediction based systems	63
4.2.2.1	Custom architecture for remote sensing and data collecting hub	66
4.2.3	Identification of programming languages.....	67
5.	Main findings.....	68
5.1	Application at the Leaf micro-grid	68
5.1.1	System description	69
5.1.2	Power production data	71
5.1.3	Prediction using Neural Network	72
5.1.4	NN model setup	72
5.2	Test of the custom data collection platform	73
5.3	Preliminary design of the Geosolar system in TUC	75
5.3.1	Ground source heating and cooling	75
5.3.2	Choice of geothermal system	76
5.3.3	Ground source heat pump principle	78
5.3.4	Solar Thermal Collectors	79
5.3.5	Solar thermal energy	80
5.3.6	Climate conditions	81
5.3.8	Geothermal energy	84
5.3.9	Geology	86
5.3.10	Location	88
5.3.11	Borehole heat exchanger.....	89
5.3.12	Underground Thermal Energy Storage	90
5.3.13	Heat production	91
5.3.14	Geo-Solar system design.....	93
6.	References	97
9.	Annexes	100

List of Figures

Figure 1: The Smart GEMS Energy model, from the building level to the large energy distribution networks.	9
Figure 2: Energy signature conceptual schema.....	15
Figure 3: Battery storage deployment in UK & Germany	17
Figure 4: EFR Results.....	21
Figure 5: Revenue build up.....	22
Figure 6: Brunel University London Campus Map	28
Figure 7: Electricity consumptions recorded by meters.....	28
Figure 8: Total electricity consumption.....	29
Figure 9: Annual trends over time (seasonal plots).....	30
Figure 10: Median daily profile.....	31
Figure 11: Median weekly profile.....	32
Figure 12: Athalassa campus and energy grid schema	33
Figure 13: Fresnel and Thermal loop Trnsys model.....	34
Figure 14: Simulation model vs Data Driven model of NTLab	34
Figure 15: Flow chart of Energy Signature generation.....	35
Figure 16: NTL Power demand.....	36
Figure 17: ETL procedure	37
Figure 18: Re-sampling algorithm	37
Figure 19: Selected data set.....	39
Figure 20: Training and test data set	39
Figure 21: Energy Signature in terms of heating and cooling consumption vs external temperature.....	39
Figure 22: Selected data set after ETL procedure	40
Figure 23: Linear regression model with scatter plot of training data.....	45
Figure 24: Two variables linear regression model with scatter plot of training data.....	47
Figure 25: Three variables linear regression model with scatter plot of training data.....	47
Figure 26: Ridge second order degree regression model with scatter plot of training data.....	50
Figure 27: Ridge second order degree regression model with scatter plot of training data.....	51
Figure 28: Ridge second order degree regression model with scatter plot of training data.....	51
Figure 29: Technical University of Crete Campus.....	52
Figure 30: HVAC system and its operating parameters.....	53
Figure 31: Heat consumption along the year.....	55
Figure 32: Cooling consumption along the year.....	56
Figure 33: Black box overview	58
Figure 34: Net overview	60
Figure 35: The TUC ANN prediction model.....	63
Figure 36: Validation of ESPr model of Indoor Temperature at the Circulation Areas of K2 Building	64
Figure 37: Measured and predicted power demand in the case study area... 64	64
Figure 39: The LEAF micro-grid.....	68
Figure 40: Thermal storage - GWHP connection.....	71
Figure 44: A common structure of an Elman network.....	74

Figure 45: Seasonal ground temperature fluctuation in relation to depth.....	77
Figure 46: Absorption Heat Pump.....	78
Figure 47: Collector efficiency vs ΔT	81
Figure 48: Selected point for PVGIS data analysis (K2 TUC)	82
Figure 49: Monthly average irradiance 2007-2016.....	84
Figure 50: Monthly average temperature 2007-2016	84
Figure 51: Horizon profile and sun path	84
Figure 52: ThermoMap analysis location	86
Figure 53: USDA texture classification (Group level)	87
Figure 54: Ground composition.....	87
Figure 55: Location of BHE systems.....	89
Figure 56: Chosen configuration for BHEs.....	90
Figure 57: Ideal volume for UTES.....	91
Figure 58: GeoT*SOL system selection.....	92
Figure 59: Heat Pump parameters.....	92
Figure 60: Borehole Heat Exchangers parameters	93
Figure 62: Design of the Geo-Solar system	94

List of Tables

Table 1: Seconded researchers and activities presented in Deliverable 4.1	Σφάλμα! Δεν έχει οριστεί σελιδοδείκτης.
Table 2: Main storage applications in the UK.....	16
Table 3: Examples of international government action to support energy storage.....	19
Table 4: Domestic, Non-Domestic and Community BESS Applications.....	20
Table 5: Dataset filters	38
Table 6: Data exploration for heating dataset.	40
Table 7: Data exploration for cooling dataset.....	40
Table 8: Correlation matrix for heating dataset	41
Table 9: Correlation matrix for cooling dataset	41
Table 12: Heat consumption data.	54
Table 13: Total heat consumption per thermal zone.	54
Table 14: Total heat consumption and peak power of the building.	54
Table 15: Cooling consumption calculation.....	55
Table 16: Average and peak cooling consumption.	56
Table 17: Input-target variables	60
Table 18: input arguments	61
Table 19: Input data for each prediction.....	73
Table 20: Shallow geothermal methods.....	76
Table 21: Fluid path configuration.....	77
Table 22: Information obtained from PVGIS	83

Summary

This report summarizes activities performed within the task 4.1 of the Smart Gems project, aimed at the optimized integration of smart buildings into local smart grids.

Promising approaches and technologies have been explored in connection with the real sites available within the framework of the Smart Gems partnership. Advanced technologies for the integration of Zero Energy Building (ZEBs), and Nearly ZEBs (NZEB), in smart grids have been considered in the context of the NTL building at the Cyprus Institute, where a LFR solar thermal collection system is available. The same approach has been applied at the TUC campus in Crete. A custom infrastructure of sensors and processing boards has been designed, which could be integrated in networks and standards already in place. Sizing, positioning and effective operation of RES and storage systems in smart grids has been also an object of study by the design of district cooling/heating based on geothermal and solar thermal technologies and a detailed analysis of study of a battery energy storage system.

Also optimization approaches by forecasting of electricity consumption has been considered, through a specific study performed at the campus of Brunel University of London.

All the activities have seen the participation of researchers both from industry and academia. The specific contribution of each seconded researcher is summarized in Table 1.

Researcher	Sending Organisation	Hosting Organisation	Research Field
Daniela Isidori (author)	AEA, Loccioni	Technical University of Crete	Advanced technologies for the integration of Zero Energy Building (ZEBs), and Nearly ZEBs (NZEB), in smart grids. Application at the TUC and NUS campus case studies.
Daniela Isidori (author)	AEA, Loccioni	Cyprus Institute	Study of technologies for the integration of Zero Energy Building (ZEBs) in connection with the Solar Thermal Fresnel collectors of NTL building
Laura Standardi (author)	AEA, Loccioni	Brunel University	Study of a battery energy storage system
Martina Senzacqua (author)	AEA, Loccioni	Brunel University	Forecast of electricity consumption of Brunel University London campus
Fernando Sanahuja (author)	Exergy	Technical University of Crete	Sizing, positioning and effective operation of RES for smart grids: Design of district cooling/heating based on geothermal / solar thermal technologies
Pietro Muratore (author)	IDEA	Technical University of Crete	Developing a custom hardware and software infrastructure of sensors and boards using the standard and already present networks

1. Introduction

A growing importance is attributed to the effective integration of Zero Energy Building (ZEBs), and Nearly ZEBs (NZEBs) in local smart grids. As a matter of fact the optimization of the grid performance at a settlement level is going to play a key role in the upcoming energy models where multiple distributed energy sources are connected and jointly cooperate in giving an efficient response to the energy demand (see the energy model considered in the Smart Gems approach, represented in Figure 1). This objective can be achieved by the combination of different approaches and technologies, involving smart energy management systems, interoperable metering, monitoring and control devices, procedures for users' active engagement and internal comfort optimisation, flexible distributed storage systems.

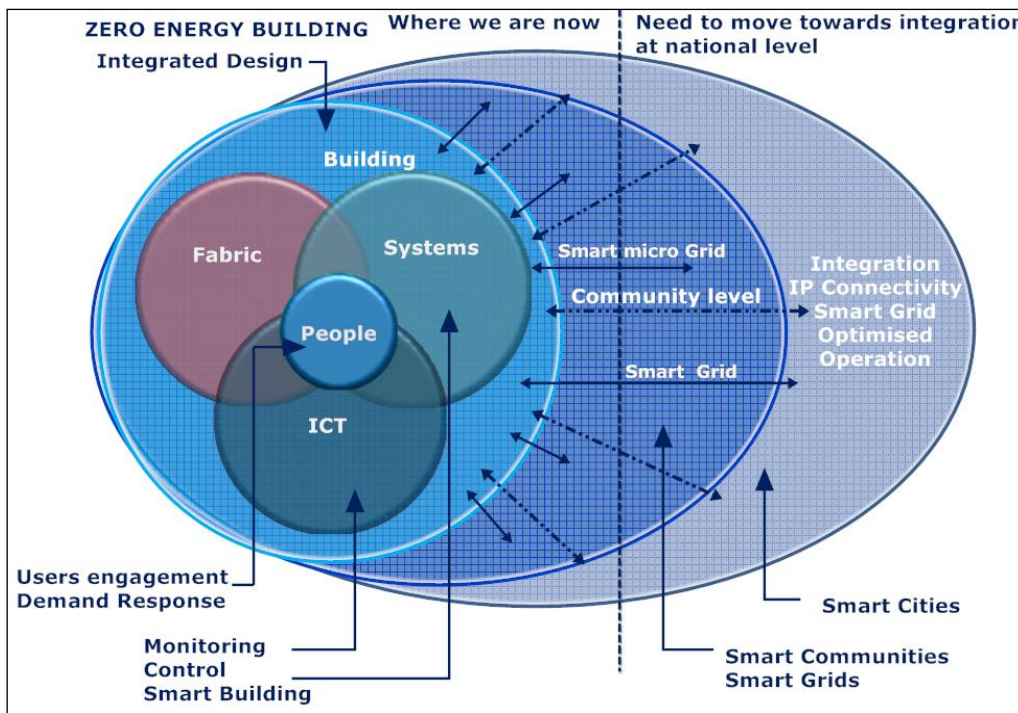


Figure 1: The Smart GEMS Energy model, from the building level to the large energy distribution networks.

Deployment of smart grids asks for innovative techniques for predicting and controlling electricity request to the grid, in order to reduce peaks, improve grid stability and optimize electricity costs. Smart grids can even contain millions of smart meters, which produce a huge amount of data about energy consumption. In addition to these time series, we can have additional correlated information about energy sources, weather, occupancy, building performance and so on.

A good interpretation of these data leads to predict in advance both electrical and thermal energy demand, both in very short and long term. The combination of predictive models and storage systems can be very effective in improving the integration of the local to the main grid, reducing peaks and decreasing electricity costs. Furthermore, the collected data can be used for the early detection of anomalies.

Smart metering application and testing as a basic component in present and future electrical grids has been addressed. As a matter of fact, interoperability among meters of various OEMs must be guaranteed as then the control system is enabled to coordinate and control all the energy systems which are monitored. For this purpose a building environment has been simulated, where the smart meters utilized belong to different firms and their interoperability is tested using dedicated protocols.

Some tasks have been devoted to characterize services and systems, through activities related to the analysis of energy consumption and users satisfaction. Also the possible engagement of users has been explored via online surveys, questionnaires and focus groups. This combined approach has paved the way for tailored control, which can maximize energy performance both from thermal comfort and energy cost perspective. These approaches have been specifically applied to buildings that host departments of the universities which are in the partnership, the NUS in Singapore and the TUC in Crete. A specific action has been addressed to the role of storage systems in the integration of smart buildings into the grids, exploring a large variety of possible applications and architectures. The goal of this report is to describe how storage systems boost the integration of smart buildings into the grids. The flexibility that such systems provide the grid and the buildings is crucial as it can be deployed in a large variety of applications addressed in this report.

The integration of solar thermal sources has been considered in the case study of the Novel Technology Lab in Athalassa campus of Nicosia. The energy signatures of the building have been calculated by starting from common data that are easy collected in such smart building, like external temperature, wind, internal temperature. An estimation of the loads has been derived and used to tune and optimize the renewable production of thermal energy, by a Trnsys model of both the building and the LFR collector, which were already available. This approach may be used to estimate the energy consumption for data sets of the outdoor temperature coming from different time—space locations with an acceptable error for a preliminary analysis. Improvements via advanced control and

data mining techniques for energy predictions have been explored with the aim exploiting the thermal production by the LFR collector as part of a smart grid approach.

A broader exploitation of thermal sources has been taken into account in the case study of the K2 building from the Department of Environmental Engineering in the Technical University of Crete. The purpose of this study was the design of a combined geothermal and solar thermal energy system, which could supply heating and cooling services achieving the highest possible efficiency along one year.

A further step was the preliminary design of a monitoring and control system for buildings connected to polygenerative solar systems, which can deliver electricity, cold and heat. Multi-Purpose Management (MPM) device networks have been considered, where Artificial Neural Network (ANN) can be used for the prediction of energy loads and fuzzy control algorithms can keep the optimal comfort conditions. Solutions developed at TUC have been considered for a possible industrialization, moving them from a scientific development framework to more commercial platforms. Portability issues have been addressed, testing options to permit a remote data exchange with the grid.

2. Methodology

2.1 Energy management systems as a key component of micro-grids

The requirement for clean energy, energy efficiency and cost-efficient energy management has given rise to the investigation of transition from traditional energy distribution grids to smart micro-grids. In traditional electricity grids energy is produced centrally and distributed to the various energy consumers that are connected to the grid. Traditional grids lack flexibility in power generation and load operation. A micro-grid includes distributed energy sources, energy loads and storage components, thus forming a semi-autonomous entity with energy management capabilities. Moreover, a micro-grid can operate connected to the main grid or in island mode. For the purpose of reliable and efficient operation the Energy Management System (EMS) has become an essential component of micro-grids.

EMS assists in the optimization of power distribution within a micro-grid through the application of appropriate controls. Measuring and monitoring and control equipment connected through Information and Communication Technologies (ICT) are necessary for “building” an EMS. These assets combined with advanced energy management techniques make a micro-grid smart. A smart micro-grid communicates with its components and through the EMS controls its loads so as to achieve an efficient and cost-effective operation. An energy management approach is tested for optimum integration and operation of a PV array and a battery for serving a micro-grid’s loads and increased efficiency and occupant satisfaction has been achieved by applying the EMS in a University Campus.

Load forecasting is invaluable to micro-grid energy management and Load forecasting for controlling charge and discharge of an electrical storage has been largely studied. Depending on the forecasted period three types of forecasting are recognised:

- short-term forecasting: 1h to 1week for optimum
- medium-term forecasting: 1week to 1year
- long-term forecasting: 1year to decades ahead.

Two methods for load forecasting have been recognised in literature, statistic mathematical models and artificial intelligence models. Artificial Neural Networks (ANN) are artificial intelligence models widely used for forecasting providing high accuracy. ANN have been extensively used for short-term load prediction. Multi-layer perceptron neural

network that uses load and weather data have been applied in order to forecast the daily load of a suburban area. Feed forward artificial neural network for hourly demand prediction have been also tested and the proposed algorithm is able to achieve a high prediction accuracy.

ANN have been applied in task activities to generate a 24h load forecasting micro-grids with the purpose to predict the day ahead excess production and apply appropriate controls for its utilisation.

2.2 Building modelling

The analysis of energy consumption data is an important instrument for the buildings management: it is crucial for energy audits, to verify the savings achieved by a retrofit and to improve the estimation of expected savings. This aspect requires the knowledge of the factors that influence the energy consumption. Usually, a validated model of the building is necessary to estimate the consumption for any operating conditions.

There are two approaches for developing such a model: the “simulation approach”, also called “forward modelling”, and the “system identification” approach, called “inverse modelling”. A third option, which can be also considered, is a hybrid approach: by starting with the description of the building and calibrating the simulation program for matching with the measured consumption data.

Energy model-based simulation requires computational tools that allow a proper modelling of the dynamic thermal interactions between a building and its outdoor and indoor environments. This approach is based on a deep understanding of the behaviour by starting from established relationships. On the other side, conducting energy model-based simulation requires significant time, resources, technical expertise and an extensive set of inputs to characterize a building (geometry, internal loads, outdoor environment, equipment, and schedules), which limits their application. Usually, sufficient resources are missing and the soft relationship between design and analysis tools does not permit rapid energy model iteration.

The system identification approach, is based on the behaviour of the building (consumption data, outdoor temperature, etc.) by assuming the structure of the model and identifying its parameters through a statistical analysis of data collected. The simplest option is to assume a steady-state model of the building and use data related to consumptions, weather conditions, etc. This leads to what is known as energy signature (ES). The energy signature of a building represents a set of parameters that describe its

energy performance by using few equations; however, a sophisticated statistical process is mandatory to make the results as reliable as possible. A very positive aspect with respect to the simulation approach, is that only data easy to obtain without a dedicated data acquisition system are required. In the literature, a classical method used for energy signature is PRISM model, a regression of consumption with respect to external temperature. But other factors can also be important, such as solar radiation, wind velocity and occupancy/operating mode that are particularly relevant for industrial buildings (unoccupied during holidays and weekends) which behaviour is obtained with two separate models: one for heating and the other for cooling period.

In the literature, numerous works have confirmed that the outdoor temperature is the central factor for buildings whose loads are dominated by heating. Energy signatures for air conditioning systems can have characteristics that are different with respect to heating systems so the assumptions can be very different.

Starting from common measurement that are easily collected in a smart building like external temperature, wind, the internal temperature, it is possible to by-pass the simulation model, and directly obtain estimation of load that can be used to tune and optimize renewable production (see Figure 2). This methodology has been applied to the NTL building at the Cyprus Institute in Nicosia. The simplified model, obtained by the statistical analysis of the available data, gives the overall heating/cooling with respect to external temperature, and it may be used to estimate the energy consumption for data sets of the outdoor temperature coming from different time—space locations with an acceptable error for a preliminary analysis. These data have been uploaded in the Trnsys model the building connected to the LFR collector, which were already available, as to understand their possible behaviour as smart grid. For this reason, improvements via advanced control and data mining techniques for energy predictions have been also taken into consideration.

operates at a flat level of baseload generation in order to reduce emission, thus, they are unable to increase output;

- b) maintaining adequate capacity margin: in the medium and long term, the capacity margin could be maintained through the capacity mechanism;
- c) increasing need for flexibility to ensure system reliability: this requires quick and reliable systems that constantly ensure the required flexibility;
- d) reduced efficiency of conventional plants: the high penetration of RES pushes conventional plants further down the merit order. Plants must provide quicker ramps, more start-ups and greater overall cycling; consequently, maintenance costs increase as well as environmental impacts due to lower efficiency and higher emission per unit output;
- e) localised distribution network impacts: massive distributed generation can cause congestion in a distribution network designed to passively distributed power from the transmission system to the end customer.

In this evolving context, storage systems can operate in different market across the electricity system to provide multiple services to multiple stakeholders as shown in Table.

	Response Service	High energy user	Domestic, Nondomestic, Community	Energy Reserve	Energy Trader
Primary Service	Enhances Frequency Response (EFR)	Transmission Cost avoidance	Generator own use	STOR or Fast Reserve or Capacity Market	Price arbitrage and peak shaving
Additional revenues	Firm Frequency Response (FFR)	Distribution cost avoidance	Aggregated own use	Transmission cost avoidance	Aggregated price arbitrage
	Capacity market	Peak-shaving	Price arbitrage and peak shaving	Distribution cost avoidance	Grid Curtailment
	Transmission cost avoidance	Frequency control	Grid Curtailment	Price arbitrage and peak shaving	
	Distribution cost avoidance	Generator own use	Frequency response		
		UPS	STOR or Capacity Market		

Table 2: Main storage applications in the UK

2.3.2 Worldwide scenario

With reference to batteries, many countries are focusing on battery installations.

The scenario described in the previous chapter related to UK, is very similar to what is happening in Germany as shown in Figure 3. Behind-the-meter installations are located

at customer's site and, in this specific case, they are con Commercial & Industrial customer. The large number of installations with more than 1 MWh of capacity installed is mainly given by the fact that batteries can provide multiple services for grid regulation at the same time.

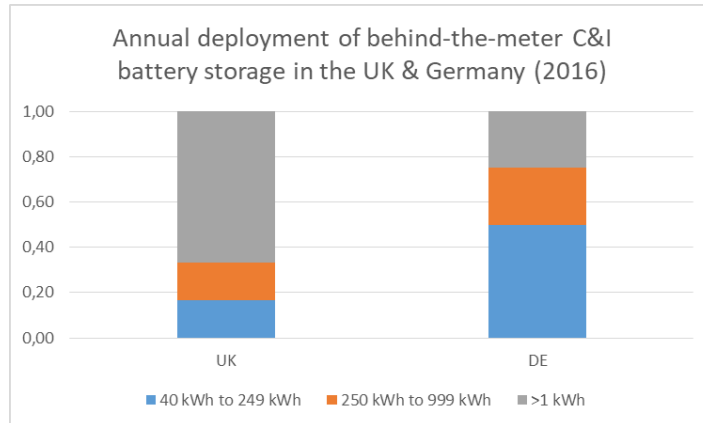


Figure 3: Battery storage deployment in UK & Germany

Considering about 1,636 storage projects installed worldwide and 193,349 MW of power, electrochemical technologies involve about 993 projects and 3,279 MW; among those installations, lithium technology have been deployed in about 631 project with 2,289 MW installed.

Many governments have also supported actions to improve the deployment of energy storage not strictly related to batteries, though (see Table).

Country	Organisation and Overview
Canada	Ontario Ministry of Energy In 2013, the government released a Long-Term Energy Plan, which included procurement target of 50MW for storage technologies. The LTEP has targets of 10,700MW of wind (11%), solar (3%) and bioenergy (3%) by 2021 (each source representing their percentage of total energy production).
China	Central Government There have been funding for demonstration projects such as the Zhangbei project in Hebei, which has 36KWh lithium-ion battery capacity, in order to evaluate the value energy storage would have when providing electricity grid flexibility. The National Energy Administration (NEA) is expected to release 13 energy policies in 2015, which include large capacity energy storage and EV charging infrastructure. It is anticipated in 2015 that the National Reform and Development Commission will implement time-of-use pricing mechanisms.
European Union	European Commission – Framework Research Programme The 'stoRE' project, co-funded by the Intelligent Energy Europe Programme of the EU, aims to create a framework that will allow energy storage infrastructure to be developed in support of higher penetration of variable renewable energy resources. Target countries to identify a series of improvements/application include, Austria, Denmark, Germany, Greece, Ireland and Spain.
Germany	Federal Ministry of the Environment, Nature Conservation and Nuclear Safety

	<p>Since May 2013, part of the support scheme for solar-plus-batter, the state-owned bank Kreditanstalt für Wiederaufbau (KfW) has granted low interest loans with an aggregate value of €163 million for 10,000 energy storage projects combined with PV installations with a power up to 30kW.</p> <p>The Ministry also covers 30% of the storage system costs. Eligible PV systems should feed maximum 60% of installed capacity into the grid.</p>
Japan	<p>Ministry of Economy, Trade and Industry</p> <p>Government support to demonstrate the ability to time-shift demand by 10% in 14 conjunction with expanded use of renewable generation resources. Within the next seven years METI funding is aiming to decrease the total cost by providing funds up to 75% of the total storage system cost.</p> <p>METI is planning to spend around 81 billion yen to resolve grid related issues and to increase renewable energy. Additionally, the Ministry is aiming to provide incentives for energy storage systems, which can be implemented onto solar power stations or substations. The budget is awaiting parliament approval.</p> <p>Ministry of Environment</p> <p>Up to 50% subsidy for storage battery for renewable energy generation (1MW) Subsidy for renewable energy in local areas (Total 1bn JPY)</p>
South Korea	<p>Ministry of Trade, Industry and Energy (MOTIE)</p> <p>Customised electric rates to stimulate the energy storage system and electric vehicle industries along with drawing investment in storage and the use of ecofriendly EVs by consumers (MOTIE, 2015).</p> <p>The government plans to install 500kWh of energy storage systems. The Korea Electric Power Corporation also plans to install 1000kWh of storage (Agency for Growth Policy Analysis, 2014).</p> <p>MOTIE also supports small and mid-sized companies with various incentives to install energy storage systems.</p> <p>Central Government</p> <p>President Park has expressed support for innovative energy systems, which includes the usage of ES within Energy Management Systems and smart grids.</p>
United States	<p>Storage Technology for Renewable and Green Energy Act of 2013 or the Storage 2013 Act</p> <p>Similar to the Storage Act of 2011 this act promotes deployment of energy storage technologies by recognising the benefits for renewables and consumers and benefits to the grid. The Act aims to level the playing field of energy tax incentives (U.S. Senate Committee, 2013).</p> <p>The Act provides 20% investment tax credit of up to \$40 million per project connected to the electric grid and distribution system. Additionally, the Act provides 30% investment tax credit of up to \$1 million per project to businesses for on-site storage (ibid).</p> <p>An important change from the Act of 2011 is that the minimum size of system eligibility had been lowered from 20kWh to 5kWh. This change helps promote deployment of systems from small businesses to the grid and it is expected to incentivise storage companies to create leasing models for residential users (ibid).</p> <p>The Act also provides 30% tax credit for homeowners for on-site storage systems to store off-peak electricity from solar panels or from the grid for later use (ibid).</p> <p>Federal Energy Regulatory Commission (Orders)</p> <p>Order 755 increases the pay for “fast” responding sources like batteries or flywheels that are bidding into frequency regulation service markets. “Fast-ramping, more 15 accurate resources are now given greater compensation in the wholesale frequency regulation markets” (DOE, 2015). The FERC is ensuring that it’s providing just and reasonable and not unduly discriminatory or preferential rates of frequency regulation.</p> <p>Order 784 expands Order 755 and focuses on third-party provision of ancillary services and accounting and financial reporting for new electric storage technologies (ibid).</p> <p>According to the Order public utilities must take into account the speed and accuracy of regulation resources, which opens the door for greater efficiency in transmission customers' purchase of regulation resources. Additionally, the order eases the barriers</p>

	<p>for third-party entry into ancillary service markets and by revising accounting and reporting requirement to improve market transparency.</p> <p>The incentives for systems that provide summer on-peak demand reduction are \$2,600/kW for thermal storage and \$2,100/kW for battery storage technologies (ibid). Proposed incentives are capped at 50% of installed project cost plus bonus incentives are available for large (>500kW) projects.</p> <p>Master Limited Partnerships Parity Act</p> <p>A Master Limited Partnership (MLP) "is a business structure that is taxed as a partnership, but whose ownership interests are traded like corporate stock on a market" (Library of Congress, 2013). However, it has only applied for fossil fuel based energy partnerships within the internal revenue code.</p> <p>The MLP Parity Act "Amends the Internal Revenue Code, with respect to the tax treatment of publicly traded partnerships as corporations, to expand the definition of "qualifying income" for such partnerships to include income and gains from renewable and alternative fuels (in addition to fossil fuels), including energy derived from thermal resources, waste, renewable fuels and chemicals, energy efficient buildings, gasification, and carbon capture in secure geological storage" (Lib. of Cong., 2013).</p> <p>The MLP Parity Act expands MLP eligibility to an array of renewable energy sources, including "electricity storage devices" (DOE, 2015). If the Act is enacted, it will allow for more equitable taxation methods across all energy sectors, and will allow for new ownership and taxation models for energy storage device partnerships (ibid).</p> <p>MLP Parity Act was introduced in 2012 and then in 2013 (with expanded qualifying resources) and still awaits approval.</p>
--	--

Table 3: Examples of international government action to support energy storage

2.3.3 The Success of Lithium Technology

Nowadays, lithium batteries are mostly deployed for grid regulation and integrated with renewables. As the lithium prices are going down, even though they are not as affordable as other battery technologies, the technological maturity of such batteries cause high performances that are required from most of the recent tenders worldwide.

The main advantages of the lithium technology, reported by the literature are:

- mature technology;
- modularity and scalability;
- power Intensive;
- high performance.

While, the disadvantages are mostly related to the, still, high prices.

2.3.4 Integration of BESS in built environments

The union between BESS and buildings typically defines two scenarios referring to Table:

(i) Domestic, Non-domestic and Community; (ii) High energy users.

2.3.4.1 Domestic, Non-Domestic and Community

A BESS can provide a variety of services when integrated with domestic, nondomestic buildings and communities as reported in Table 4. Primary service denotes the main type

of services that an electrical storage can provide when integrated in building applications, while, additional revenues represent other services that the BESS can simultaneously provide. Domestic, non-domestic and community include residential, industrial, office, and other types of buildings or group of buildings.

	Domestic, Non-Domestic & Community
Primary Service	Generator own use
Additional revenues	Aggregated own use
	Price arbitrage and peak shaving
	Grid Curtailment
	Frequency response
	STOR or Capacity Market

Table 4: Domestic, Non-Domestic and Community BESS Applications

Generator own use

The energy to satisfy the energy demand in a single building or a group of buildings, also defined as community, for both domestic and nondomestic cases, is typically taken from the national grid. However, it is also possible to use the energy used by Renewable Energy Sources on site, in case of prosumers. Another option is then a diesel generator. On the other hand, a storage system enables such users to withdraw the required energy from it whenever necessary. This scenario characterizes off-grid solutions where the union of RESs, storage systems, loads, and a possible back-up diesel generator, guarantee the balance of energy demand and supply.

Aggregators

Buildings and community easily fit in being aggregated in both demand and response. In this scenario, the aggregators balance the energy consumption and production within the aggregated buildings in order to minimize any imbalances. Storage systems boost aggregation because they provide flexibility aimed to enhance the internal energy balance that aggregated buildings ask for.

Price arbitrage and peak shaving

Storage systems enable users to store the extra energy produced by renewables or bought at low prices, and then use it when prices are high. Moreover, peaks in consumption can be shaved by withdrawing energy from the energy storage. Both strategies yield to savings for the customers and support grid stability.

Grid Curtailment

In this situation, the energy produced by a wind farm is curtailed at certain times. Clearly, this loss of energy can be mitigated by storing it in a storage system and then withdrawn into the grid whenever is possible.

Frequency response, STOR and Capacity market

As the grid frequency must be secured at 50 Hz as long as possible, TSOs are addressing storage systems that improve grid stability by providing and absorbing power from the grid if required.

In this view, National Grid (the TSO in the United Kingdom) have issued in 2016 a tender for the Enhanced Frequency Response (EFR) service. In such tender, 61 offers involved battery storage systems, while 2 were Demand Side Response (DSR) and 1 was a thermal generator. The eight projects that have won are shown in Figure 4: **EFR Results**.

Provider Name	Enhanced Response (MW)	Estimated Start Date (mmm-yy)	Tender Cost (£)	Average price of tender £ per MW of EFR h
EDF Energy Renewables	49	Dec-17	£12,035,184	£7.00
Vattenfall	22	Apr-17	£5,749,148	£7.45
Low Carbon	10	Dec-17	£2,680,544	£7.94
Low Carbon	40	Mar-18	£12,668,253	£9.38
E.ON UK	10	Nov-17	£3,891,259	£11.09
Element Power	25	Feb-18	£10,079,028	£11.49
RES	35	Feb-18	£14,650,994	£11.93
Belectnc	10	Oct-17	£4,200,034	£11.97
	201			£9.44

Figure 4: EFR Results

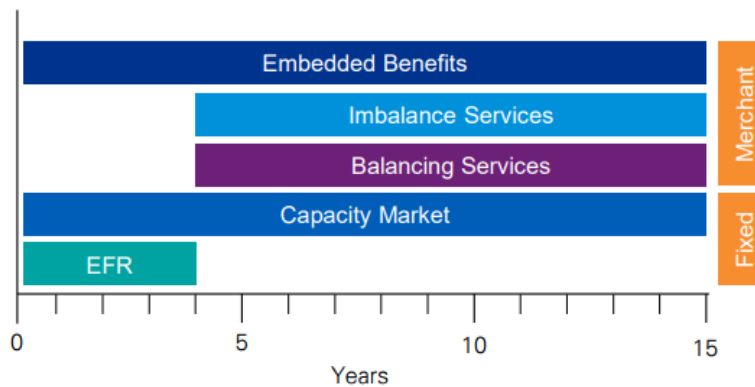
The success of lithium storage deployment in the EFR tender is related to the sub-second response times that NG required. The success of such tender was also given by the fact that tenderers can deploy the battery systems for multiple services at the same time. Clearly, this yields to an increase in revenues through the following market mechanisms:

- a. **Imbalance market:** imbalance prices are supposed to reach 6000 £/MWh in times of system stress. Flexibility can, then, be a crucial future revenue stream.
- b. **Capacity Market (CM):** National Grid buys capacity ahead of delivery. Market participants can bid for contracts in auctions held four years ahead of the delivery date, even if longer term agreements (15 years) are available for new plant, to encourage investment in new generation assets. Generators, CHPs, electricity storage systems, interconnectors, and DSRs can participate to the capacity market.

Participants are notified, usually, four hours ahead of the required delivery time and further information related to the settlement period and the percentage of their total obligations are provided as well.

- c. **Embedded benefits:** triads are supposed to be removed by 2020 and this may provide benefits in the long term.

Scenario 1 – revenue build up incl. triad periods



Scenario 2 – revenue build up excl. triad periods

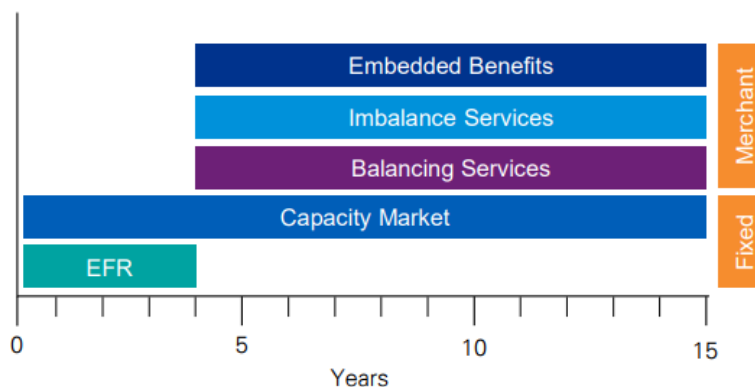


Figure 5: Revenue build up.

2.3.4.1 High Energy users

High Energy users, most likely to be related to the industrial and commercial sectors, are subject to high payments if they have peaks in consumption.

The main goals for such energy users, related to the deployment of storage systems might be:

1. Transmission and Distribution Costs Avoidance

The reduction of the energy withdrawn from the grid and the power peak causes a decrease in the transmission and distribution costs for the users.

2. Peak shaving

Governments in the UK, and many countries in Europe, are supporting users setting an upper limit in their annual consumption. By guaranteeing their maximum consumption below such threshold, users avoid payment peaks and TSOs provide more stability to the grid.

Peak shaving strategies involve software and hardware solutions, such as storage systems and diesel generators.

As UK is highly addressing peak reduction in high energy users, Germany has dealt with this years ago with the STROMNEV legislation; in such scenario, many industrial consumers were attracted by high savings and, firstly, decided to look for solutions such as diesel generators integrated with storage batteries. However, due to the uncertainty of such law, few investments have been finalized for peak reduction, as consumers were reluctant to invest thousands of euro for a law that could have been canceled the following year.

3. Increase self-consumption of the renewable energy produced

High energy users that have installations of Renewable Energy Sources (RESs), might be interested in increasing their deployment through storage systems. This will yield to a reduction in the amount of energy withdrawn from the national grid.

4. Uninterruptible Power Supplies (UPS)

Batteries can also operate as UPS when it is not possible to withdraw power from the national grid due to failures and breakout.

5. Frequency Control

In many countries, like in the UK, batteries can provide multiple services at the same time. In this view, storage systems can also provide services for grid regulation and, so, increase the revenue streams.

6. Generator own use

Batteries can easily act as generators whenever they are charged.

2.4 Combined geothermal and solar thermal energy storage systems

The combination of geothermal and solar thermal energy systems may support the achievement of the highest efficiency possible in heating and cooling renewable based plants. The main energy source is the thermal solar field, which takes the heat from solar energy and the ground source heat pumps, which energy is extracted from boreholes on the ground, and can be used for heating, cooling and storage purposes. The excess

energy can be stored under the ground to preserve it until needed.

As a matter of fact, the solar source can usually generate much more energy than with geothermal, but its main drawback of this kind of renewable energy is the lack of constancy in the extraction, since the sun is not shining at night and during the non-sunny days. The adoption of the sole geothermal energy has some inconveniences as well. For example, the efficiency of the system will decrease with time, as the ground temperature cools down because of its energy use.

The two sources can be associated to solve the drawbacks they individually have. Most of the time during the year, the solar energy warms the flowing water at higher temperature than needed for heating the building. In order to not waste the surplus of water temperature, the solar system pipes can be redirected to the borehole. This way, the warm water will heat up the ground, letting the geothermal system be able to extract more energy, as well as keeping the ground temperature from cooling down. In the periods when the water circulating through the solar system has similar temperature as the needed for the building thermal needs, this energy will be used directly to heat up the heating system. That means, the solar system will have more than one direction, one towards the borehole, other to heat pump and a final one directly connected with the space heating system.

The parameters to consider regarding the building are mainly the heating, cooling and electricity consumption. In the case study of the K2 building of the Environmental Engineering Department in TUC, this information can be taken from the existing simulation of the model building K1 in OpenStudio software, which has similar characteristics as the object of study. The model contains the same external and internal dimensions of the real building, as well as, all the distribution, installations and facilities, so that the data obtained will be reliable. To simulate the model, a heating and cooling temperature set point is defined, so when a certain room temperature increases above the specified degree in the case of cooling, or below in the case of heating, the HVAC system will switch on and consume energy. In this way, the thermal energy consumption is calculated.

About the climate conditions, the daily average temperature and the sun irradiance will be useful when dimensioning the solar thermal collectors. The data have been acquired from the Photovoltaic Geographical Information System (PVGIS), which also provides the average optimal inclination angle of the collector, for having the maximum efficiency

possible at the specific location.

It is also necessary to study the geology of the area, for knowing the characteristics of the terrain below the ground surface and its different strata. This data will be useful when dimensioning the borehole heat exchangers for the geothermal energy extraction and storage. The information will be taken from the ThermMap, an Interactive Online Platform that provides the average thermal conductivity and heat capacity of the ground, among other parameters.

Once all the data are gathered, the dimensioning of the energy sources is performed. The geothermal boreholes extract energy from the ground, so the potential of this source decreases with time, as the more heat is drawn out, the faster the ground is cooled down. For overcoming this fact, the part or all the energy obtained (depending on the needs) by solar collectors will be redirected to the borehole in order to maintain the temperature of the ground above certain level, as well as, serving as the heat source for the Underground Thermal Energy Storage.

The solar collectors have been dimensioned taking into account the heat consumption needed to be extracted from the boreholes. For that, the collector type is specified and the thermal energy produced is calculated considering the collector parameters (efficiency and area) and the climate conditions (solar irradiance).

For the dimensioning of the geothermal boreholes, the GeoT*SOL software has been utilized, which simulates the Borehole Heat Exchanger (BHE) system and specifies the best configuration, the number of boreholes needed, heat produced and energy consumed by the heat pump. After energy sources dimensioning, the final conceptual design of the system combining both energy sources connected with the Space Conditioning System is presented, followed by a description of the systems functioning and different modes of operation.

2.5 Design of a platform for monitoring and controlling building integrated solar polygeneration systems

A research-to-market applicative approach has been adopted, starting from the results that TUC obtained in terms of data collection infrastructures and processing algorithms based on ANN and fuzzy logic. Data models have been described, as well as the storage and calculation procedures. ARM processor based platforms have been considered porting the experimental architecture on a robust and scalable platform. The ARM boards

under consideration are adopting for Linux OS that allows the adoption of rapid, affordable and robust development environments.

Once an open framework for sensing and controlling has been designed, a pilot porting activity has been operated in order to validate the envisaged approach.

3. Optimised Operation of Renewables for Smart Grids

3.1 Energy forecast at the Brunel University London

Brunel University London is a medium-sized university based in Uxbridge on the outskirts of London. Formed in 1966, it has grown steadily through the incorporation of additional colleges and further education providers, but retains an emphasis on engineering, science and technology. Today, it numbers around 15,000 students and 2,000 staff.

The campus (see Figure 6) is composed by three different type of buildings:

- **Residentials**, with ten residential complexes, each one of them composed by a variable number of buildings.
- **Academic**, with almost twenty buildings consisting of halls, offices, labs and libraries.
- **Social**, including sport centers, art centers, cafes and restaurants.

For what concerns the electricity supply, the whole campus is directly connected to the national grid. There are some production plants (both solar and wind) also connected to the national grid. Hot water and heating systems are fed by a gas system, so electricity is used for lighting, cooling and for electrical devices supply.

In 2011 a system of 21 meters has been installed within the campus. Each meter records every 30 minutes data about electricity consumption of one or more buildings.

Data provided, is related to electricity consumption recorded by each meter distributed at the campus of Brunel University London from 8th of February 2011 to 31st of March 2017.

Data are recorded every 30 minutes, 24 hours a day (48 samples per day). Each meter is connected to one or more neighbouring buildings. In Figure 7 different meters records are plotted. As it can be noticed, loads can vary a lot according to the number of buildings connected to the meter, and to their use.

The highest consumption is recorded by the “CBS 1” meter, its main contribution is given by Hamilton Centre, a complex that hosts most of restaurants and social area.

On the other hand, the lowest contribution to the electricity demand is given by the “Health” meter, related to Mary Seacole building, including gyms, art rooms, laboratories, observation rooms and work rehabilitation rooms.

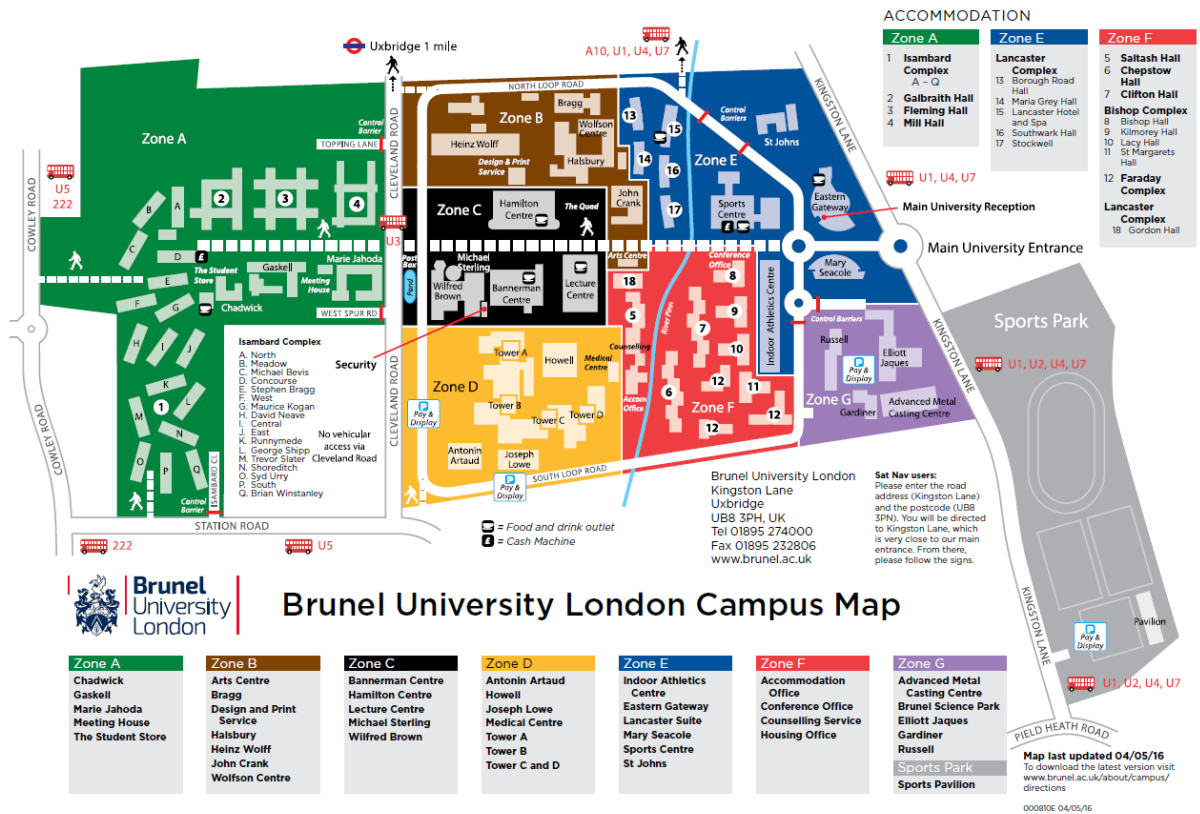


Figure 6: Brunel University London Campus Map

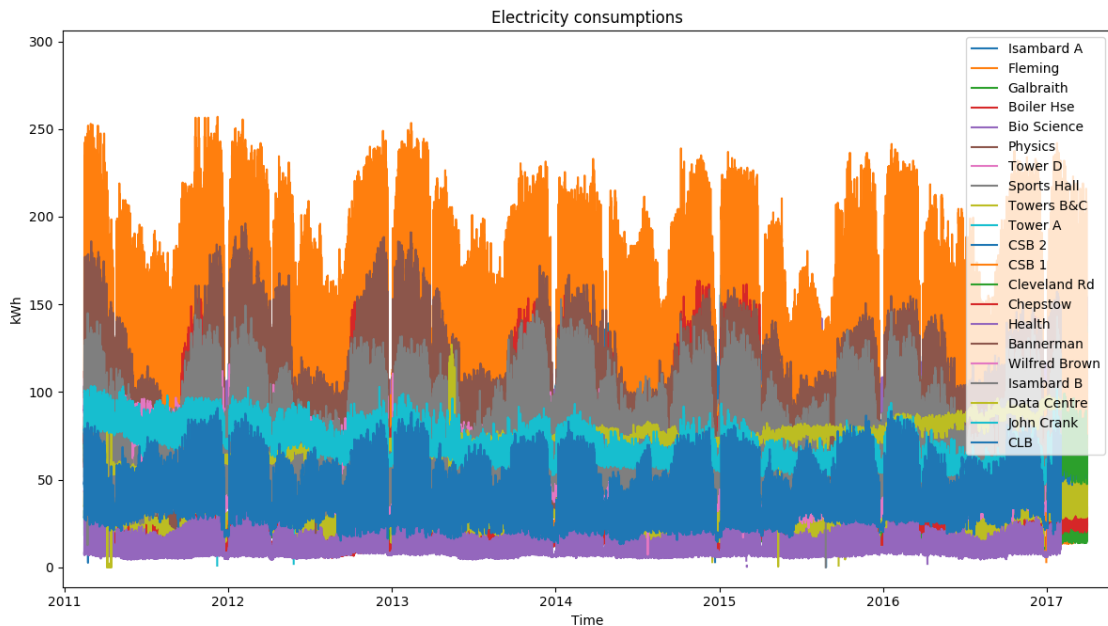


Figure 7: Electricity consumptions recorded by meters

3.1.1 Data preparation

Before proceeding to the development of the forecast model, data collected have been “prepared” for the analysis. In particular:

- outliers have been detected and replaced by the average value of the time series
- missing values have been filled through linear interpolation
- periods during which data from particular meters are not available have not been included in the analysis.

Once the data of each single meter were ready to be analysed, they have been summed and the total amount of electricity consumption was studied. Further steps of this work will include a separate analysis of the consumption profiles differentiated for each meter. In Figure 8 the total electricity demand is shown.

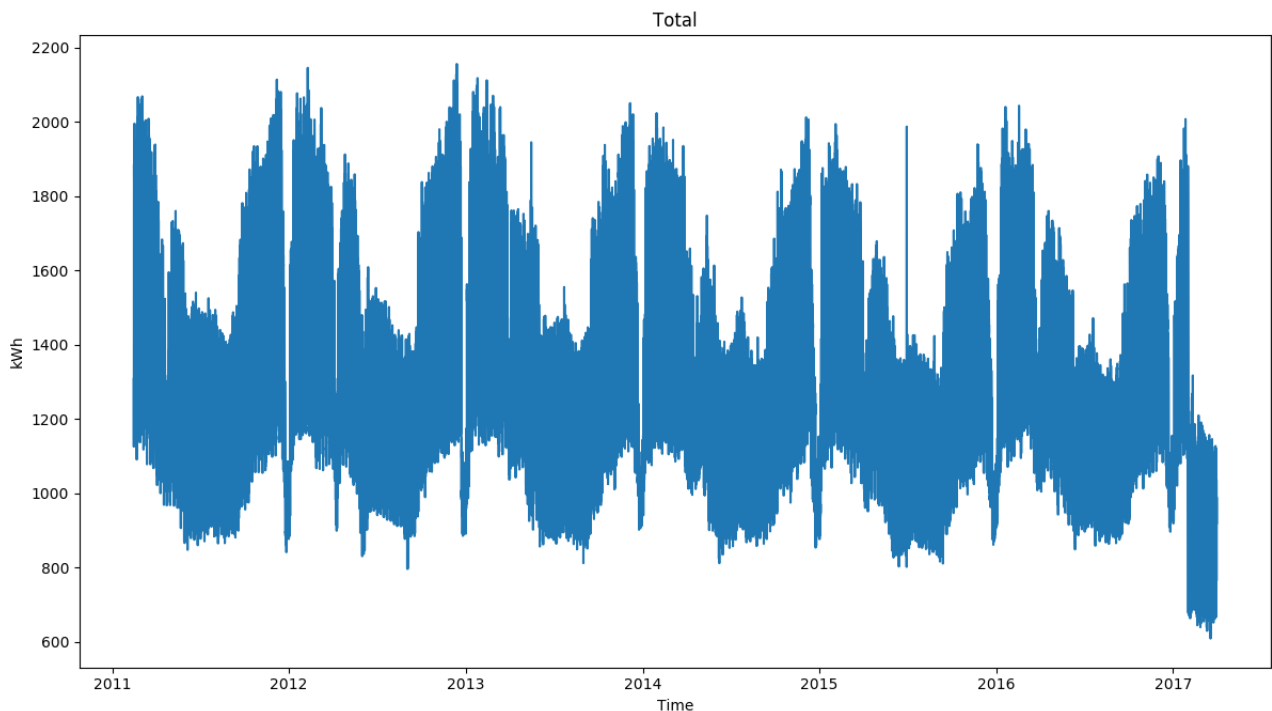


Figure 8: Total electricity consumption

Some preliminary considerations can be made by observing the plot:

- There is a clear annual seasonal profile.
- During summer period, when classes are stopped and many students are out for holidays the electricity demand is lower.
- During winter holidays (around from 24th of December to 5th/6th of January) a steep decrease of electricity consumption is observed possibly due to Christmas holidays.
- Data relative to 2017 show a deceptive decrease of consumption. It is actually due to missing measurements of some meters. For this reason, as mentioned before,

data of 2017 have been removed from the dataset in order to not affect the model with systematic errors.

For the dataset preparation and this first data exploration of the programming language Python was employed.

3.1.2 Forecast

To predict future values of energy consumption data, a preliminary study of the behaviour of the campus have been performed. Once evaluated the main characteristics of the electric demand trend over time, two forecasting models have been implemented and evaluated: ARIMA and Exponential Smoothing. Their analysis is performed using R programming language.

3.1.2.1 Yearly, weekly and daily profiles

The dataset of the total electricity consumption from February 2011 to December 2016, has been used to develop the forecast model.

In addition to the annual trend of the electricity consumption, in Figure 9 overlapping annual profiles are shown.

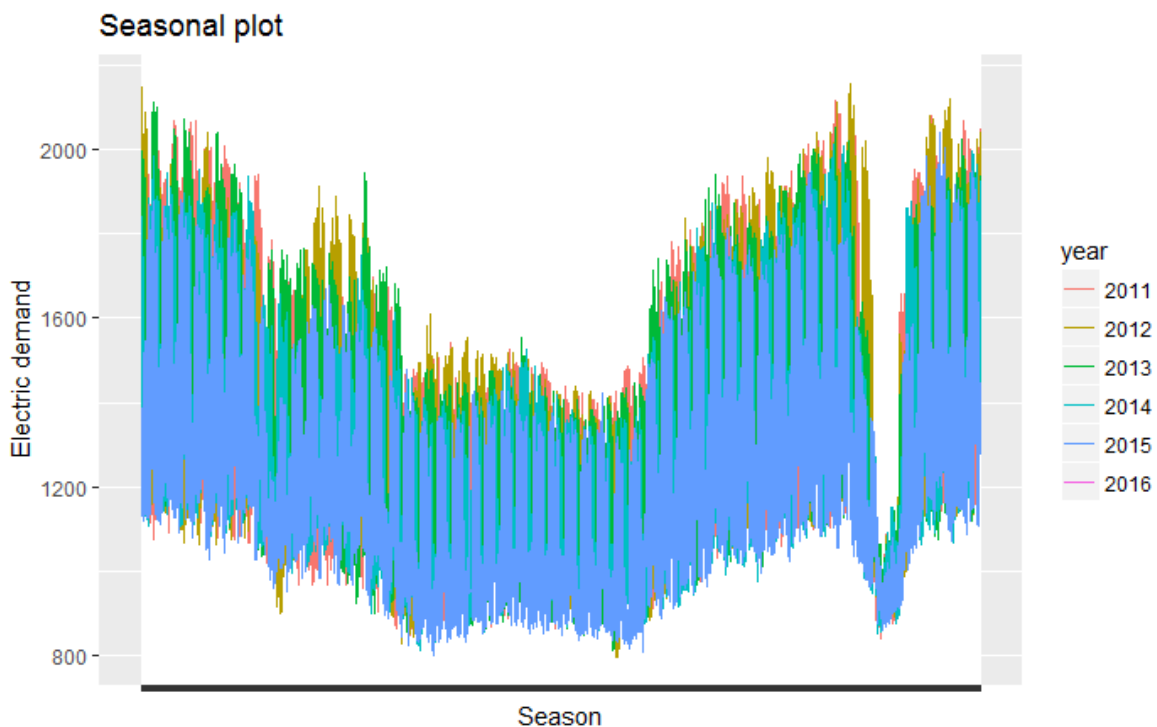


Figure 9: Annual trends over time (seasonal plots)

Early observations can be confirmed by observing the seasonal plot: trends repeat over the years, there is a decrease of the consumption during the summer vacations and a steep drop is observed in Christmas holidays.

In order to better understand the characteristic behaviour of the campus and to analysing at different depths the trend over time of the demand, median daily and weekly profiles have been produced. In Figure 10 and Figure 11 the median pattern and the Median Absolute Deviation (MAD) are shown.

From the daily profile an increase of the demand in the first half of the morning (from 7 a.m. to 10 a.m.) is evident and then the profile remains almost flat until the evening (around 8 p.m.). Such a profile can be justified as the combined result of the residential buildings demand- which have a predominant request in the early morning when students wake up and in the evening- and the academic and social buildings- which have a predominant consumption in the central part of the day.

In the median weekly profile the difference between the working days and the weekend is very clear. For the working days in fact the profile is higher and shows an increasing pattern in the morning, with a peak occurring around 12 a.m. and a decreasing pattern in the second part of the day, with a minimum recorded during the night around 4 a.m.

As it can be expected, during Saturday and Sunday the request is lower and the daily peaks are delayed to the late evening (around 19 p.m.).

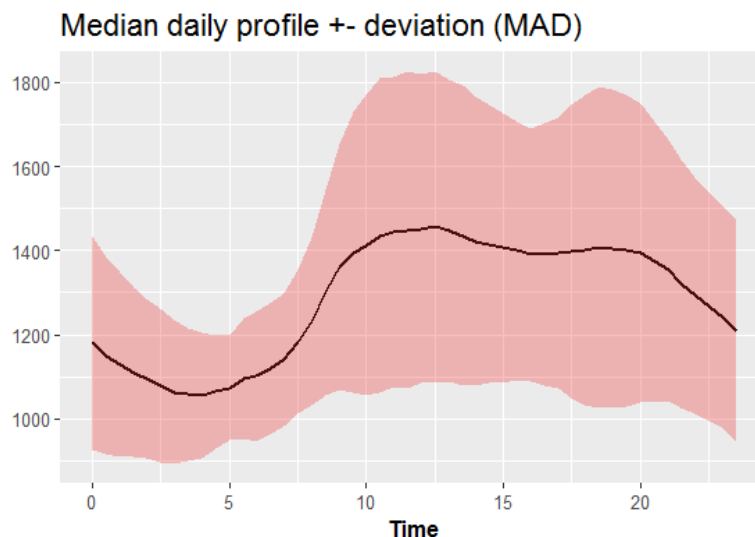


Figure 10: Median daily profile.

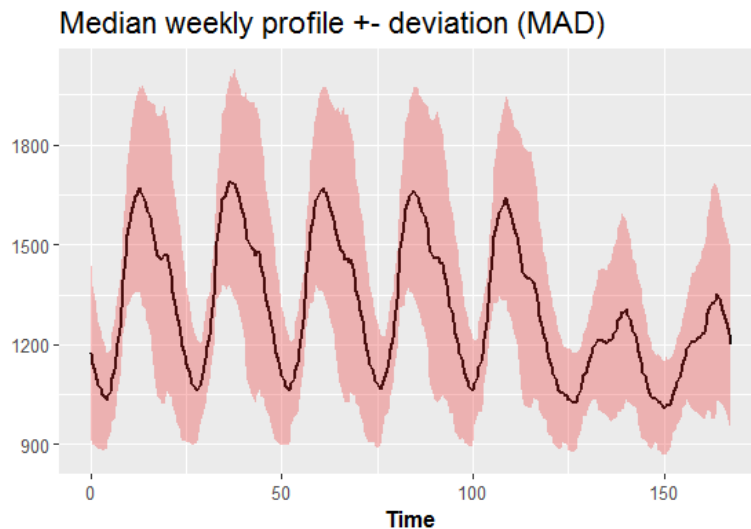


Figure 11: Median weekly profile.

3.1 Athalassa Campus and NTL building

The Fresnel technology started to be part of a grid, composed by several buildings of Athalassa campus (adjacent to Franco Cypriot School) within Aglantzia Municipality in Nicosia, where Cyprus Institute is located. The Cyprus Institute started to add non-used buildings at the Campus to expand its research activity with needed laboratory and office space. The renovation and extension work commenced at the end of 2014.

The main facilities within the Campus are:

- The Guy Ourisson Building (2007): the first renovated building of Cyl that includes a mixture of offices (for faculty, researchers and administration), seminar and conference rooms as well as auxiliary common areas, a small number of research laboratories, office space for students and a students' common area.
- The Novel Technologies Laboratory (2014): it is designed as a "green building", using specific standards that allow it to be a near zero energy building. The Laboratory hosts offices and laboratory teams from the Energy, Environment and Water Research Centre and is equipped with latest technology equipment for scientific research.
- The Cy-Tera, Cyl's High Performance Computing Facility (2012): one of most powerful Supercomputers in the region used for scientific research. The Building includes office space for the researchers and the technical team.

- STARLab Laboratory: research infrastructure for the scientific research, documentation and preservation of the cultural heritage of Cyprus. The Facility includes both a fixed and a mobile laboratory.

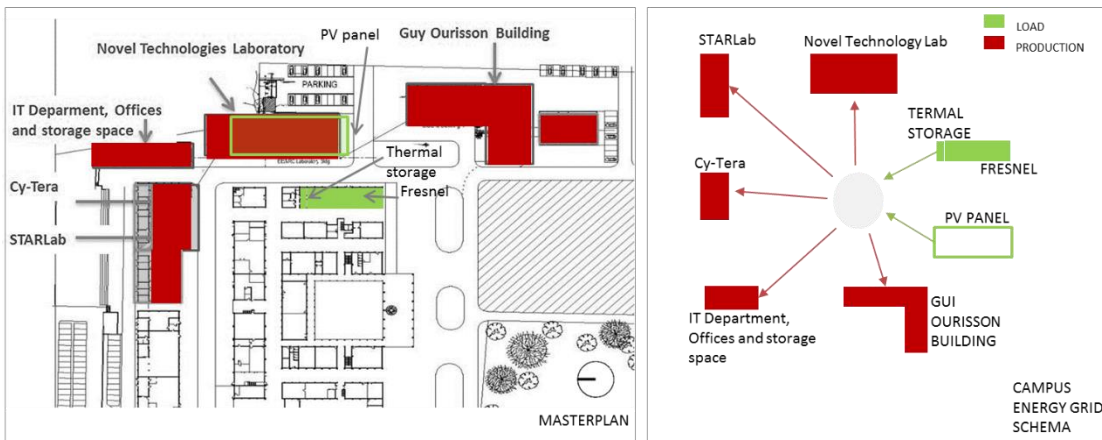


Figure 12: Athalassa campus and energy grid schema

Activities initiated with a preliminary focus on the campus by considering the buildings as load (consumption) or production nodes that compose the smart grid. Smart Grids provide the integration of traditional and renewable energy resources, with new elements in a distributed, open, and self-managed way. Innovative models for energy infrastructure and the self-management of the power grid are required, suitable for open and distributed infrastructures. Such a shift would ensure the scalability of smart grids and enable the management of autonomous operations throughout the power network.

In this context, we consider the existing integrations between two nodes of the Athalassa Campus “potential” grid, as the Novel Technologies Laboratory (NTLB) and Linear Fresnel Collector with thermal storage. The system is constituted by a Fresnel solar collector, an oil buffer storage, a heat exchanger to generate hot water and a single stage chiller to be integrated with the existing HVAC units. The solar collector has been designed by Idea Srl and it is implementing the possibility to install PV panels on the back of the primary optics, to produce electricity when the direct solar radiation is poor.

The aim of the Linear Fresnel Collector is to explore the opportunities offered by solar poly-generation for Near to Zero Energy Buildings and maximize the utilization of the collected solar energy. The research activities during the first year of Smart GEMS have been devoted to the study of the main issues emerging in such a kind of integrated system and, specifically, on tuning, liability, automation, building integration and hybridization with the in-place air conditioning systems.

NTLB with a Linear Fresnel Collector and combined HVAC systems has been assessed in terms of minimization of consumption and full exploitation of solar plant integration. In addition, dynamic modelling and evaluation of Concentrated Solar Power (CSP) technology and in specific, the IDEA FRESCO system was investigated as a solution for integration in Near Zero Energy Buildings (NZEBS) and smart grids.

A model of the Fresnel System was developed and exploited to fully understand the operational phase and coupling possibilities of such systems. In such context, the goal is to give an overall estimation of energy consumption by using a data driven model obtained with the data collected in Novel Technology Laboratory.

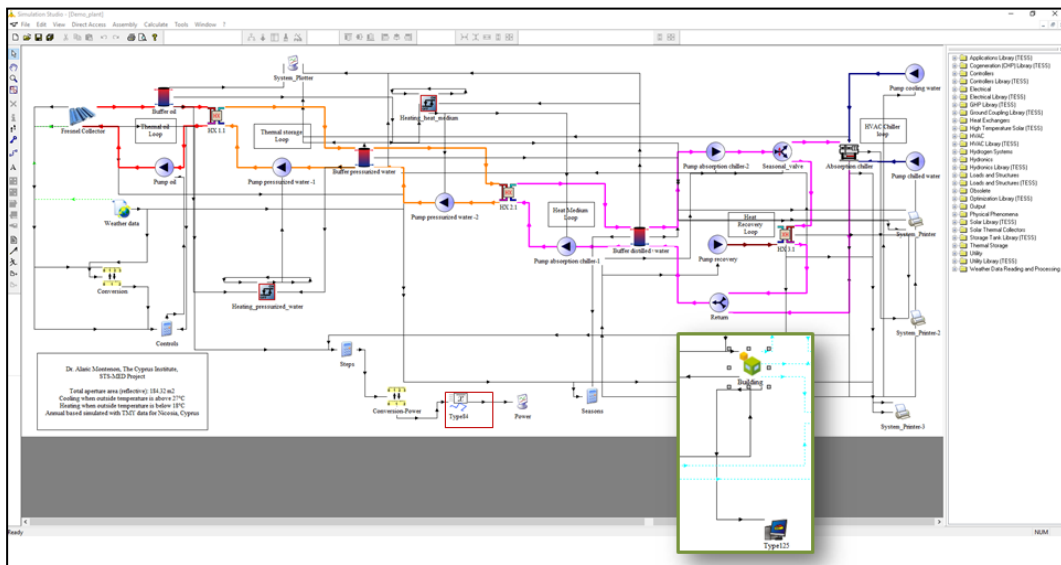


Figure 13: Fresnel and Thermal loop Trnsys model

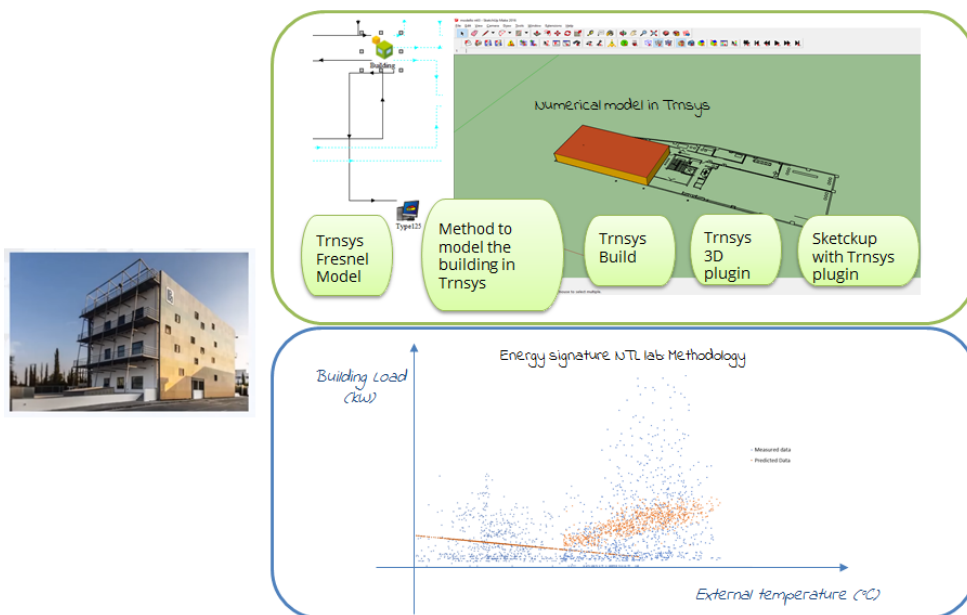


Figure 14: Simulation model vs Data Driven model of NTLab

3.2.1 Correlation with weather data

Data analysis general methodology is composed by several fundamental steps including problem definition, data exploration and data preparation, and finally data analysis through the test of several algorithms, related to supervised and unsupervised techniques.

Data preparation has been obtained through Microsoft Excel and Labview software environment while algorithms used for data analysis have been developed in Python programming language.

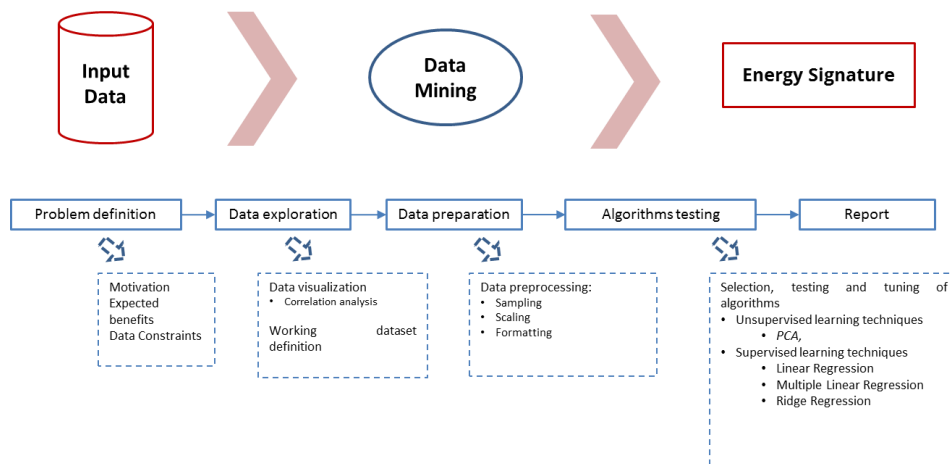


Figure 15: Flow chart of Energy Signature generation

In this case, we decided to employ regression analysis in order to model its relationship among energy load, external temperature, and other collected data.

Then, we try to predict the outcome (Y) based on values of a set of predictor variables (X_i) by using regressive method.

Regression analysis is widely used for prediction and forecasting of a quantity and helps to understand how the value of the dependent variable changes when any one of the independent variables (or 'predictors') is varied, while the other independent variables are held fixed. The estimation target is a function of the independent variables called the regression function.

These methods allow to assess the impact of multiple variables in the same model. In the literature, there are various types of regression analysis.

We started from linear regression by adding each time a new (X_i) variable in order to better fit the (Y). Since, the first results with a linear model were not so good, non-linear

regression with Ridge technique was introduced to create a reliable model for predicting building consumption.

3.2.2 Novel Technology case study description

As previously introduced, Novel Technologies Laboratory mainly contains offices and laboratories in four levels; basement, ground floor, first floor and second floor. The basement encloses laboratories, WC and two offices. Ground floor is composed of the main lobby/entrance, two laboratories, six offices, a storage room, a small kitchen and WC. First floor has a lecture hall, five offices and a conference room, a small kitchen and WC. Second floor contains a laboratory, five offices, a kitchen and WC.

The Novel Technologies Laboratory operates 8 hours/day, Monday to Friday and for about 240 days/year.

The demand of energy in NTL has a distribution that is typical in hot countries. Figure 16 shows the power demand required during a year: the red line indicates the average basic load demand (general appliances elevator, ventilation, hot water) the blue line artificial lighting, and the green line represents electricity consumption, in cold and warm months, to manage demand for heating and cooling.

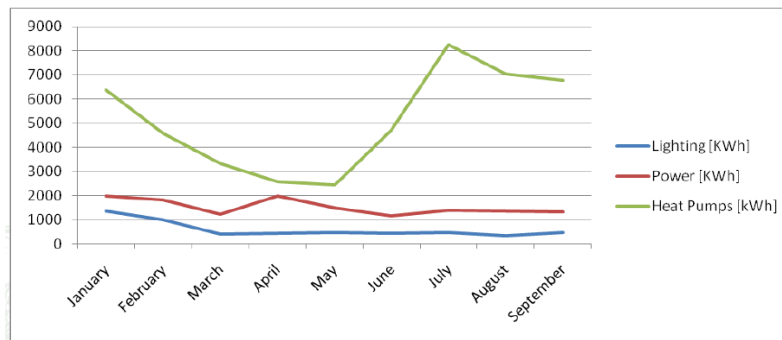


Figure 16: NTL Power demand

Extract Transform Load procedures (ETL) started from “load demand” data and “meteo station” data that has been collected in two separates files with a different sample rate (Figure 17).

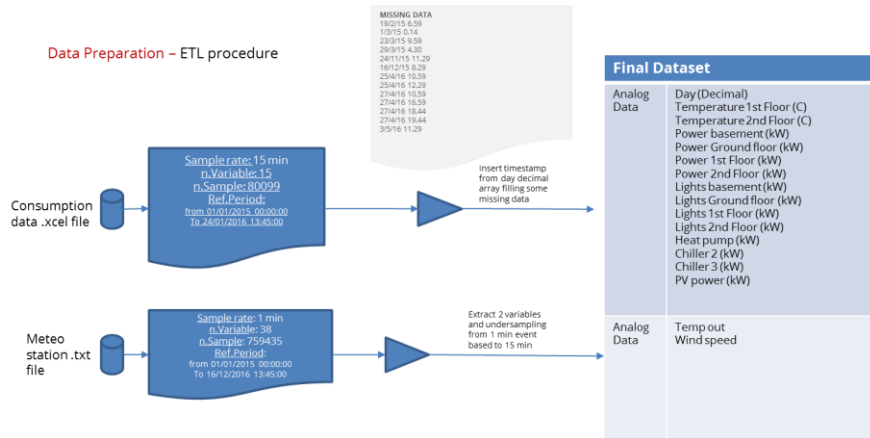


Figure 17: ETL procedure

Sub-sampling procedures have been developed to be scalable and programmed in Labview platform (Figure 18).

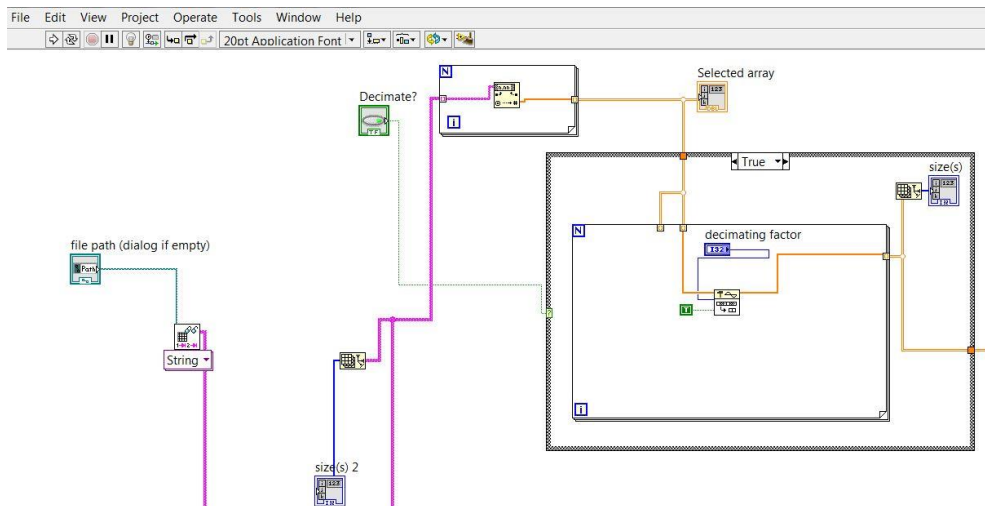


Figure 18: Re-sampling algorithm

Another important aspect is to consider the correct timestamp in order to understand the real consumptions in operative settings. For this reason, we added several conditions related to working time, week end, and national holidays, in order to select only the most relevant data and exclude all data collected when the building is not fully operative. Moreover, we split in two datasets the original data, in order to obtain the two basic components of energy signature: one related the heating consumption, and the other one related to cooling consumption. For this reason, we consider both for 2015 and 2016 the period from January 01 to May, 01 and the period after November 14 for the heating data set and the other for cooling dataset.

We added another condition related to maximum or minimum external temperature, because, for a fully operative condition, during heating period the external temperature has to be minor than 25°C and during summer has to be higher than 25°C. While for the heating dataset we considered only the consumption of the Heat Pump, for cooling period we considered the sum among Heat Pump, Chiller 2 and Chiller 3. In Table all the added conditions are explained.

Select working time	Dataset from 9:00 am to 05:00 pm
Delete week end day	Delete all samples collected during Saturday and Sunday
Delete National Holiday	Delete all samples collected during National Holiday and expected vacation
Heating variable HEATING (kW)	-Time $t > 01/01/2015$ and $t < 01/05/2015$ or $t > 14/11/2015$ - Weather Temperature $T < 25^\circ\text{C}$ HEATING (kW)=Heat Pump (kW)
Cooling variable COOLING (kW)	-Time $01/01/2015 < t < 01/05/2015$ or $t > 14/11/2015$ - Weather Temperature $T > 25^\circ\text{C}$ COOLING (kW)=Heat Pump (kW) +Chiller 2 (kW) +Chiller 3 (kW)

Table 5: Dataset filters

The Final Dataset consists of 27 columns, corresponding to the observed variables, and a number of rows corresponding to the various samples collected, with 15 minutes, between 01/01/2015 and 31/12/2016 (Figure 19).

Other two additional variables are added. One, called “orari”, is obtained by extracting single hour from timestamp. The other one, called “deltaT”, is obtained by calculating the difference between the average of internal and external temperature.

Figure 19: Selected data set

2015											
January	February	March	April	May	June	July	August	September	October	November	December
HEATING PERIOD				COOLING PERIOD				HEATING PERIOD			
TRAINING PERIOD											
2016											
January	February	March	April	May	June	July	August	September	October	November	December
HEATING PERIOD				COOLING PERIOD				HEATING PERIOD			
TEST PERIOD											

Figure 20: Training and test data set

Finally, we split again the dataset in order to obtain the training data set completely different from the test dataset. Training set is a set of data used to discover potentially predictive relationships and test set is a set of data used to assess the strength and utility of a predictive relationship. Initial discovery of relationships is usually done with a training set while a test set and a validation set are used for evaluating whether the identified relationships hold. In this case, we have the whole 2015 as training set and 2016 as test set (Figure 20).

The energy signature (heating and cooling consumption vs external temperature) of selected dataset with respect to the original dataset is shown in Figure 21.

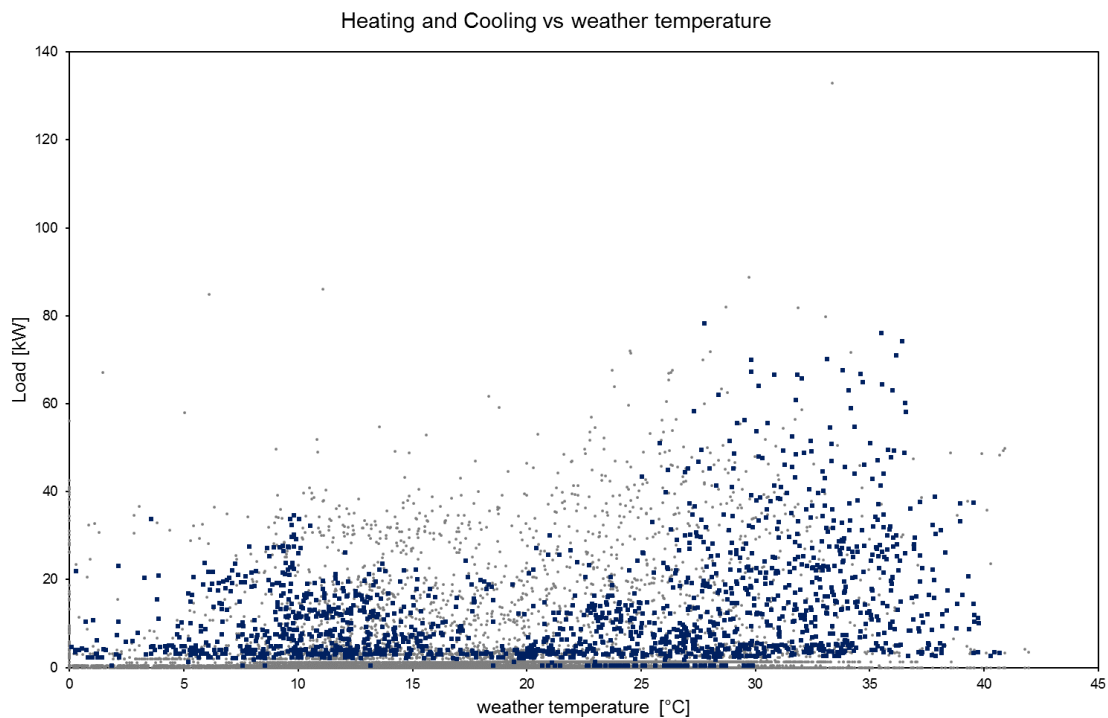


Figure 21: Energy Signature in terms of heating and cooling consumption vs external temperature

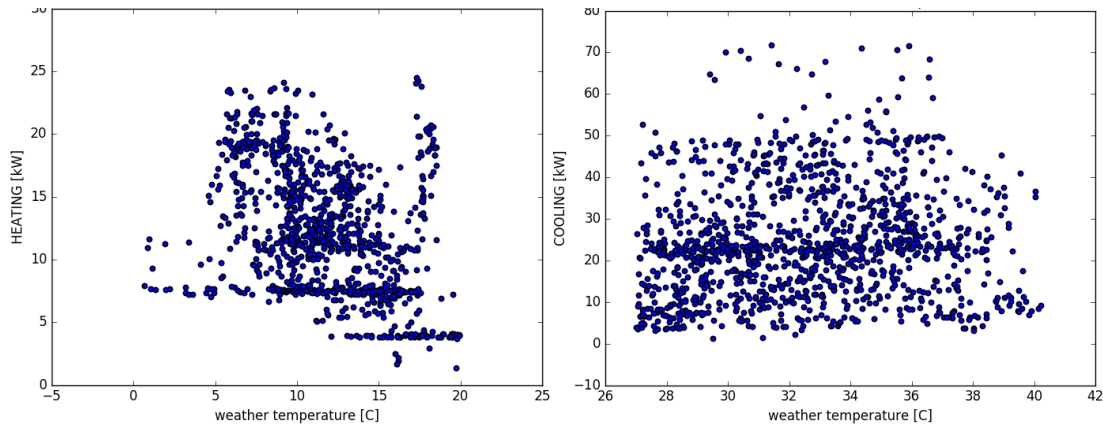


Figure 22: Selected data set after ETL procedure

3.2.3 Data exploration

Data exploration is the first step in data analysis and typically involves summarizing the main characteristics of a dataset. Before a “prescribed” data analysis, we must know how many cases are in the dataset, what variables are included, how many missing observations there are, which is the average value and what general hypotheses the data is likely to support. An initial exploration of the dataset helps in answering these questions and familiarizing with the data.

From this step, one can identify variables that are likely to have interesting observations. For example, by displaying the mean external temperature variable we can simply check if the two clusters for heating and cooling are appropriated and coherent with thermal conditions. In Table and Table the information related to number of samples, mean value, standard deviation, min, 25%, 50%, 75% and maximum values are shown for each variable.

	Temperature 1st Floor [C]	Temperature 2nd Floor [C]	Heat pump [kW]	Chiller 2 [kW]	Chiller 3 [kW]	PV power [kW]	weather_temperature	orari	weekdays	deltaT	heating
count	2396	2396	2396	2396	2396	2396	2396	2396	2396	2396	2396
mean	17.16255843	19.0924207	10.52388982	0.180033389	0.400617696	4.181619366	11.78800793	12.62	2.071368948	-6.3394816	10.5238898
std	1.51954765	1.846996587	6.967868963	0.200660285	0.01267361	4.191526521	3.814949122	2.36	1.392913156	3.8761798	6.96786896
min	11.73	12.51	1.04	0	0.36	0	0.593	9	0	-20.723	1.04
25%	16.31	18.15	4.04	0	0.4	0.12	9.4	11	1	-8.942	4.04
50%	17.11	19.41	7.84	0	0.4	2.84	11.78	13	2	-6.3415	7.84
75%	17.82	20.2	15.32	0.4	0.4	7.97	14.1685	15	3	-3.8895	15.32
max	23.01	23.95	36.16	0.44	0.44	13.68	19.907	17	4	3.66	36.16

Table 6: Data exploration for heating dataset.

	Temperature 1st Floor [C]	Temperature 2nd Floor [C]	Heat pump [kW]	Chiller 2 [kW]	Chiller 3 [kW]	PV power [kW]	weather_temperature	orari	weekdays	deltaT	cooling
count	2362.000	2362.000	2362.000	2362.000	2362.000	2362.000	2362.000	2362	2362.000	2362.000	2362.000
mean	25.0292083	25.8142337	10.2473277	4.840321761	5.129077053	6.61703641	32.31518967	12.74	2.038022862	6.8934687	20.2167316
std	2.085831047	2.445781115	16.49763977	10.39229874	10.52949692	3.783842645	3.245778846	2.25	1.420999436	3.2185138	16.5229615
min	20	21.87	0.32	0.36	0.36	0	27.013	9	0	-2.297	1.12
25%	23.58	23.91	0.44	0.44	0.44	2.89	29.5485	11	1	4.61775	6.97
50%	25	24.94	0.44	0.44	0.44	7.5	32.307	13	2	6.56	16.02
75%	26.59	27.37	14.42	1.35	2.79	10.2	34.6115	15	3	9.21925	27.16
max	30.49	30.63	87.24	85.2	69.96	12.04	40.727	17	4	17.142	88.12

Table 7: Data exploration for cooling dataset.

3.2.4 Correlation Matrix

Pearson’s correlation coefficient between two variables is defined as the covariance of the two variables divided by the product of their standard deviations.

Correlation is computed into what is known as the correlation coefficient, which ranges between -1 and +1. Perfect positive correlation (a correlation coefficient of +1) implies that as one variable moves, either up or down, the other variable will move in lockstep, in the same direction. Alternatively, perfect negative correlation means that if one variable moves in either direction the variable that is perfectly negatively correlated will move in the opposite direction. If the correlation is 0, the movements of the variables are said to have no correlation; they are completely random.

In Table 8 and Table 9 corresponding to correlation matrices for both datasets, one can observe several levels of correlation.

HEATING	Temperature 1	Temperature 2	Power basement	Power Ground	Power 1st Floor	Power 2nd Floor	Lights basement	Lights Ground	Lights 1st Floor	Lights 2nd Floor	Heat pump	Chiller 2 (kW)	Chiller 3 (kW)	PV power (kW)	weather_temp	orari	deltaT	heating	
Temperature 1st Floor (C)	1.00	0.73	0.09	0.22	0.25	0.11	0.12	0.20	0.15	0.19	-0.05	-0.13	0.19	0.00	0.16	0.13	0.13	-0.21	-0.05
Temperature 2nd Floor (C)	0.73	1.00	0.14	0.32	0.40	0.16	0.23	0.28	0.21	0.41	0.28	-0.28	0.13	0.06	0.15	0.06	0.15	0.06	0.28
Power basement (kW)	0.09	0.14	1.00	0.23	0.09	0.54	0.46	0.05	0.05	0.29	0.25	0.20	-0.02	0.05	0.13	-0.02	0.07	0.25	0.15
Power Ground floor (kW)	0.22	0.32	0.23	1.00	0.43	0.18	0.23	0.20	0.09	0.56	0.54	-0.07	-0.02	0.18	-0.03	-0.28	-0.15	0.54	0.25
Power 1st Floor (kW)	0.25	0.40	0.09	0.43	1.00	0.03	0.14	0.14	0.14	0.40	0.48	-0.08	0.00	0.19	0.00	-0.28	-0.14	0.48	0.25
Power 2nd Floor (kW)	0.11	0.16	0.54	0.18	0.03	1.00	0.55	0.23	0.03	0.30	0.10	0.57	-0.06	0.05	0.39	0.01	0.33	0.10	0.10
Lights basement (kW)	0.12	0.23	0.46	0.23	0.14	0.55	1.00	0.28	0.13	0.55	0.20	0.41	-0.03	0.01	0.21	-0.06	0.13	0.20	0.20
Lights Ground floor (kW)	0.20	0.28	0.05	0.20	0.14	0.23	0.28	1.00	0.52	0.31	0.19	0.28	-0.14	-0.46	0.02	0.37	-0.08	0.19	0.19
Lights 1st Floor (kW)	0.15	0.21	0.05	0.09	0.14	0.03	0.13	0.52	1.00	0.16	0.15	-0.03	-0.09	-0.32	-0.07	0.34	-0.15	0.15	0.15
Lights 2nd Floor (kW)	0.19	0.41	0.29	0.56	0.40	0.30	0.55	0.31	0.16	1.00	0.43	0.16	-0.04	0.08	0.06	-0.21	-0.07	0.43	0.43
Heat pump (kW)	-0.05	0.28	0.25	0.54	0.48	0.10	0.20	0.19	0.15	0.43	1.00	-0.10	-0.07	0.01	-0.12	-0.13	-0.18	1.00	1.00
Chiller 2 (kW)	-0.13	-0.29	0.20	-0.07	-0.08	0.57	0.41	0.28	-0.03	0.16	-0.10	1.00	-0.11	-0.16	0.21	0.00	0.30	-0.10	-0.10
Chiller 3 (kW)	0.19	0.13	-0.02	-0.02	0.00	-0.06	-0.03	-0.14	-0.09	-0.04	-0.07	-0.11	1.00	0.09	-0.03	0.05	-0.10	-0.07	-0.07
PV power (kW)	0.00	0.06	0.05	0.18	0.19	-0.05	-0.01	-0.46	-0.32	0.08	0.01	-0.16	0.09	1.00	0.11	-0.34	0.09	0.01	0.01
weather_temperature	0.16	0.15	0.13	-0.03	0.00	0.39	0.21	0.02	-0.07	0.06	-0.12	0.21	-0.03	0.11	1.00	-0.11	0.92	-0.12	-0.12
orari	0.13	0.06	-0.02	-0.28	-0.28	0.01	-0.06	0.37	0.34	-0.21	-0.13	0.00	0.05	-0.74	-0.11	1.00	-0.15	-0.13	-0.13
deltaT	-0.21	-0.23	0.07	-0.15	-0.14	0.33	0.13	-0.08	-0.15	-0.07	-0.18	0.30	-0.10	0.09	0.92	-0.15	1.00	-0.18	-0.18
heating	-0.05	0.28	0.25	0.54	0.48	0.10	0.20	0.19	0.15	0.43	1.00	-0.10	-0.07	0.01	-0.12	-0.13	-0.18	1.00	1.00

Table 8: Correlation matrix for heating dataset

COOLING	Temperature 1	Temperature 2	Power basement	Power Ground	Power 1st Floor	Power 2nd Floor	Lights basement	Lights Ground	Lights 1st Floor	Lights 2nd Floor	Heat pump	Chiller 2 (kW)	Chiller 3 (kW)	PV power (kW)	weather_temp	orari	deltaT	cooling	
Temperature 1st Floor (C)	1.00	0.81	-0.07	-0.04	-0.56	-0.06	-0.13	-0.47	-0.35	-0.59	-0.04	-0.22	-0.19	-0.09	0.37	0.16	0.16	-0.26	-0.29
Temperature 2nd Floor (C)	0.81	1.00	-0.12	-0.08	-0.52	-0.08	-0.15	-0.50	-0.33	-0.66	-0.13	-0.21	-0.22	-0.10	0.29	0.16	0.16	-0.35	-0.40
Power basement (kW)	-0.07	-0.12	1.00	0.01	0.21	0.18	0.99	0.14	0.01	0.20	-0.04	0.21	0.21	0.10	0.23	-0.02	0.80	0.22	0.22
Power Ground floor (kW)	-0.04	-0.08	0.01	1.00	0.07	0.07	0.01	0.07	0.02	0.07	0.09	0.03	0.05	0.06	0.00	-0.08	0.05	0.14	0.14
Power 1st Floor (kW)	-0.56	-0.52	0.21	0.07	1.00	0.22	0.23	0.48	0.38	0.62	0.26	0.20	0.29	0.30	-0.04	-0.31	0.33	0.57	0.57
Power 2nd Floor (kW)	-0.06	-0.08	0.18	0.07	0.22	1.00	0.16	0.22	-0.03	0.08	0.39	0.05	0.18	0.06	0.18	-0.07	0.23	0.54	0.54
Lights basement (kW)	-0.13	-0.15	0.99	0.01	0.23	0.16	1.00	0.17	0.09	0.26	-0.03	0.20	0.16	0.10	0.17	-0.04	0.27	0.20	0.20
Lights Ground floor (kW)	-0.47	-0.59	0.14	0.07	0.48	0.22	0.17	1.00	0.26	0.56	0.09	0.16	0.22	0.18	-0.14	-0.18	0.20	0.33	0.33
Lights 1st Floor (kW)	-0.35	-0.33	0.01	0.02	0.38	-0.03	0.09	0.26	1.00	0.37	0.09	0.01	0.08	0.03	-0.21	-0.08	0.03	0.15	0.15
Lights 2nd Floor (kW)	-0.59	-0.66	0.20	0.07	0.62	0.08	0.26	0.56	0.37	1.00	0.19	0.21	0.21	0.28	-0.19	-0.29	0.25	0.45	0.45
Heat pump (kW)	-0.04	-0.13	-0.04	0.09	0.26	0.39	-0.03	0.09	0.09	0.19	1.00	-0.25	-0.26	0.11	-0.03	-0.15	0.03	0.67	0.67
Chiller 2 (kW)	-0.22	-0.21	0.21	0.03	0.20	0.05	0.20	0.16	0.01	0.21	-0.25	1.00	-0.19	0.16	0.05	-0.13	0.20	0.26	0.26
Chiller 3 (kW)	-0.19	-0.22	0.21	0.05	0.29	0.18	0.16	0.22	0.08	0.21	-0.26	-0.19	1.00	0.14	0.13	-0.14	0.28	0.26	0.26
PV power (kW)	-0.09	-0.10	0.10	0.06	0.30	0.06	0.10	0.18	0.03	0.28	0.11	0.16	0.14	1.00	-0.07	-0.87	-0.01	0.30	0.30
weather_temperature	0.37	0.29	0.23	0.00	-0.04	0.18	0.17	-0.14	-0.21	-0.19	-0.03	0.05	0.13	-0.07	1.00	0.26	0.78	0.09	0.09
orari	0.16	0.16	-0.02	-0.08	-0.31	-0.07	-0.04	-0.18	-0.08	-0.29	-0.15	-0.13	-0.14	-0.87	0.26	1.00	0.15	-0.32	-0.32
deltaT	-0.26	-0.35	0.30	0.05	0.33	0.23	0.27	0.20	0.03	0.25	0.03	0.20	0.28	-0.01	0.78	0.15	1.00	0.33	0.33
cooling	-0.29	-0.40	0.22	0.14	0.57	0.54	0.27	0.33	0.15	0.45	0.67	0.26	0.26	0.30	0.09	-0.32	0.33	1.00	1.00

Table 9: Correlation matrix for cooling dataset

About heating data set results obtained are:

- Average correlated variables: *Power Ground floor, Power 1st floor, and Light 2nd floor.*
- Weakly correlated variables: *weather temperature, orari, delta T, Light basement, Light Ground floor, Light 1st floor, Chiller 2, Chiller 3, PV power.*

About cooling data set results obtained are:

- Average correlated variables: *Power 1st floor, Power 2nd floor, Light 1nd floor and Light 2nd floor.*

- Weakly correlated variables: *orari*, *delta T*, *Light basement*, *Light Ground floor*, *Light 1st floor*, *Chiller 2*, *Chiller 3*, *PV power*.

Obviously, both heating and cooling variables have a very strong correlation with Heat Pump (in the case of heating variable it is perfect). Instead, the cooling dataset is very weakly correlated with external temperature and for this reason a multivariable regression model is necessary to obtain more reliable results.

3.2.5 Regression model

The techniques for implementing regression analysis are several: parametric, such as linear regression and ordinary least squares regression, and non-parametric regression. Regression models are often fitted using the least squares method but they may also be fitted by minimizing the "lack of fit" in some other norm (as with least absolute deviations regression), or by minimizing a penalized version of the least squares loss function as in ridge regression (L2-norm penalty) and lasso (L1-norm penalty).

In this case, as described in the previous paragraph, two arrays, *x_train* and *y_train* have been created: *x_train* is related to the independent variable, *y_train* is instead the dependent variable.

The performance of regression analysis methods depends on the form of the data generating process, and how it relates to the regression approach being used.

Scikit-Learn package in Python has been applied as machine learning tool. There are 3 different APIs in Scikit-Learn to evaluate the quality of predictions of a model:

- Estimator score method: Estimators have a score method providing a default evaluation criterion for the problem they are designed to solve.
- Scoring parameter: Model-evaluation tools using cross-validation rely on an internal scoring strategy.
- Metric functions: The metrics module implements functions assessing prediction error for specific purposes.

In this work, regression metrics are used by considering several losses, score, and utility functions to measure regression performance. Some of those have been enhanced to handle the multi-output case: mean squared error, mean absolute error, explained variance score and *r2_score*.

The *r2_score* and explained variance score accept an additional value 'variance weighted' for the multioutput parameter. This option leads to a weighting of each

individual score by the variance of the corresponding target variable. This setting quantifies the globally captured unscaled variance. If the target variables are of different scale, then this score puts more importance on well explaining the higher variance variables.

3.2.6 Explained variance score

The explained variance score computes the explained variance regression score. If $y_{i\text{ pred}}$ is the predicted value and $y_{i\text{ train}}$ is the corresponding true value, and Var is variance, the square of the standard deviation, then the explained variance is estimated as

$$\text{Explained variance} (y_{\text{train}}, y_{\text{pred}}) = 1 - \frac{\text{Var} \{y_{i\text{ train}} - y_{i\text{ pred}}\}}{\text{Var} \{y_{i\text{ train}}\}}$$

Best possible score is 1.0.

3.2.7 Mean absolute percentage error

Another metric normally used to evaluate prediction accuracy of the regression model is the *mean absolute percentage error* (MAPE). It usually expresses accuracy as a percentage, and is defined by the formula:

$$M = \frac{100}{n} \sum_{t=1}^n \left| \frac{A_t - F_t}{A_t} \right|$$

where A_t is the actual value and F_t is the forecast value.

The difference between A_t and F_t is divided by the Actual Value A_t again. The absolute value in this calculation is summed for every forecasted point in time and divided by the number of fitted points n . Multiplying by 100 makes it a percentage error.

It cannot be used if there are zero values (which sometimes happens for example in demand data).

3.2.8 Mean absolute error

The mean absolute error function corresponds to the expected value of the absolute error loss or L1-norm loss.

If $y_{i\text{ pred}}$ is the predicted value of the i^{th} sample, and $y_{i\text{ train}}$ is the corresponding true value, then the mean absolute error (MAE) estimated over n is defined as

$$\text{MAE} (y_{\text{train}}, y_{\text{pred}}) = \frac{1}{n} \sum_{i=1}^{n-1} |y_{i\text{ train}} - y_{i\text{ pred}}|$$

3.2.9 Mean squared error and Root mean squared error

The mean squared error function and root squared error computes mean square error and its root, a metric corresponding to the expected value of the squared (quadratic) error loss or root error loss.

If $y_{i\ pred}$ is the predicted value of the i^{th} sample, and $y_{i\ train}$ is the corresponding true value, then the mean squared error (MSE) and the root mean squared error (RMSE) estimated over n defined as

$$MSE(y_{train}, y_{pred}) = \frac{1}{n} \sum_{i=1}^{n-1} (y_{i\ train} - y_{i\ pred})^2$$

$$RMSE(y_{train}, y_{pred}) = \frac{1}{n} \sum_{i=1}^{n-1} \sqrt{(y_{i\ train} - y_{i\ pred})^2}$$

3.2.10 Median absolute error

The median absolute error is calculated by taking the median of all absolute differences between the target and the prediction.

If $y_{i\ pred}$ is the predicted value of the i^{th} sample, and $y_{i\ train}$ is the corresponding true value, then the median absolute error (MedAE) estimated over n is defined as

$$MedAE(y_{train}, y_{pred}) = median(|y_{1\ train} - y_{1\ pred}|, \dots, |y_{n\ train} - y_{n\ pred}|)$$

3.2.11 R² score function

The R² score function computes R², the coefficient of determination. It provides a measure of how well future samples are likely to be predicted by the model. It can also be interpreted as the amount of variation of the dependent variable explained by the regression equation. Best possible score is 1.0. A constant model that always predicts the expected value of y , disregarding the input features, would get a R² score of 0.0.

If $y_{i\ pred}$ is the predicted value of the i^{th} sample, and $y_{i\ train}$ is the corresponding true value, then the score R² estimated over n is defined as

$$R^2(y_{train}, y_{pred}) = 1 - \frac{\sum_{i=1}^{n-1} (y_{i\ train} - y_{i\ pred})^2}{\sum_{i=1}^{n-1} (y_{i\ train} - \bar{y})^2}$$

where $\bar{y} = \frac{1}{n} \sum_{i=0}^{n-1} y_{i\ train}$

3.2.12 Linear regression model

The simple linear regression model to express the dependence of the expected response μ_i on the predictor x_i can be written as

$$Y = \beta_0 + \beta_i x_i$$

where β_0 is called the constant or intercept, and represents the expected response when $x_i=0$; β_i is called the slope, and represents the expected increment in the response per unit change in x_i .

In this case, the sklearn. linear regression model developed for Python is used.

The programming code used for linear regression calculates by default the intercept and obviously, the coefficients of the model, by fitting the model on the base of true training data x_{train} and target value y_{train} arrays, without any normalization. Once the model is fitted, we can obtain the predicted values array y_{plot} on the base of the linear regression model. A regression model example representing heating dataset (regreH1) is shown below.

Train the regrH1 model using the training sets

```
regrH1= linear_model.LinearRegression()
```

```
regrH1.fit(x_trainH, y_trainH)
```

```
y_plotH1reg = regrH1.predict(x_trainH)
```

In Figure 23 the linear regression model of training data, the x_{train} values vs the x_{plot} predicted value in the scatter plot for heating and cooling dataset are shown.

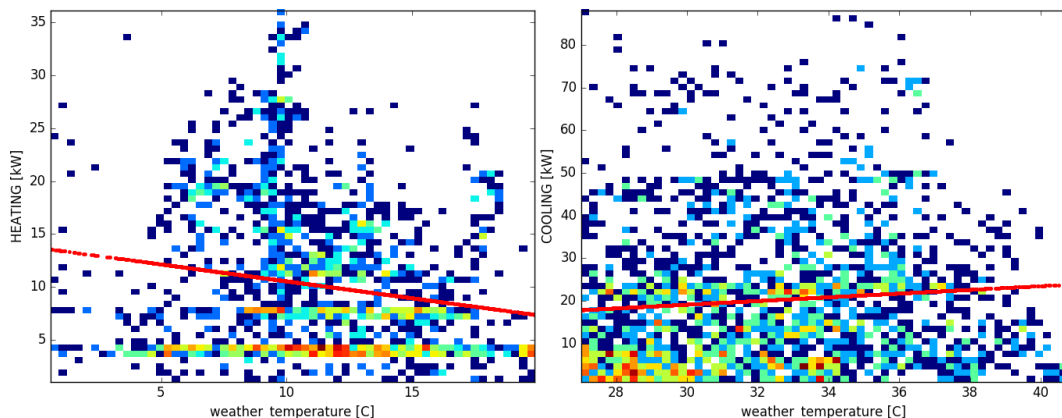


Figure 23: Linear regression model with scatter plot of training data.

As explained in the previous paragraph several metrics are calculated in order to quantify the accuracy of the model. As expected, the scores obtained from metrics in this case

are very low as you can see from Figure 23 **Σφάλμα! Το αρχείο προέλευσης της αναφοράς δεν βρέθηκε..**

3.2.13 Multiple regression model

In order to obtain a more accurate model, two different variables, are added in the x_train predictor, that in this case become a 3D-array with 3 columns: external temperature, *orari* and *deltaT* variables, (explained in the previous paragraph). This procedure is called multiple linear regression analysis and aims to establish a relationship between $y=y_train$ array, that is the energy consumption variable (dependent variable) and the $X=x_train(X_1, X_2, X_3)$ predictor in the form:

$$y = \beta_0 + \beta_1 X_1 + \beta_2 X_2 + \dots + \beta_n X_n + \varepsilon$$

where X_1 =external temperature, X_2 =*orari*, X_3 =*deltaT* and $\beta_0 \dots \beta_n$ are the regression coefficients to be estimated based on a record of observations and ε is the error. This is normally done by curve fitting based on the least square method with the aim of minimizing the difference between the observed and estimated values. The last term in the equation (ε) is referred to as the residual (or fitted error) and is used for testing of the significance of each regression coefficient.

3.2.14 Two variables linear regression

As previously described, the linear regression model calculates by default the intercept and obviously, the coefficients of the model, by fitting the model on the base of true training data x_train , that in this case is a 2D-array – composed by *external temperature* and *orari* variables - and target value y_train arrays, without any normalization. Once the model is fitted, we can obtain the predicted values array y_plot on the base of the linear regression model in the form

$$y_{pred} = y_{plot} = \beta_0 + \beta_1 X_1 + \beta_2 X_2$$

where X_1 =external temperature, X_2 = *orari* and $\beta_0 \dots \beta_2$ are the regression coefficients to be estimated based on a record of observations.

In Figure 24 the linear regression model is presented. In this case, we plot external temperature variable, vs the x_plot predicted value in the scatter plot of training data both for heating and cooling dataset.

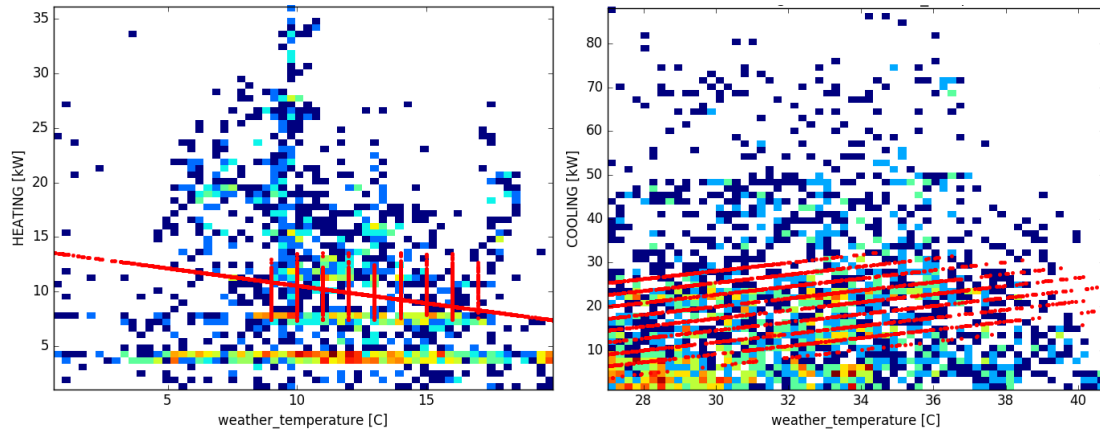


Figure 24: Two variables linear regression model with scatter plot of training data.

3.2.15 Three variables linear regression

Three variables linear regression model calculates the intercept and the coefficients of the model, by fitting the model on the base of 3D - arrays – composed by *external temperature*, *orari* and *deltaT* variables - and target value *y_train* arrays, without any normalization. Once the model is fitted, we can obtain the predicted values array *y_plot* on the base of the linear regression model in the form:

$$y_{plot} = \beta_0 + \beta_1 X_1 + \beta_2 X_2 + \beta_3 X_3$$

where X_1, X_2, X_3 are external temperature, *orari* and *deltaT* and $\beta_0 \dots \beta_3$ are the regression coefficients to be estimated based on a record of observations.

In Figure 25 the linear regression model is illustrated. Also in this case, we plot external temperature variable, vs the *x_plot* predicted value in the scatter plot of training data (*x_train* and *y_train*) both for heating and cooling dataset.

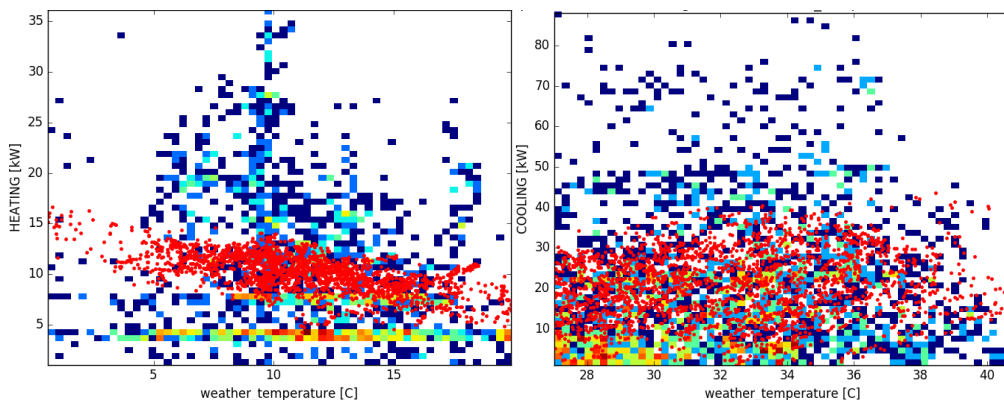


Figure 25: Three variables linear regression model with scatter plot of training data.

3.2.16 Ridge regression

Ridge regression, also known as Tikhonov regularization or, in machine learning, as weight decay, is related to the Levenberg–Marquardt algorithm for non-linear least-squares problems. This method has also built-in support for multi-variate regression, and this method solves a regression model where the loss function is the linear least squares function and regularization is given by the L2-norm regularization.

Usually, the equation with A matrix and b vector

$$Ax = b$$

is solved with the ordinary least squares linear regression. Ordinary least squares seek to minimize the sum of squared residuals, which can be written as

$$\|Ax - b\|^2$$

Ridge regression model is solved by including a regularization term in this minimization

$$\|Ax - b\|^2 + \|\Gamma x\|^2$$

where Γ is Tikhonov matrix [26]. In many cases, this matrix is chosen as a multiple of the identity matrix giving preference to solutions with smaller norms; this is known as L2 regularization. L2 loss function minimizes the sum of the square of the differences between the true value and the estimated values as

$$L2 = \sum_{i=1}^n (y_{i \text{ train}} - y_{i \text{ pred}})^2$$

where $y_{i \text{ train}}$ is the i true value and $y_{i \text{ pred}}$ the estimated i values.

The Ridge Regression procedure addresses some of the problems of Ordinary Least Squares by imposing a penalty on the size of coefficients. The ridge coefficients minimize a penalized residual sum of squares introducing α , a fixed positive constant that has to be tuned in order to obtain a good calibration of the penalty term.

α is a complexity parameter that controls the amount of shrinkage and so regularization strength. Regularization improves the conditioning of the problem and reduces the variance of the estimates. Larger values specify stronger regularization. When $\alpha=0$ a classical linear regression is obtained.

In order to validate α , a built-in cross-validation is used. RidgeCV sklearn command implements ridge regression with built-in cross-validation of the alpha parameter. Then α is obtained by creating a function that tests each value of α by fitting x_{train} , y_{train} and checking the score on the base of mean absolute error. Below an example is shown.

```
alphas = 10**np.linspace(10,-2,100)*0.5
```

```

ridge = Ridge(normalize=True)
coefs = []
for a in alphas:
    ridge.set_params(alpha=a)
    ridge.fit(x_train, y_train)
    coefs.append(ridge.coef_)
np.shape(coefs)
ridgecv=RidgeCV(alphas=alphas, scoring='mean_absolute_error', normalize=True)
ridgecv.fit(x_trainH, y_trainH)
ridgecv.alpha_

```

The α value obtained is equal to 0.005.

3.2.17 Single variable linear regression

In this case, the sklearn. polynomial features and ridge regression estimator developed for Python are used in order to consider a second-degree model. Since, a second-degree model is used, the regression model to express the dependence of the expected response on the predictor can be written as

$$Y_{pred} = \beta_0 + \beta_1 x^2 + \beta_2 x$$

where $Y_{pred}=y_{plot}$ is the predicted value and $x=x_{train}$ is the external temperature variable.

As previously described, α is equal to 0.005 and an automatic solver is used based on the type of data. This automatic solver can select among Singular Value Decomposition of X to compute the Ridge coefficients, 'standard scipy.linalg.solve' function to obtain a closed-form solution, 'sparse_cg' using the conjugate gradient solver as found in scipy.sparse.linalg.cg, regularized least-squares routine and 'sag' using a Stochastic Average Gradient descent.

Also in this case it is possible to extract the intercept and obviously, the coefficients of the second-degree model, by fitting the model on the base of true training data x_{train} and target value y_{train} arrays, without any normalization. Once the model is fitted, we can obtain the predicted values array y_{plot} on the base of ridge regression model. A regression model example is shown below.

Train the model using the training sets

```

modelH1 = make_pipeline(PolynomialFeatures(degree), Ridge(alpha=0.005, copy_X=True,
fit_intercept=True, max_iter=None, normalize=False, random_state=None, solver='auto', tol=0.001))
modelH1.fit(x_trainH, y_trainH)
y_plotH1 = modelH1.predict(x_trainH)

```

In Figure 26 the non-linear regression model, that is the x_{train} values vs the x_{plot} predicted value in the scatter plot of training data is shown (x_{train} and y_{train}) both for heating and cooling dataset.

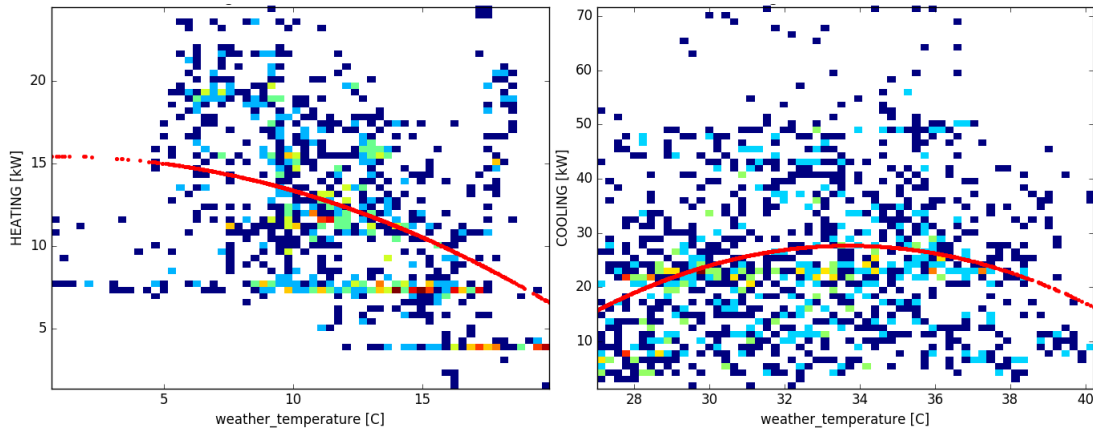


Figure 26: Ridge second order degree regression model with scatter plot of training data.

In this case, the same metrics previously described are calculated in order to quantify the accuracy of the model.

3.2.18 Two variables linear regression

By adding orari variable, x_{train} becomes a 2D-array composed by external temperature array and orari array. The regression model to express the dependence of the expected response on the predictor can be written as

$$Y_{pred} = \beta_0 + \beta_1x^2 + \beta_2y^2 + \beta_3xy + \beta_4x + \beta_5y$$

where $Y_{pred}=y_{plot}$ is the predicted value, predictor x is external temperature and predictor y is orari variable, and $\beta_0 \dots \beta_5$ are the regression coefficients to be estimated based on a record of observations.

Figure 27 shows the scatter plot of non-linear regression model obtained by fitting two variables, both for heating and cooling dataset and considering weather temperature in the x-axis.

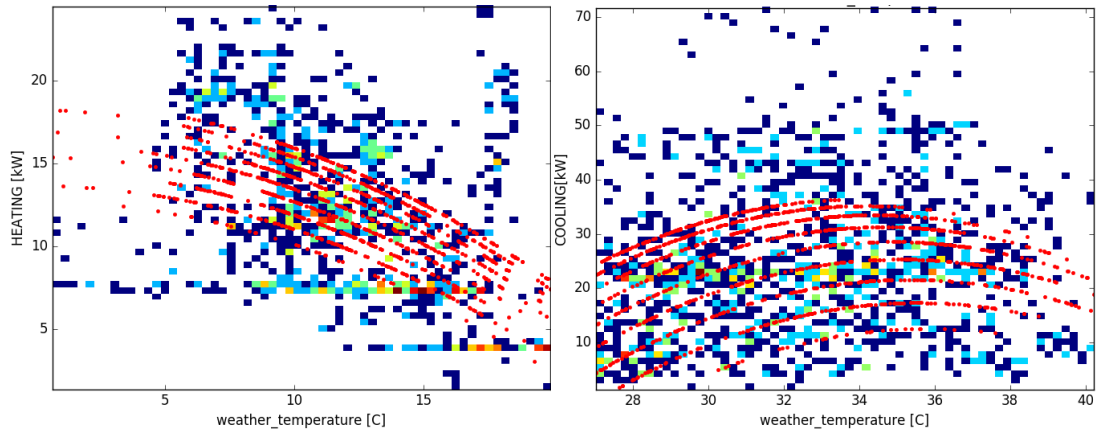


Figure 27: Ridge second order degree regression model with scatter plot of training data.

3.2.19 Three variables linear regression

Finally, also in this case, by adding deltaT variable, x_{train} becomes a 3D-array composed by external temperature array, orari and deltaT arrays. The regression model to express the dependence of the expected response on the predictor is

$$Y_{pred} = \beta_0 + \beta_1 x^2 + \beta_2 y^2 + \beta_3 z^2 + \beta_4 xy + \beta_5 yz + \beta_6 zx + \beta_7 x + \beta_8 y + \beta_9 z$$

where $Y_{pred} = y_{plot}$ is the predicted value, predictor x is external temperature and predictor y is orari variable, z deltaT variable and $\beta_0 \dots \beta_9$ are the regression coefficients to be estimated based on a record of observations.

Figure 28 shown the scatter plot of non-linear regression model obtained by fitting three variables both for heating and cooling dataset considering ambient temperature in the x-axis.

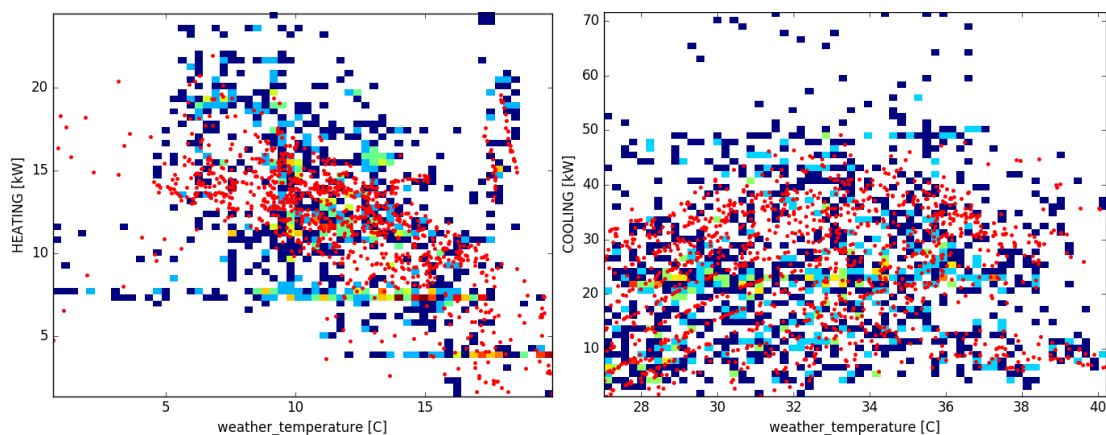


Figure 28: Ridge second order degree regression model with scatter plot of training data.

3.2 The Geosolar integration at TUC

The study has been focused on the building K2 and surroundings of the Environmental Engineering Department in the Campus of the Technical University of Crete.



Figure 29: Technical University of Crete Campus

The building has rectangular shape as can be seen in Figure 29, made of two symmetric parts or wings, with 2,032.21 m² and 1,135.43 m² of conditioned and non-conditioned area, respectively. The building is composed of a ground floor, 2 upper floors and a roof, where the solar collectors will be placed.

The thermal comfort is provided by an HVAC system (Heating Ventilation and Air Conditioning) that supplies heated or cooled air to the conditioned rooms when needed. The heat pump of the system is a Hitachi Air Conditioner Model RAS-20FSG, as can be seen in Figure 30. The model has a maximum input of 35.5 kW, an input power for the compressor of 23.6kW and 22.7 kW, and for the fan of 1.39 kW-1.61 kW for heating and cooling operations respectively.



Figure 30: HVAC system and its operating parameters.

3.3.1 Energy consumption

The Combined Geothermal and Solar Thermal System is designed to produce heating and cooling, in order to meet the energy needs of the building K2 in TUC. For that, it is necessary to know the energy consumption of the building for covering the demand and ensuring thermal comfort.

The Department of Environmental Engineering in TUC developed, using OpenStudio software, a model for K1 building, with similar characteristics to those of the one being studied (K2). This model is based on the features and parameters of the real building and is able to simulate its behaviour and needs along the year with reliable values. In this way, and as the two buildings share analogous dimensions, distribution, components and activities building K2 is assumed to have the same energy consumption as the one provided by the K1 building model simulations.

3.3.2 Heat consumption

The model presents the heat consumption in every thermal zone of the building throughout the year. The building model is divided in 30 thermal zones with different consumptions, from which the simulations give values in intervals of 1 hour, from the 1st of January until the 31st of December, forming a total of 8,760 values per thermal zone. In Table part of the Heat Consumption data from the K1 building model simulation is shown. Consumption is zero in cells denoted with (-). The simulation presents the data in Joules, which is then converted to kWh for further processing.

Hourly	THERMAL ZONE 1: Zone Air System Sensible Heating Energy	THERMAL ZONE 2: Zone Air System Sensible Heating Energy	THERMAL ZONE 3: Zone Air System Sensible Heating Energy	THERMAL ZONE 4: Zone Air System Sensible Heating Energy	THERMAL ZONE 5: Zone Air System Sensible Heating Energy	THERMAL ZONE 6: Zone Air System Sensible Heating Energy
2009-Jan-01 01:00:00	-	-	-	400,544.85	145,130.97	36,643.93
2009-Jan-01 02:00:00	-	-	-	476,046.47	181,391.44	118,263.71
2009-Jan-01 03:00:00	-	-	-	486,751.77	181,440.51	121,128.26
2009-Jan-01 04:00:00	-	-	-	459,399.68	162,486.06	91,321.92
2009-Jan-01 05:00:00	-	-	-	426,728.52	141,333.11	59,396.05
2009-Jan-01 06:00:00	-	-	-	397,036.44	121,833.69	31,107.83
2009-Jan-01 07:00:00	-	-	-	370,598.46	103,961.50	6,751.75
2009-Jan-01 08:00:00	-	-	-	344,170.22	86,324.43	-
2009-Jan-01 09:00:00	203,520.46	21,284.11	26,598.67	583,913.82	208,125.22	209,923.72
2009-Jan-01 10:00:00	120,592.10	151,804.12	-	725,242.64	284,505.88	357,513.01
2009-Jan-01 11:00:00	372,746.44	777,658.89	52,278.18	1,237,008.95	547,521.33	797,120.66
2009-Jan-01 12:00:00	697,541.43	1,232,685.82	321,186.65	1,624,858.47	755,681.80	1,118,636.03
2009-Jan-01 13:00:00	624,424.82	1,241,174.12	245,151.92	1,624,322.76	765,904.64	1,125,223.86
2009-Jan-01 14:00:00	626,804.53	1,277,365.04	237,397.63	1,663,232.04	795,062.01	1,163,339.67
2009-Jan-01 15:00:00	531,525.03	1,444,358.64	114,881.76	1,815,482.42	885,977.48	1,304,425.22
2009-Jan-01 16:00:00	645,780.16	1,660,654.87	199,270.89	2,013,825.64	1,005,998.19	1,481,233.33
2009-Jan-01 17:00:00	532,493.41	1,437,520.75	90,889.08	1,870,978.88	945,463.78	1,360,854.23
2009-Jan-01 18:00:00	364,584.34	1,091,576.77	10,088.45	1,617,863.29	819,544.19	1,145,252.30
2009-Jan-01 19:00:00	199,756.41	740,290.99	-	1,345,078.02	676,615.45	907,096.37
2009-Jan-01 20:00:00	75,787.68	427,514.79	-	1,103,842.93	545,343.86	691,835.57
2009-Jan-01 21:00:00	11,610.43	171,127.12	-	913,258.27	437,831.64	519,635.99
2009-Jan-01 22:00:00	-	20,063.13	-	766,962.51	353,195.25	384,348.23
2009-Jan-01 23:00:00	-	-	-	647,505.03	282,622.86	262,682.75
2009-Jan-02 00:00:00	-	-	-	535,682.17	218,364.56	144,386.45

Table 10: Heat consumption data.

Summing up all the values from each thermal zone, the total heat consumption per area is obtained. To know the peak power of the system, the highest value of the consumption for the whole year is checked, as shown in [Table](#) .

Hourly	THERMAL ZONE 12: Zone Air System Sensible Heating Energy	THERMAL ZONE 13: Zone Air System Sensible Heating Energy	THERMAL ZONE 14: Zone Air System Sensible Heating Energy	THERMAL ZONE 15: Zone Air System Sensible Heating Energy	THERMAL ZONE 16: Zone Air System Sensible Heating Energy	THERMAL ZONE 17: Zone Air System Sensible Heating Energy
TOTAL (J)	5,165,793,714.14	192,267,086,856.18	2,732,441,655.95	663,742,247.30	15,722,413,646.22	733,516,783.79
Average Power (J)	589,702.48	21,948,297.59	311,922.56	75,769.66	1,794,796.08	83,734.79
Peak Power (J)	11,990,531.46	185,336,857.63	43,654,723.35	15,672,164.46	103,091,769.15	12,280,135.46
TOTAL (kWh)	1,434.94	53,407.52	759.01	184.37	4,367.34	203.75
Average Power (kW)	0.16	6.10	0.09	0.02	0.50	0.02
Peak Power (kW)	3.33	51.48	12.13	4.35	28.64	3.41

Table 11: Total heat consumption per thermal zone.

Finally, the total heat consumption of the building is obtained summing up the total consumption in every thermal zone. For the system peak power, the highest value from summing up all the thermal zones is taken as a reference [Table](#) .

Total heat consumption	Average power	Peak power
549,655,792,622 J	2,091,536 J	185,336,858 J
82,301.97 kWh	0.58 kWh	51.48 kW

Table 12: Total heat consumption and peak power of the building.

Figure 31 presents the heat consumption along the year, having the greatest consumption in the month of January with 17,104.96 kWh, the lowest in October with 9,610.22 kWh, and no consumption from May to September, included.

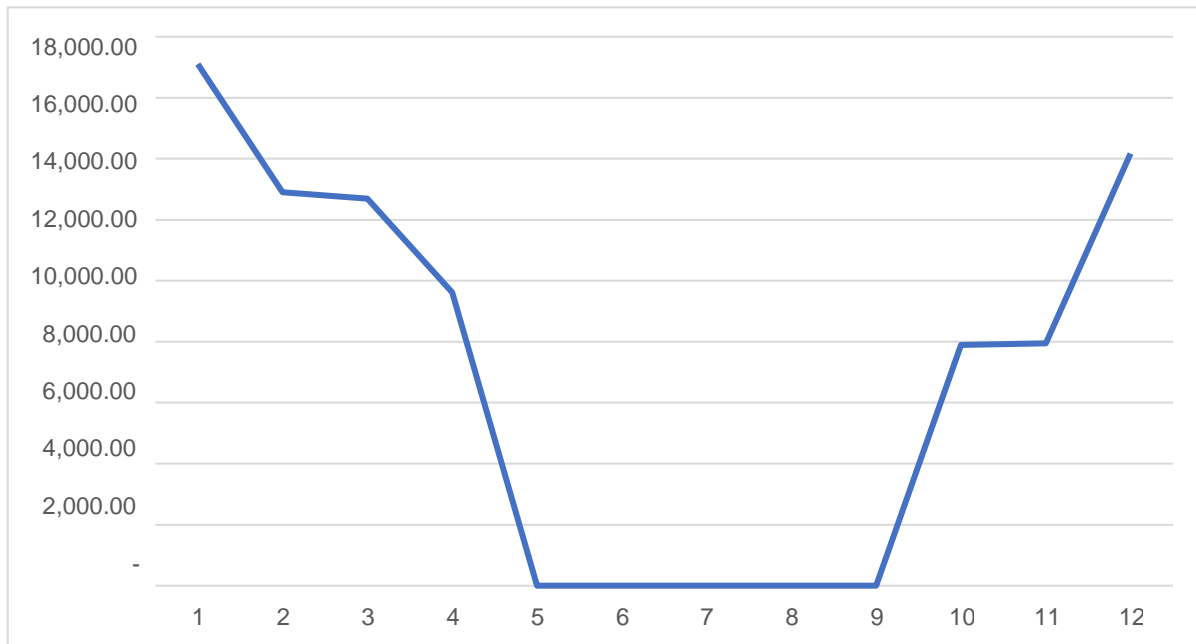


Figure 31: Heat consumption along the year.

3.3.3 Cooling consumption

The cooling consumption has been taken from the academic paper “*Development of a web based energy management system for University Campuses: The CAMP-IT platform*” based on both K1 and K2 buildings of Technical University of Crete. The peak power has been taken from the OpenStudio model.

Months	Cooling Degree days (2014)	Cooling Degree days (2015)	Energy Consumption per Cooling Degree Day (2014)	Energy Consumption per Cooling Degree Day (2015)	Total energy consumption for cooling (2014)	Total energy consumption for cooling (2015)
Units	DD	DD	kWh	kWh	kWh	kWh
May	84	85	205.4	204.7	17,253.60	17,399.50
June	188	173	120.9	122.8	22,729.20	21,244.40
July	257	252	131.3	127.9	33,744.10	32,230.80
August	288	282	77.4	66.5	22,291.20	18,753.00
September	193	205	161.3	120.1	31,130.90	24,620.50
October	71	91	272.6	190.3	19,354.60	17,317.30
TOTAL					146,503.60	131,565.50

Table 13: Cooling consumption calculation.

Months	Total energy consumption for cooling (2014)	Total energy consumption for cooling (2015)	Average 2014-2015	Peak power
Units	kWh	kWh	kWh	kWh
May	17,253.60	17,399.50	17,326.55	226
June	22,729.20	21,244.40	21,986.80	
July	33,744.10	32,230.80	32,987.45	
August	22,291.20	18,753.00	20,522.10	
September	31,130.90	24,620.50	27,875.70	
October	19,354.60	17,317.30	18,335.95	
TOTAL	146,503.60	131,565.50	139,034.55	

Table 14: Average and peak cooling consumption.

The deployed value for consumption is the average between the cooling energy consumption in 2014 and 2015. Figure 32 presents the cooling consumption along the year, starting in May, having the greatest consumption in the month of July with about 33,000 kWh, ending in October, with and no consumption from November to April, included.

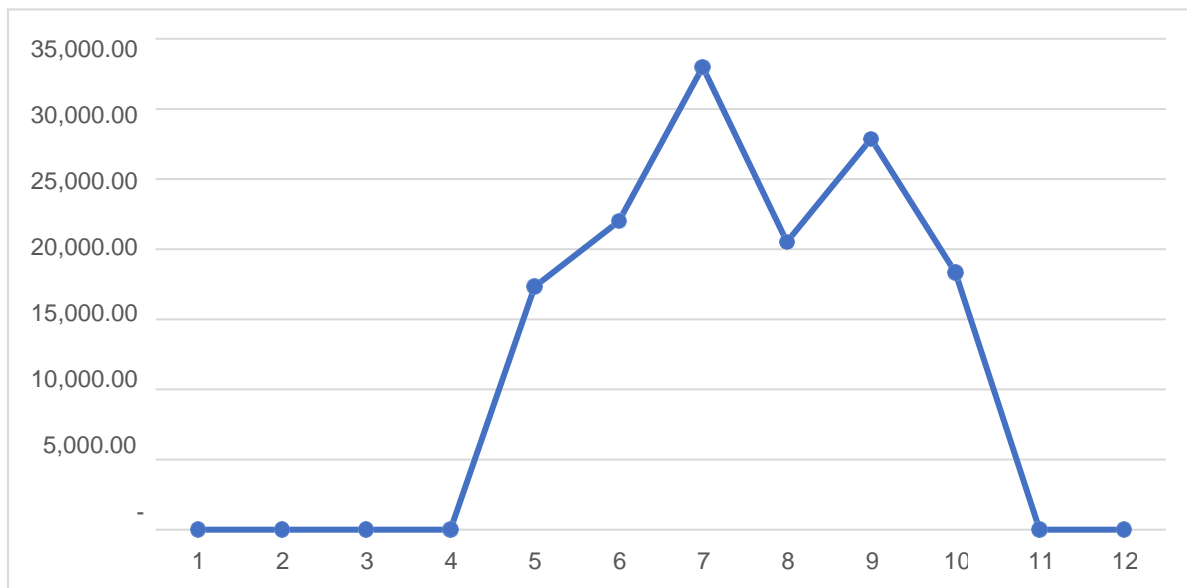


Figure 32: Cooling consumption along the year.

4. Research activities in the Smart GEMS Project

4.1 Neural Network toolbox integration through a DLL

The possibility to use an energy consumption model in batch by integrating it in a data acquisition system is a very important aspect in data analysis. Integration refers to bringing together the component sub-systems (like software application) into one system and ensuring that the subsystems work together as a system. In this work, the overall idea is to integrate the algorithm related to energy consumption forecasting into the Energy Management System (EMS) in order to control the consumption of Smart Grid buildings. Then, the activities started from the study of 24h load forecasting of a micro-grid using artificial neural networks conducted by TUC in Loccioni. The purpose was the integration of the thermal storage with the micro-grid and in particular the availability of excess production in the micro-grid during weekends, so as to schedule the charging of the thermal storage using this excess production: In order to obtain this, the mentioned work has been focussed to predict the day ahead excess production of the micro-grid so as to apply appropriate controls for its utilisation. Thermal storage is connected to the Leaf Lab and the automation system for its charge and discharge was set considering this building. Currently, the automation system is set to charge the thermal storage during weekends, when there is excess production from Leaf Lab's PV. This kind of automation will charge the storage while energy is not needed from Leaf Lab, but it could be needed from the micro grid. Consequently, there is a requirement to change the settings so that the thermal storage will be charged when there is real excess production at micro-grid level.

Consequently, this work is focussed on the integration and testing of a part of the algorithm that is necessary to predict excess production of the micro-grid: the forecasting of Energy Consumption. In this way, it is possible to check if this methodology is robust and reliable to reach the final goal of the optimization of power distribution within the micro-grid through the application of appropriate controls.

To obtain this result, the integration of the neural network algorithm for Energy Consumption estimation is necessary to avoid the use of an external software application to generate an output, like in this case MATLAB. This is possible by creating the data analysis algorithm in MATLAB and through a Dynamic Link Library (DLL), export the algorithm with the same programming language used in Energy Management tool. DLL

is Microsoft's implementation of the shared library concept that contains code and data used by multiple programs at the same time.

In this way, it is possible to obtain the results of a trained network by knowing the internal data processing of the neural network and by programming a function in .NET that can read all this data (the training result) when a user introduces his input data (Figure 33) without calling MATLAB.

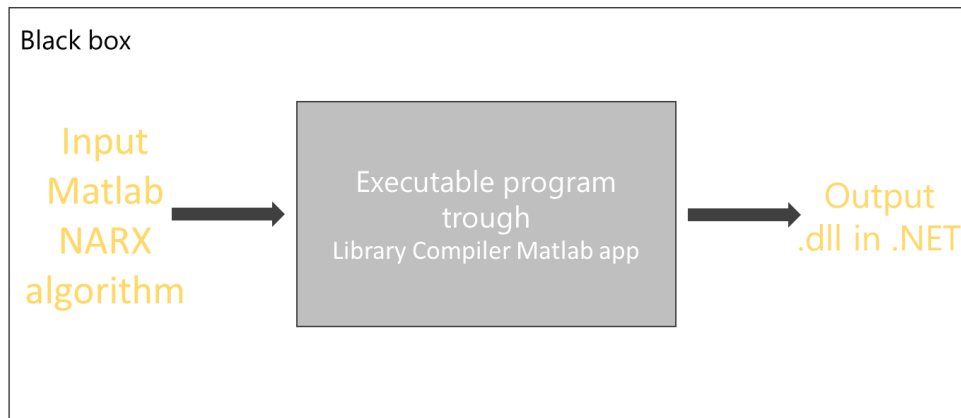


Figure 33: Black box overview

By building a black box, one has to decide the number of input and output variables. As previously explained, the objective of the algorithm is one day forecast of the Leaf Lab Energy Consumptions by considering as input the training variables related to past collected consumption data, the external temperatures, the network topology and the weights (in term of number of neurons and delays).

4.1.1 Neural Network toolbox and Nonlinear autoregressive neural network with external input

MATLAB Neural Network Toolbox provides algorithms, to create, train, visualize, and simulate deep neural networks. One can perform classification, regression, clustering, dimensionality reduction, time-series forecasting, and dynamic system modelling and control. In this case, as previously described, the goal is a time-series forecasting related to Energy consumption of Leaf Lab building trough NARX (Nonlinear autoregressive with external input) algorithm. The standard NARX network is a two-layer feedforward network, with a sigmoid transfer function in the hidden layer and a linear transfer function in the output layer. This network also uses selected delay lines to store previous values

of the $x(t)$ and $y(t)$ sequences. The output of the NARX network, $y(t)$, is fed back to the input of the network (through delays), and is a function of

$$y(t-1), y(t-2), \dots, y(t-d)$$

In fact, this network can learn to predict one-time series given past values of the same time series, the feedback input, and another time series, called the external or exogenous time series. The NARX model will provide better predictions than this input-output model, because it uses the additional information contained in the previous values of $y(t)$.

Neural Network tool, *ntstool* can be used to solve three different kinds of time series problems:

- to predict future values of a time series $y(t)$ from past values of different time series.
- to predict future values of a time series $y(t)$ only from past values of that series.
- to predict values of $y(t)$ from previous values of $x(t)$, but without knowledge of previous values of $y(t)$.

In the first type of time series problem, one would like to predict future values of a time series $y(t)$ from past values of that time series and past values of a second-time series $x(t)$. This form of prediction is called nonlinear autoregressive with exogenous (external) input, or NARX, and can be written as

$$y(t) = f(y(t-1), \dots, y(t-d), x(t-1), \dots, x(t-d))$$

In the second type of time series problem, there is only one series involved. The future values of a time series $y(t)$ are predicted only from past values of that series. This form of prediction is called nonlinear autoregressive, or NAR, and can be written as

$$y(t) = f(y(t-1), \dots, y(t-d))$$

Also in third type, time - series problem, two series are involved, an input series $x(t)$ and an output/target series $y(t)$. In this case, it is possible to predict values of $y(t)$ from previous values of $x(t)$, but without knowledge of previous values of $y(t)$. This input/output model can be written as follows:

$$y(t) = f(x(t-1), \dots, x(t-d))$$

To define the time series problem for the toolbox, one has to:

- train a network to fit a time series data set, by using the neural network time series tool GUI called *nnstool*,
- arrange a set of time series input vectors as columns in a cell array,

- arrange another set of time series target vectors (the correct output vectors for each of the input vectors) into a second cell array.

4.1.2 Case study

As previously explained, the case study is the micro-grid of the Leaf Community, in Angeli di Rosora, Italy. In particular, the energy consumption of Leaf Lab building is forecasted by using energy consumption monitored data and external temperature collected during 2016.

TARGET $y(t)$	INPUT $x(t)$
Energy consumption [kW]	External Temperature shifted of 1 day

Table 15: Input-target variables

Since true output (power consumption [kW] in 2016) and the other input are available (external temperature [$^{\circ}$ C] in 2016) during the training of the network, the nonlinear autoregressive with exogenous (external) input in which the true output is used instead of feeding back the estimated output, has been set up. This has two advantages. The first is that the input to the feedforward network is more accurate. The second is that the resulting network has a purely feedforward architecture, and therefore a more efficient algorithm can be used for training.

4.1.3 Case study

As already explained, this network has two inputs. One is an external input, and the other is a feedback connection from the network output (Figure 34).

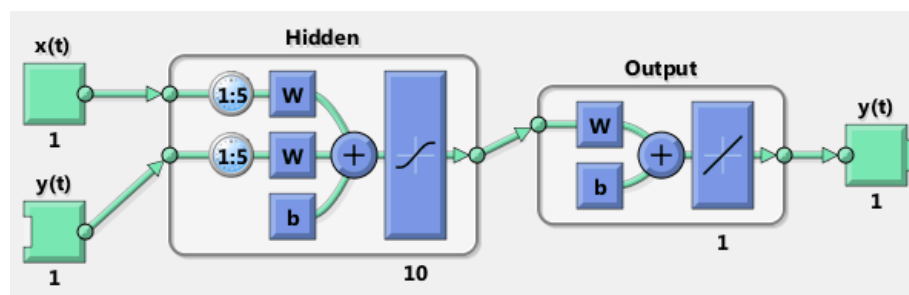


Figure 34: Net overview

For each of these inputs, there is a selected delay line to store previous values. To assign the network architecture for a NARX network, we select the delays associated with each

tapped delay line, and also the number of hidden layer neurons. The network architecture is described below.

```
inputDelays = 1:5;
feedbackDelays = 1:5;
hiddenLayerSize = 10;
net = narxnet(inputDelays,feedbackDelays,hiddenLayerSize);
```

These inputs become variables that can be adjusted if the network training performance is poor. By increasing the number of neurons and the number of delays obviously requires more computation, and this can overfit the data when the numbers are set too high, but it allows the network to solve more complicated problems.

4.1.4 Prepare the data for training

By training a network containing selected delay lines, it is necessary to fill the delays with initial values of the inputs and outputs of the network to keep the original time series data unchanged. The command *preparets* is used to facilitates this process. This function simplifies data preparation task by reformatting input and target time series and shifting input and target time series as many steps as are needed to fill the initial input and layer delay states. This function can reformat the data each time a network is transformed with *openloop*, *closeloop*, *removedelay* or *adddelay*, .

The function has three input arguments: the network, the input sequence and the target sequence and can be called as follows:

```
[Xs,Xi,Ai,Ts,EWs,shift] = preparets(net,Xnf,Tnf,Tf,EW)
```

where Table shows the input arguments.

net	Neural network
Xnf	Non-feedback inputs
Tnf	Non-feedback targets
Tf	Feedback targets
EW	Error weights (default = {1})
Xs	Shifted inputs
Xi	Initial input delay states
Ai	Initial layer delay states
Ts	Shifted targets
EWs	Shifted error weights

Table 16: input arguments

4.1.5 Set up Division of Data for Training, Validation, Testing

A particular attention has to be conducted in the way to split the dataset. In order to check the accuracy and reliability of the algorithm, the whole dataset has to be subdivided in three parts: training, validation and testing, that allows. In this application, the input vectors and target vectors will be randomly divided into three sets:

- 70% will be used for training. These are presented to the network during training and the network is adjusted according to its error.
- 15% will be used to measure network generalization and to stop training before overfitting.
- The last 15% will be used as a completely independent test of network generalization and provide a measure of network performance.

The lines commands are written as follows:

```
net.divideParam.trainRatio = 70/100;  
net.divideParam.valRatio = 15/100;  
net.divideParam.testRatio = 15/100;
```

The network uses the Levenberg-Marquardt algorithm for training. The Levenberg-Marquardt (LM) algorithm is an iterative technique that locates the minimum of a function, expressed as the sum of squares of nonlinear functions. It can be assumed as a combination of steepest descent and the Gauss-Newton method.

For problems in which Levenberg-Marquardt does not produce as accurate results as desired, we use the Bayesian Regularization.

Each time a neural network is trained, it can result in a different solution due to different initial weight and bias values and different divisions of data into training, validation, and test sets. Different neural networks trained on the same problem can give different outputs. For the same input, for these reasons, the initial conditions of Neural Network have been tried several times to ensure a good accuracy.

The following code calculates the network outputs, errors and overall performance. The lines commands are written as follows:

```
outputs = net(inputs,inputStates,layerStates);  
errors = gsubtract(targets,outputs);  
performance = perform(net,targets,outputs)
```

In order to improve the results obtained, several operations has been conducted:

- Increased the number of hidden neurons or the number of delays.

- Increased the number of training vectors.
- Tried a different training algorithm

4.2 Study of TUC experiences in NN prediction based systems

TUC has used neural network to predict the energy loads and the outside ambient air conditions, In order o do this as input parameters for the neural network predicting the energy load of the buildings, the exterior temperature, measured by a weather station close the building studied, the day of the week, time (hh:mm) and the energy demand, recorded every five minutes by smart meters were used.

In the same way, the exterior temperature, the total horizontal radiation, the relative humidity, the wind speed and direction and time of day (hh:mm) were used as inputs for the neural network that predicts the exterior temperature for the 24 h following a given moment; also in this case the weather data was collected from a weather station close to the studied buildings.

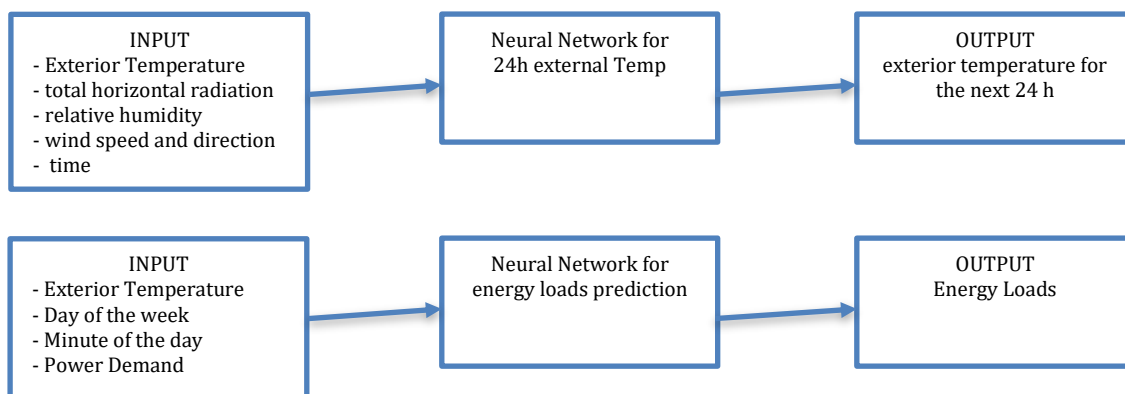


Figure 35: The TUC ANN prediction model.

The neural network used in both cases was an Elman neural network [2] with feed forward, below are the parameters used to configure the network in the Matlab environments:

- Number of Hidden Layers: 3
- Size of Hidden layers: 322
- Performance function/indicator: Run Mean Square Error (RMSE)
- Initial training dataset: 1,000
- Epochs: 3,000
- Number of maximum fails: 3,000
- Transfer function: Tangent sigmoid function

Modelling the environment temperature with neural network and predicting power demand gave good result (see Figure 36 and Figure 37).

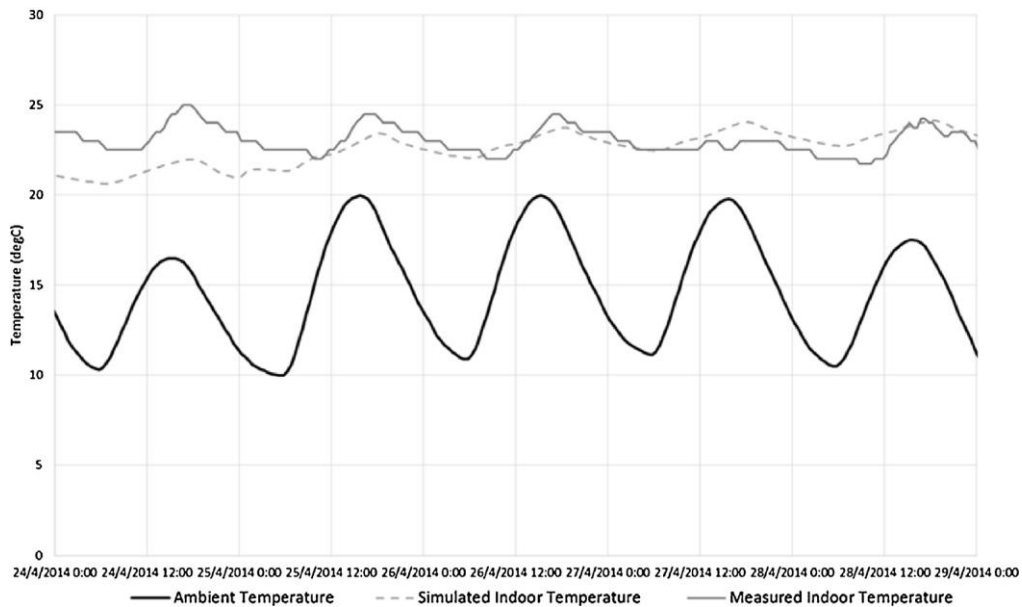


Figure 36: Validation of ESPr model of Indoor Temperature at the Circulation Areas of K2 Building

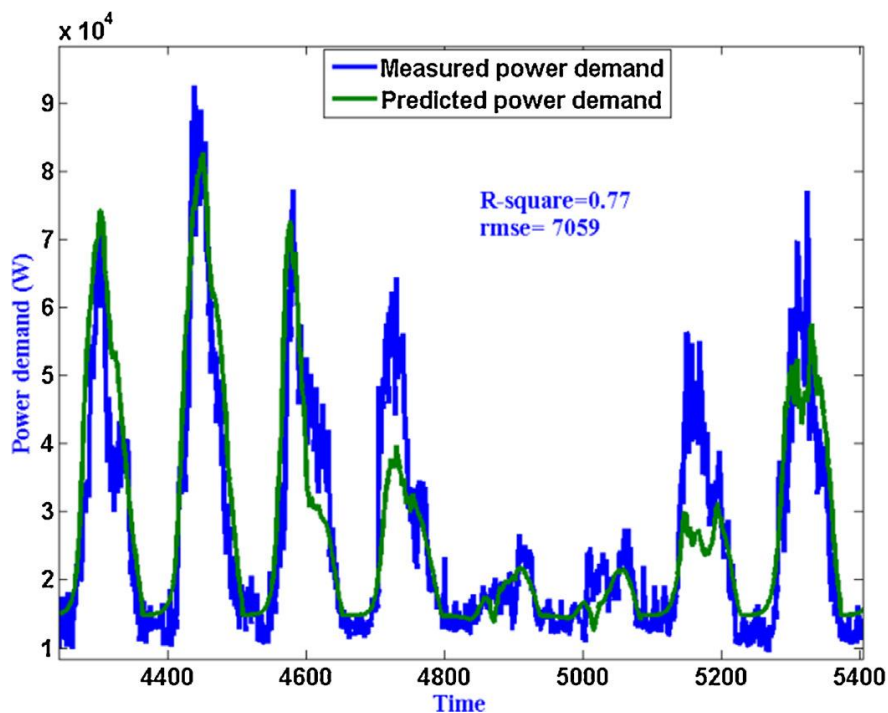


Figure 37: Measured and predicted power demand in the case study area

The prediction techniques developed by TUC have been considered for the prediction of the energy production of the LFR solar collector operating at the Idea premises.

A specific dataset has been prepared with this aim. The first activity was the adaptation of the query for the DBMS to get data every 5 minutes and not every 5 seconds, then the Date/Time field has been split in two different fields, the first one with the number of the

day and the second one with only HH:MM:SS at the end of the process the data we have obtained was:

- Day Number: the day of the week from 1 to 5 because the system normally is not working on Saturday and Sunday
- Time: hours:minutes:seconds
- Tin: Temperature of the oil at the beginning of the absorption pipe
- Tout: Temperature of the oil at the beginning of the absorption pipe
- Flow: Flow of the oil in m³/h
- DNI: Direct Normal Irradiation
- Tamb: Ambient Temperature
- Status: 0 if the system is not focalized, 1 if the system is focalized.
- Power: the power produced in kW.

At this point we used this dataset for training a neural network implemented in MatLab in order to verify the quality of the prediction: six training session have been launched, two for 8 hours prevision, two for 12 hours prevision and two for 24 hours prevision; for every couple a network with 10 neurons and 2 delays and a network with 30 neurons and 5 delays have been used.

Other configurations MatLab have been:

- NARX Network, Nonlinear Autoregressive with External (Exogenous) Inputs
- Input time series $x(t)$: all data less the power
- Target time series for the output $y(t)$: the power
- Validation and Test data: Training 70%, Validation 15%, Testing 15%
- Training Algorithm: Levenberg-Marquardt

The preliminary results should require a further improvement as they depend on the quality of the data given to the neural network, and, as a matter of fact, training data have been collected before the commissioning of a thermal energy storage which will stabilize the operability of the whole circuit. Presently the maximum working temperature is reached very fast and the collectors must be defocused many times during the day, resulting in many fluctuations of the energy generation process.

4.2.2.1 Custom architecture for remote sensing and data collecting hub

TUC have used some Schneider electronic devices for the measurement and collection of indoor air data. In particular sensors communicate the values to a collecting unit using ZigBee. A custom architecture has been conceived which would use the standard WiFi network for data exchange, compact microcontrolled sensing boards and a powerful ARM board running an OS Linux as data collector and manager.

For the main board the Beagle Bone green has been selected. It has a powerful processor, an on-board full linux distribution, a high number of reconfigurable GPIO, seven 12 Bit ADC, 8 pwm generator and a variety of connection interfaces (Ethernet, usb, I2C, Uart, etc.).

The main specs are reported below (hardware specs and the pinout of the board are available in Annex D-J).

- Processor: AM335x 1GHz ARM Cortex-A8
- RAM: 512MB DDR3
- on-board Flash Storage: 4GB eMMC
- CPU Supports: NEON floating-point & 3D graphics accelerator
- Micro USB Supports: powering & communications
- USB: Host 1
- Grove Connectors: 2 (One I2C and One UART)
- GPIO: 2 x 46 pin headers
- Ethernet: 1

The sensor board should be ready to be interfaced with different kind sensors and to communicate with standard Wi-Fi network. The selected module is based on ESP8266 chip, basically a TTL "Serial to Wireless Internet" device. ESP8266 is a system-on-a-chip (SoC) with 2.4 GHz Wi-Fi (802.11 b/g/n, supporting WPA/WPA2), general-purpose input/output (16 GPIO), Inter-Integrated Circuit (I²C), analogue to digital conversion (10-bit ADC), Serial Peripheral Interface (SPI), I²S interfaces with DMA (sharing pins with GPIO), UART (on dedicated pins, plus a transmit-only UART can be enabled on GPIO2), and pulse-width modulation (PWM). It employs a 32-bit RISC CPU based on the Tensilica Xtensa L106 running at 80 MHz (or overclocked to 160 MHz). It has a 64 KB boot ROM, 64 KB instruction RAM and 96 KB data RAM. External flash memory can be accessed through SPI.

(Specifications and images of the selected board can be found in Annex K)

4.2.3 Identification of programming languages

Neural Networks can be implemented through a large number of specific libraries and frameworks available in almost all developing languages [4]. Nevertheless, the most popular languages are C++ and Python and one of these is used for developing a custom implementation of machine learning procedures. C++ is a much harder language to deal with than Python, but it would be a plus to use C++ instead of a more “user-friendly” language because of its efficiency.

5. Main findings

5.1 Application at the Leaf micro-grid

The Leaf micro-grid is the micro-grid of the Leaf Community, in Angeli di Rosora, Italy, as represented in Figure 38.

The energy production sources connected to the grid are:

- a micro-hydropower plant, of 48kWp
- four rooftop PV installations of total 421.3kWp
- a dual axis Solar Tracker of 18kWp
- five buildings are currently connected to the micro-grid:
- the Leaf Lab, industrial building
- the AEA, office building
- the SUMMA, office building
- the Leaf Farm, office building
- the KITE, industrial building.



Figure 38: The LEAF micro-grid.

All buildings are equipped with ground water heat pumps (GWHP). A 224kWh electrical storage system and a thermal storage with heat capacity 523.25kWh/K are also part of the micro-grid.

All the previously mentioned power loads, renewables and storage components are connected in parallel to one single Point of Delivery (POD). All nodes as well as the collective operation of the micro-grid are monitored and controlled via My Leaf web based platform.

The rooftop PVs are installed on four of the five interconnected buildings of the micro-grid. The production by each rooftop PV installation is consumed by the respective building first. If there is residual production, it is fed to the micro-grid. The production of the micro-hydropower plant is also fed to the micro-grid. When the production is not enough to cover the micro-grid's loads, energy is withdrawn from the main grid. Energy is also given to the main utility grid if the demand of the micro-grid has been fulfilled, storages are fully charged and there is excess production. Regarding the storages, both have been recently connected to the grid and their operation and integration currently being tested.

The integration of the thermal storage with the micro-grid has been studied. Specifically, the availability of excess production in the micro-grid during weekends is of interest, so as to schedule the charging of the thermal storage using this excess production.

The thermal storage is connected to the Leaf Lab and the automation system for its charge and discharge has been set considering this building. Currently, the automation system is set to charge the thermal storage during weekends, when there is excess production from Leaf Lab's PV. This kind of automation will charge the storage when energy is not needed from Leaf Lab, but it could be needed from the micro grid. Consequently, there is a requirement to change the settings so that the thermal storage will be charged when there is real excess production at micro-grid level. To this end, excess production of the micro-grid during weekends needs to be predicted in a robust way so that charging of the thermal storage is controlled accordingly.

5.1.1 System description

Ground water heat pumps

There are three water to water heat pumps in Leaf Lab. GWHP1 is connected to the chilled beams installed in the offices for space heating and cooling. GWHP2 and GWHP3

are connected to four HVAC units that service the offices, the laboratory and the warehouse.

The heat pumps are connected to the storage as shown in Figure 39 GWHP2 and GWHP3 are used for charging the thermal storage. When the thermal storage is discharged, thermal energy is provided to the chilled beams, thus avoiding activation of GWHP1 during the first three days of the week.

Thermal storage

The TES is a water tank with dimensions 12.3 X 11 X 3.4 m (400m³). The water tank is buried and insulated with 16 cm of XPS. The heat stored is sensible heat intended to cover the thermal loads of Leaf Lab. The thermal storage is charged during weekends using the excess production of the Leaf Labs' rooftop PV installation. The excess production is used to operate GWHP2 and GWHP3

System settings

The charging process begins when there is an excess in Leaf Lab's PV power production over 60kW. This is the threshold for activation of GWHP3. After activation of GWHP3, if there is excess of 50kW, GWHP2 is activated.

The activation of the heat pumps for charging the thermal storage is allowed only during weekends, from 8:00am to 16:00pm in winter weekends and from 7:00am to 18:00pm in summer weekends. The pumps are switched off at the end of each schedule or if PV production is significantly reduced over a sustained period of time. In case PV power is instantly reduced power is withdrawn from the grid in order to keep the heat pumps, which provide heat to the thermal storage, activated. For the deactivation of the heat pumps if the power from the grid is greater than 130kW GWHP3 is switched off and following this GWHP2 is switched off when energy withdrawn from the utility grid exceeds 90kW.

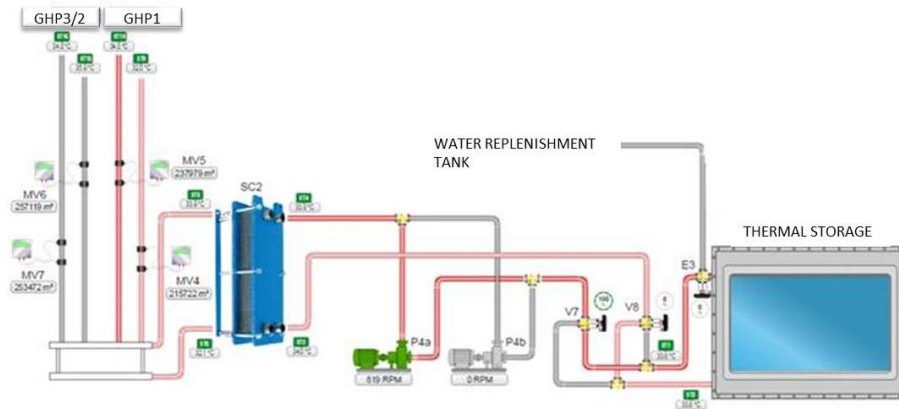


Figure 39: Thermal storage - GWHP connection.

5.1.2 Power production data

Power data as well as environmental data have been collected from the My Leaf platform. The power production of each energy source and the power taken from and exported to the main grid are being measured.

The total production of the micro-grid can be calculated as follows:

$$P_{MG} = P_{LLPV} + P_{AEAPV} + P_{SUMMAPV} + P_{KITEPV} + P_{TUV} + P_{HYDRO4}$$

Where:

P_{LLPV} is the power production of the Leaf Lab PV, in kW

P_{AEAPV} is the power production of the AEA PV, in kW

$P_{SUMMAPV}$ is the power production of the SUMMA PV, in kW

P_{KITEPV} is the power production of the KITE PV, in kW

P_{TUV} is the power production of the solar tracker, in kW

P_{HYDRO4} is the power production of the micro-hydro power plant, in kW

The production of the micro-grid is self-consumed and excess production is given to the main grid. Since there are measured data of the power exported to the grid, the power production self-consumed at any time in the micro-grid can be calculated as follows:

$$P_{SC} = P_{MG} - P_{OUT}$$

Where:

P_{SC} is the power production self-consumed, in kW

P_{OUT} is the amount of excess power production that is exported to the main-grid, in kW

5.1.3 Prediction using Neural Network

The collected data is used for prediction of excess power of the micro-grid. A good prediction of excess production has to be achieved. For this purpose the Matlab [14] Neural Network (NN) tool was utilised. Alternative combinations of input parameters were tested so as to investigate which set of input parameters were suitable for achieving an accurate prediction of excess production. Furthermore alternative training algorithms were tested and neural network structures in order to conclude which algorithm and structure could give the best prediction results.

5.1.4 NN model setup

The excess production of energy that can be used for charging the thermal storage can be determined from the measured data of power exported to the main grid. The prediction of excess production is a non-linear autoregressive problem. Past values of excess production as well as past values of day, time, irradiance, temperature and total production were used for prediction of excess power in 24h time horizon.

As already discussed, the excess production is related to parameters that determine production. For prediction of PV production, day of the week, time of day, temperature and radiation have been used as inputs. Prediction of hydro power production using as inputs the river water level and machine water level was attempted but a high accuracy prediction could not be achieved.

As a first step, day of the week, time of day and irradiance was used for prediction of excess production. Subsequently, a second prediction approach is tested using the first step's inputs plus ambient air temperature as input. A third prediction model is attempted using as input parameters the day of the week, the time of the day and total micro-grid production since excess production follows the trend of total production.

	Inputs	Target	Output
1 st prediction	day of week	excess	excess
	time of day	production	production
	irradiance	(P _{OUT})	(P _{OUT})
2 nd prediction	day of week	excess	excess
	time of day	production	production
	irradiance	(P _{OUT})	(P _{OUT})
	temperature		

3 rd	day of week	excess	excess
prediction	time of day	production	production
	micro-grid	(P _{OUT})	(P _{OUT})
	production		

Table 17: Input data for each prediction.

5.2 Test of the custom data collection platform

Algorithms applied by TUC are based on the work of Jeffrey L. Elman. Before starting the development of the machine learning platform, C++ sample code for implementing an Elman Neural Network has been prepared; the example code was successfully compiled and executed on a beagle bone green.

Accordingly with Elman: “in the implemented code input units and context units activate the hidden units; and then the hidden units feed forward to activate the output units. The hidden units also feed back to activate the context units. This constitutes the forward activation. Depending on the task, there may or may not be a learning phase in this time cycle. If so, the output is compared with a teacher input and backpropagation of error is used to incrementally adjust connection strengths. Recurrent connections are fixed at 1.0 and are not subject to adjustment. At the next time step $t+1$ the above sequence is repeated. This time the context units contain values which are exactly the hidden unit values at time t . These context units thus provide the network with memory.”

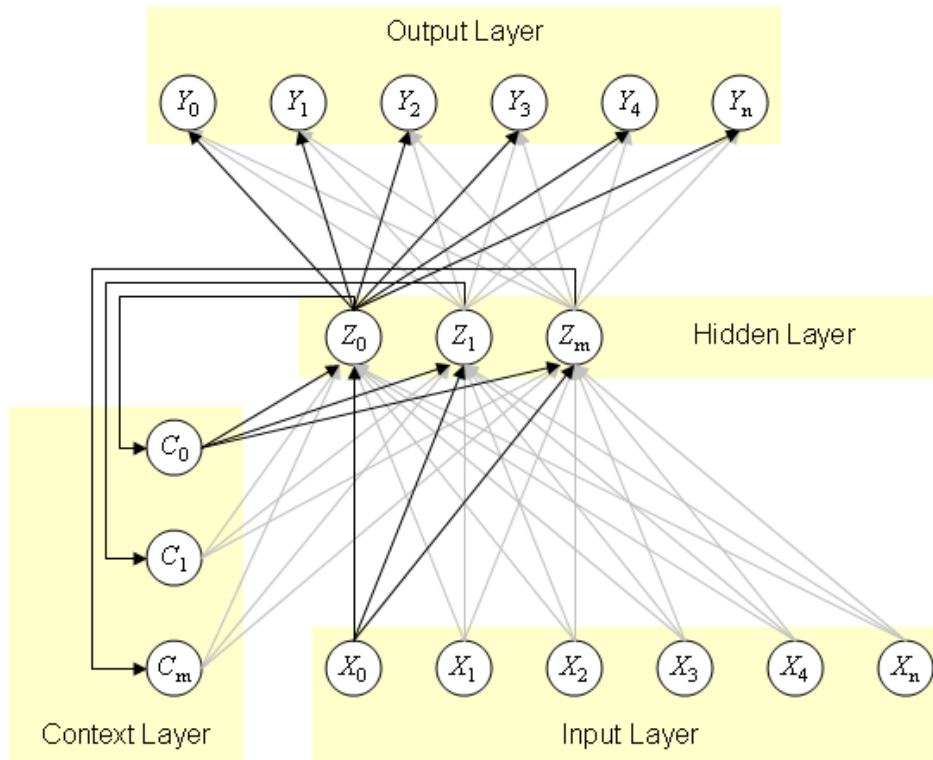


Figure 40: A common structure of an Elman network.

Elman intended the input and output units to represent individual letters, with could train the network to predict the next letter in a string of letters.

Based on this we used an example where the neural net architecture has six input, and six output units (for numbers 1 through 5, plus 0 for the terminal symbol). There are three hidden units, with three corresponding context units.

Training the net for a particular string involves several steps, the number depending on the length of the string. At the beginning of training, the activations of the context units are set to 0.5. The terminal symbol is first presented to the input units, and the net predicts the successor. The error (the difference between the predicted and the actual successor specified by the training string) is determined and back propagated, and the weights are adjusted. The context units receive a copy of the hidden unit's activations, and the next symbol in the training string (which was the target for the output units on the first step of training) is presented to the input units. Training continues in this manner until another instance of the terminal symbol (0) is reached.

The structure of the algorithm is the following:

For each training string, do steps 1 through 7.

Step 1: Set activations of the context units to 0.5.

Step 2: Do Steps 3 through 7 until second instance of terminal symbol.

- Step 3: Present input symbol.
- Step 4: Present successor to output units as target response.
- Step 5: Calculate predicted successor.
- Step 6: Determine error, backpropagate, and update weights.
- Step 7: Test for stopping condition:

If target = second instance of terminal symbol, then

Stop

Otherwise,

Copy hidden unit activations to context units and continue at Step 3.

After training, the net can be used to determine whether any given string of numbers is a valid sequence, according to the training string. As each symbol is presented, the net predicts the possible valid successors of that symbol. The output unit with the highest activation value indicates that the symbol it represents is a valid successor to the current input. Ideally, the net should be trained with enough iterations and just the right learning rate, resulting in a target activation of 0.3 or better, with the others falling well below.

To determine whether a string of numbers is valid, the symbols (numbers) are presented to the net sequentially, as long as the net predicts valid successors in the string. If the net fails to predict a successor, the string of numbers is rejected. If all successors are predicted, the string is accepted as valid.

The code is reported in as an Annex.

5.3 Preliminary design of the Geosolar system in TUC

The demand of heating and cooling needed to be supplied by the Combined System has been calculated. The next step is producing an initial system design to establish the different characteristics of this type of system based on the principles of the energy extraction, transportation and storage. The technology used is described along with the procedures followed to obtain the desired objectives.

5.3.1 Ground source heating and cooling

In the design of borehole heat exchangers, many factors come into play that carry different variants of a design for a system. So, the most suitable configuration must be found to address the specificities of the project, obtaining an optimum yield at the lowest possible cost.

5.3.2 Choice of geothermal system

The several shallow geothermal methods to transfer heat out of or into the ground are reported in **Table**:

Shallow geothermal methods	Depth (m)	Loops	Reason
Horizontal ground heat exchangers	1.2-2.0	Horizontal	The underground temperature is constant after 8 to 15 meters depth, so in this case, the system would be affected by the temperature seasonal variations
Borehole heat exchangers	10-250	Vertical	It is the method chosen for the heating and cooling extraction of the terrain, as is the most suitable design for both storage and extraction
Energy piles	5-45	Vertical	Designed for a heating plant, so there are no foundations to put the energy pipes
Ground water wells	4-50	Vertical	The idea is use the geothermal boreholes as thermal storage, so if the aquifers of the zone are used, the heat stored would be lost
Water from mines and tunnels	10-300	Vertical	There are no mines/tunnels nearby for the extraction of the heating from the ground

Table 18: Shallow geothermal methods

Generally, horizontal systems are used for low temperature heating installations when large surfaces are available. Vertical systems, however, are used when large areas of land are not available, the heat demand is higher, for better efficiency or heat storage. The chosen shallow geothermal method is the Vertical Borehole Heat Exchanger, since is the most suitable for the specific case being studied. The desired depth range will be between 5 and 15 meters, trying to avoid the effect of the seasonal temperature variations but not exceeding a reasonable depth, in order to prevent high drilling costs.

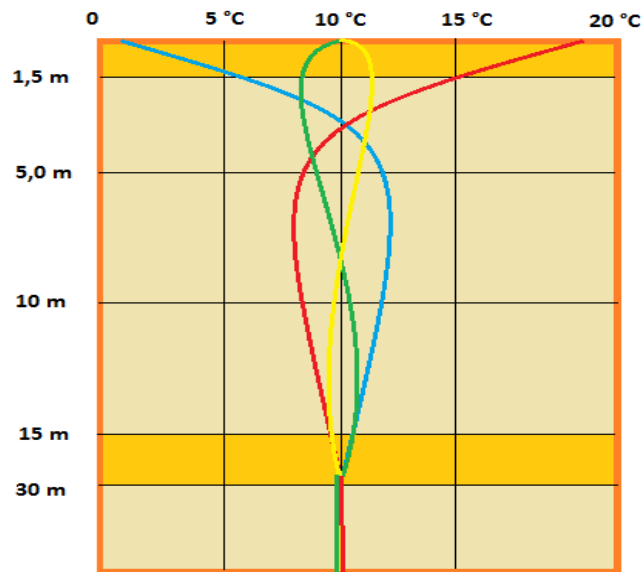


Figure 41: Seasonal ground temperature fluctuation in relation to depth.

Figure 41 presents an example of the ground temperature fluctuation in relation to depth, due to different seasonal climates along the year. As can be seen in red the ground temperature in summer is represented. From one side, the shallow layers of terrain are heated by the warm temperatures of this season, but on the other side, the inner layers are colder due to the low conductivity of the soil, as well as, the distance between the heating source and the strata blocking the absorption or extraction of thermal energy. Similar effects take place in other seasons, with the respective temperatures during those periods. Another parameter to consider is the choice of the fluid path (serial or parallel), based on the advantages and disadvantages of both options.

	Advantages	Disadvantages
System in series	Higher thermal operation per meter of pipe since it requires a larger diameter	A larger diameter pipe is needed, which means an increase in the amount of fluid
	Easier purge	The length is limited due to the pressure drop of the fluid
	Fluid path defined	
System in parallel	Less costs of installation, since the diameters are smaller	Purging operation more complicated
	Less amount of fluid used	Balance of fluid in the various complicated loops

Table 19: Fluid path configuration

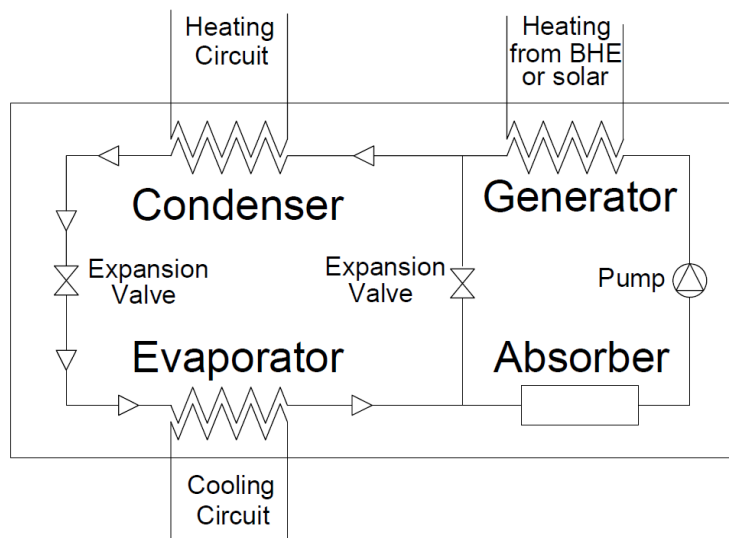
Considering **Table** for the supply of heating and cooling in the building a parallel system is proposed, as even if this configuration it does not give as high thermal operation per meter, the cost of installation is much lower, since the diameters of the pipes are smaller. Moreover, the amount of fluid is less, so it is possible to further reduce costs. Even if the purging operations could be more complicated, the maintenance is minimum.

5.3.3 Ground source heat pump principle

To extract thermal energy from the ground, Borehole Heat Exchangers (BHE) is proposed. This kind of system will be closed loop, which means the cold/warm water goes along the length of the pipe until the bottom, and goes up again being heated/cooled by the ground temperatures. The pipe system will extend from the mentioned ground to the Absorption Heat Pump (AHP), and returned to the ground forming a closed loop without exchange of water.

The water will be the same but its temperature will vary along the circuit, being heated up below the terrain and cooled down in the heat pump, or the opposite. As the final element supplying the energy is the Air Conditioning system, it will be defined as Water-to-Air Heat Pump. The diagram shown in **Figure 42** presents the closed loop system of the absorption heat pump combined with the borehole heat exchanger, the heating and cooling circuits.

Figure 42: Absorption Heat Pump



The hot water from the Solar Collectors and/or the Boreholes heats the fluid/refrigerant solution in the Generator via heat exchanger, increasing the temperature and pressure. The strong refrigerant vapour travels to the condenser meanwhile the weak solution is recirculated to the Absorber. The high temperature and pressure refrigerant transfers the heat to the heating system in the Condenser, making the vapour become liquid. The high-

pressure refrigerant flows through the expansion valve, where the pressure decreases. Because of that, the refrigerant has now a reduced boiling point, and the liquid changes phase again to vapour. Then, the vapour reaches the Evaporator, where ambient air is drawn by a fan through the low temperature vapour refrigerant, exchanging heat and leaving cooled air for cooling purposes. The now heated, low pressure vapour passes on to the Absorber. In the Absorber, the weak refrigerant solution recombines with the heated vapour, changing its state into a liquid. These releases further heat to the heating system. The now recombined solution is pumped back to the Generator where the process starts again. A second expansion valve controls the flow of weak refrigerant between the Generator and the Absorber.

5.3.4 Solar Thermal Collectors

The solar thermal collectors are a type of heat exchangers that absorb the incoming solar radiation, convert it into heat, and transfer this heat to a fluid (usually air, water, or oil) flowing through the collector. The solar energy collected is carried from the circulating fluid to the final destination of consumption or to the thermal energy storage tank from which can be drawn for use at night and/or cloudy days.

There are basically two types of solar collectors: non-concentrating or stationary and concentrating. A non-concentrating collector has the same area for intercepting and for absorbing solar radiation, whereas a sun-tracking concentrating solar collector usually has concave reflecting surfaces to intercept and focus the sun's beam radiation to smaller receiving area, thereby increasing the radiation flux.

The main difference between concentrating and non-concentrating solar collectors is that the first ones track the sun in its trajectory across the sky and the second ones are permanently fixed in position. The concentrating collectors need electricity to run their tracking devices and they are also more expensive. For these reason, the non-concentrating solar collectors are chosen. Inside this category there are three different types of collectors: Flat plate collectors (FPC), Stationary compound parabolic collectors and Evacuated tube collectors (ETC).

- The FPC consist of a dark flat-plate absorber, a transparent cover that reduces heat losses, a heat- transport fluid (air, antifreeze or water) to remove heat from the absorber, and a heat insulating backing.
- The CPC have the capability of reflecting to the absorber all of the incident radiation within wide limits. The necessity of moving the concentrator to

accommodate the changing solar orientation can be reduced by using a trough with two sections of a parabola facing each other.

- The ETC are composed of multiple evacuated glass tubes each containing an absorber plate fused to a heat pipe. The heat is transferred to the transfer fluid and then to the heating system.

Flat-plate collectors usually lose more heat than evacuated tubes and if they are compared on the basis of absorber plate area, the last ones are more efficient per square meter than equivalent flat plate systems.

However, the evacuated tube collectors are more expensive and normally used for irregular roofs and/or when the roof area is limited, as they require less overall space. Moreover, they work with higher temperatures in the system, which is not good for long periods of low hot water use. They are also perceived as more fragile.

In the cases with flat roof and enough space for placing several solar collectors, as it is the case of K2 building, some low cost flat plate collectors can be more cost-efficient than evacuated tube collectors. For that reason, the proposed solar collector type will be flat-plate, as they cost less and considered to be more efficient in this particular application. The collector used in terms of its technical characteristics is the ARCON Solar Collector type HT- HEATstore 35/10. The parameters of the chosen Thermal Solar Collector are detailed in the data sheet (Annex B).

5.3.5 Solar thermal energy

To calculate the energy that the collector can provide, its efficiency factors, as well as, the area of the collector: $A_c = 13,57 \text{ m}^2$ (included in the data sheet in Annex B) need to be taken into account. In the case of the chosen panels, ARCON Solar Collector type HT-HEAT store 35/10, those factors are the collector loss coefficients (a_1 and a_2), the monthly average $\tau\alpha$ product ($\tau\alpha$) and the corrected collector heat removal factor (F_R), among others.

$$a_1 = 1.118 \left[\frac{W}{m^2 K} \right]; a_2 = 0.032 \left[\frac{W}{m^2 K^2} \right]; F_R = 0.97 \left[\frac{W}{m^2 K} \right]; \tau\alpha = 0.96$$

Those factors are needed in the next formula (equation taken from the collector data sheet) to calculate the collector efficiency (η_c), which also depends on the irradiation (G) and the efficiency when the difference of temperature is equal to 0 (η_0), the maximum efficiency of the collector:

$$\eta_c = \eta_0 - \frac{a_1(T_m - T_a)}{G} - \frac{a_2(T_m - T_a)^2}{G}$$

$$\eta_0 = 0,827 \quad G = \text{Total (global) irradiation on the collector surface} \left[\frac{W}{m^2} \right]$$

$$T_m = \text{Mean collector fluid temperature (}^\circ\text{C)} \quad T_a = \text{Ambient temperature of the environment (}^\circ\text{C)}$$

It is very difficult to calculate the mean collector fluid temperature as it can vary from one day to another in the same month. The efficiency is influenced by the temperature difference between the collector and the environment; the smaller temperature difference, the higher the efficiency is, and the opposite.

In summer, as the ambient temperature increases, so does the collector temperature but at a higher level, as the thermal conductivity of it is greater than the air. For that, the temperature difference is bigger, decreasing the efficiency of the solar collector. In winter the same thing reversed happens, the ambient and collector temperature are lower, but the difference is not as significant as in summer.

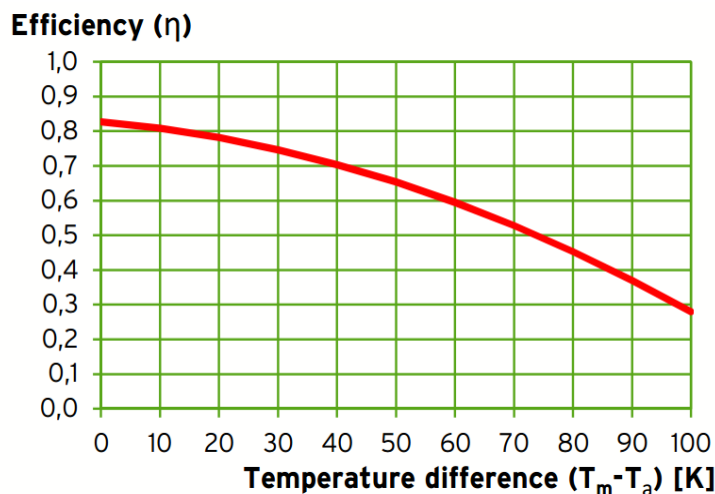


Figure 43: Collector efficiency vs ΔT.

The efficiency of the collector is going to be calculated, assuming that in the location being studied the maximum temperature difference between the collectors and the ambient will be 70°C in summer, and the minimum will be 30°C in winter. Checking the next graph of evolution of the efficiency with respect to the temperature difference, it can be seen that at the maximum temperature mentioned the efficiency is 52% and at the minimum 75%.

Figure 43 is taken from the data sheet of the selected type of collector.

5.3.6 Climate conditions

Other parameters that influence the solar energy production are the ambient temperature average and the solar irradiation. These values are taken from the *Photovoltaic*

Geographical Information System (PVGIS). The solar thermal collectors will be placed facing south to achieve the maximum efficiency concerning orientation.

For using the PVGIS data, it needs to be determined the point in the world where the information is to be obtained for. In this case, the exact point of K2 building in the database map, inside the TUC campus in the city of Chania, Greece (Figure 44) is defined. This corresponds to the geographical coordinates of 35°31'57" North and 24°4'7" East, with Elevation of 139 m.a.s.l. (meters above the sea level).



Figure 44: Selected point for PVGIS data analysis (K2 TUC)

The PVGIS-5 geo-temporal irradiation database (PVGIS-CMSAF) estimates the monthly irradiation data for the certain position desired, among other information such as the optimal inclination angle for the collectors, the average daytime temperature, the number of heating degree-days, etc., shown in Table.

Month	H_h	H_{opt}	$H_{(90)}$	DNI	I_{opt}	T_L	D/G	T_D	T_{24h}	N_{dd}
	Wh/m ² /day	Wh/m ² /day	Wh/m ² /day	Wh/m ² /day	deg	-	°C	-	°C	-
Jan	2,400	3,630	3,620	3,380	59	1.9	0.44	12.2	10.4	210
Feb	3,170	4,290	3,720	3,890	51	1.9	0.42	13.1	11.2	192
Mar	5,000	6,000	4,190	5,510	39	2.2	0.38	14.9	12.8	146
Apr	6,270	6,630	3,320	6,720	25	2.4	0.32	18	15.8	35
May	7,390	7,090	2,510	7,780	10	3.1	0.28	21.7	19.8	3
Jun	8,420	7,650	2,040	9,720	0	2.9	0.20	25.1	23.4	2
Jul	8,340	7,750	2,230	9,910	4	3	0.18	27.8	26.1	1
Aug	7,600	7,750	3,190	9,150	17	3.1	0.20	28	26.2	2
Sep	5,880	6,810	4,200	7,050	34	2.8	0.28	25.8	23.8	4
Oct	4,130	5,410	4,400	5,080	48	2.2	0.37	21.2	19.3	24
Nov	2,810	4,170	4,050	3,990	58	2.2	0.40	17.6	15.8	89
Dec	2,040	3,150	3,250	2,950	61	2	0.46	14.1	12.4	171
TOTAL	63,450	70,330	40,720	75,130		29.7	3.93	239.5		879
Average	5,288	5,861	3,393	6,261	29	2.5	0.3275	19.95833	18.08333	

H_h – Irradiation on horizontal plane
 H_{opt} – Irradiation on optimally inclined plane
 $H_{(90)}$ – Irradiation on plane at angle: 90 degrees
DNI – Direct normal irradiation
 I_{opt} – Optimal inclination
 T_L – Linke turbidity
D/G – Ratio of diffuse to global irradiation
 T_D – Average daily temperature
 T_{24h} – 24-hour average temperature
 N_{dd} – Number of heating degree-days

Table 20: Information obtained from PVGIS

The database provides the average optimal angle values in each month, depending on the sun positioning and the irradiance obtained. Since the chosen solar collector is stationary, its angle will be the given optimal inclination plane for the whole year, which is 29 degrees. As can be seen in Table, the total irradiation at optimal angle (H_{opt}) is greater than the horizontal (H_h) or vertical one ($H_{(90)}$).

The Direct normal irradiation (DNI) shows the amount of solar radiation received per unit area in the case of a solar collector held always perpendicular (or normal) to the rays that come in a straight line from the direction of the sun at its current position in the sky. It could be interpreted as the maximum solar irradiance that the collector can obtain. This could be achieved with concentrating solar thermal installations and non-stationary/tracking devices. The difference between the maximum irradiance and the one at optimal angle is not very wide, meaning that even with a stationary solar collector high efficiency can be obtained.

The annual irradiation deficit due to shadowing can be depreciated as there are no elements in the roof that can block the sun rays.

In **Figure 45** and **Figure 46** are shown the monthly average irradiance values from 2007 until 2016, either horizontal, optimal angle and direct normal irradiation [kWh/m²]; and the monthly average temperature for the same period [deg C].

Figure 45: Monthly average irradiance 2007-2016

Figure 46: Monthly average temperature 2007-2016

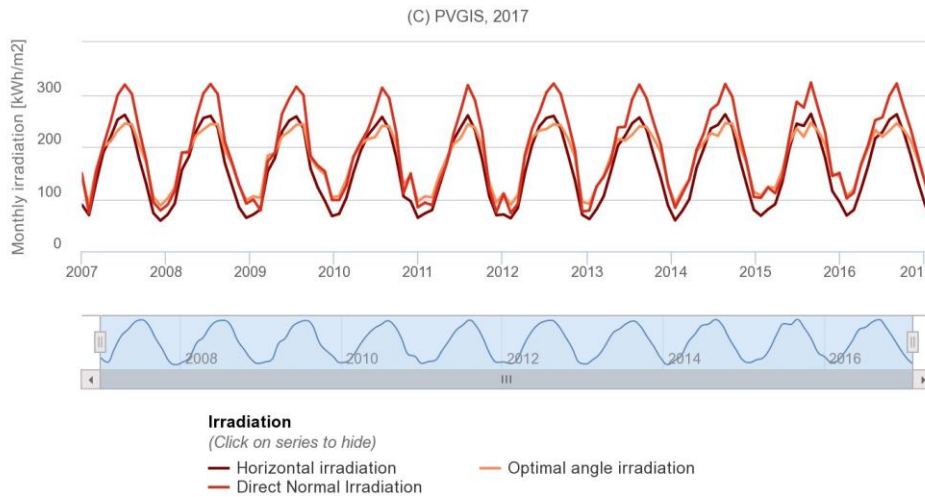


Figure 47 shows the outline of horizon at the studied location.

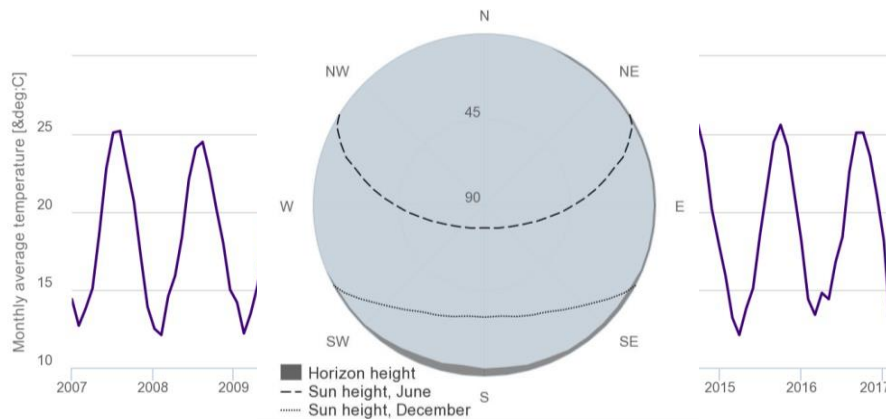


Figure 47: Horizon profile and sun path

5.3.8 Geothermal energy

To obtain the greatest amount of energy for the ground source heating and cooling, the soil characteristics must be considered. The best way to know precisely the geomorphological characteristics of the strata or layer that make up the ground, is executing a Thermal Response Test (TRT) in the same place where the vertical geothermal probe will be located. This allows to obtain the strata typology and the ground temperature evolution at different depths.

Since this test is very expensive and its execution would not be inside the scope of the project, information by the *Institute of Geology & Mineral Exploitation*⁵ (IGME) and in the

*ThermoMap*⁶, was used regarding the different composition of the ground around the whole country.

The initial plan is to develop a shallow geothermal system. The main reasons are that the the campus of *Technical University of Crete* has adequate temperature levels at low depths, plus this type of systems require lower capital investment. Moreover, the heat pumps will increase the water temperature coming from the ground until reaching the desired temperature.

The hydrology is also an important factor that influences the ground temperature. When there is water flowing through any ground layer in the intended location of the Borehole Heat Exchanger, the temperature of the ground decreases and the thermal conductivity is higher due to better thermal properties of water against ground materials. The study of the hydrology of the terrain is essential, either for taking advantage of the underground water for higher thermal conductivity (*heat extraction*), or to avoid heat losses and know how to proceed in order to counteract its negative effects when the aim is keeping the heat underground (*heat storage*).

Depending on the system needs, the conductivity can be an advantage or inconvenient. High conductivity can reheat the ground faster when it is being used for extraction, so it would be a benefit. However, if the ground is intended for heat storage, the heat would be wasted, as the high conductivity removes the heat faster. On the other hand, low conductivities do not affect too much the transport of heat, so it would be a good option for heat storage, and not for heat extraction, as ground would cool down without quick refill of heat.

In this case of study, the ground will be used both for extraction and storage. It has been decided to place two different Underground Thermal Energy Storage Systems, one for storing heat and the other for storing cold. The main reason for this is to have two independent sources where energy can be stored or extracted at the same time.

On the one hand, in summer, the demand for heating is very low, but the irradiance of the sun much greater than in winter. Since the system studied will be combined with solar collectors, these will produce heat and store it under the ground, as there is no need for heating in that period. In this case, cooling will be provided to the building.

On the other hand, in winter, heat stored in the borehole will be extracted to cover the demand of heating in the building. And, as there are no cooling needs, the cooling circuit coming from the absorption heat pump will store the energy in another underground system intended for cooling.

5.3.9 Geology

To know the ground properties in the place where the boreholes are going to be located, a study of the geology needs to be performed. For that, ThermoMap gives a good analysis of the ground characteristics in Chania, and specifically in the area of the Technical University of Crete (See original document in Annex C). The key aim of the ThermoMap project was to develop an efficient estimation system for the creation of pan-European superficial geothermal potential maps as a supportive and informative planning tool for installing (very) shallow vertical and horizontal geothermal installations. For this purpose, it has made use solely of existing geoscientific datasets and information which do not necessarily reflect the real on-site conditions with regard to all available parameters.



Figure 48: ThermoMap analysis location

Figure 48 shows the ground average thermal conductivity in Chania, identifying the area of TUC as medium-low thermal conductivity, which could be appropriate for the thermal storage activities.

Possible limitations of usage

Based on the specified data it can be stated that the chosen site is not located in a protected zone. The topographical analysis revealed a slope, less than 15° . Therefore, when installing a (very) shallow geothermal system, no issues with the venting and installation procedure should occur. The determined dominant soil type according to the acknowledged WRB classification system is here Cambisol. With this type of soil in principle no restrictions regarding a sustainable and efficient installation and operation of a (very) shallow geothermal system are known.

Climatic conditions

The climate data, averaged over several years, results in a mean annual air temperature of 18.75 °C whereas the minimum annual air temperature is 9.00 °C. The amount of the annual precipitation is 665 mm. The maximum monthly precipitation of 120 mm occurs in the month(s) of January, December. This implies sub-humid conditions for the chosen area.

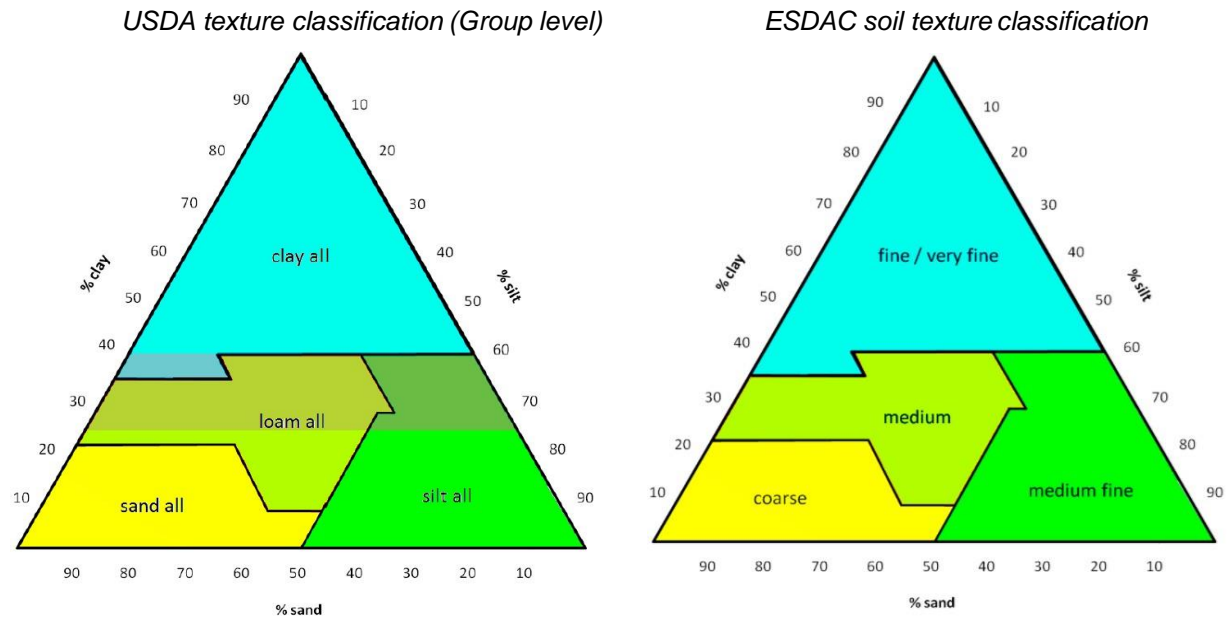


Figure 49: USDA texture classification (Group level)

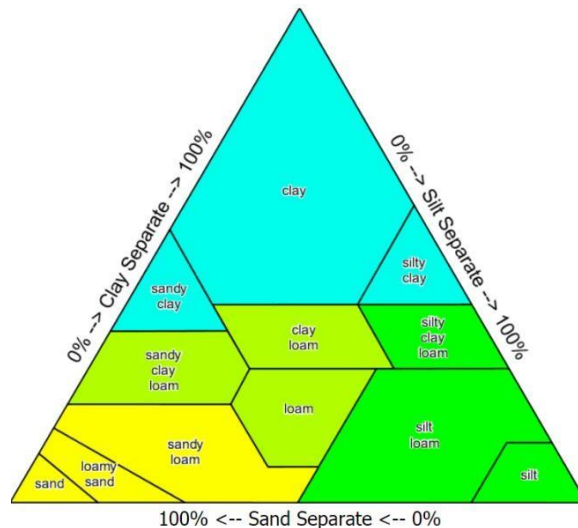


Figure 50: Ground composition

Soil properties

The dominant grain size distribution according to the USDA soil texture classification is loam all (Group level) (see Figure above for the USDA classes with estimated separates of sand, clay and silt), and according to the ESDAC soil texture classification is medium (see Figure above for the ESDAC classes with estimated separates of sand, clay and silt).

Geothermal situation

The thermal heat conductivity of the soil matrix is defined essentially by its texture, water content and bulk density. At the chosen site, the values under unsaturated conditions can range from 0.83 W/mK to 1.07 W/mK. On the basis of humid/unsaturated conditions a value of 1.07 W/mK is probable. These parameters were calculated by use of the KERSTEN (1949) formulas. The heat capacity of NaN MJ/m³K is calculated according to formulas after DEHNER (2007). For these calculations, a bulk density of 1.3 g/cm³ was used which generally describes the relation between mass and volume. The analysis of these geoscientific parameters indicate that the chosen location has medium low conductivity as very Shallow Geothermal Potential (vSGP7) without any limitations.

Summary of parameters given by the ThermoMap

Soil characteristics

Soil texture (ESDAC): Medium

Hydrological system status: Humid/Unsaturated

Climatic conditions

Annual precipitation: 665 mm

Annual mean temperature: 18.75 °C

Annual minimum temperature: 9 °C

Monthly maximum precipitation: 120 mm

Thermal properties

Heat conductivity: 1.07 W/mK

Heat capacity DEHNER (2007): 2.03 MJ/m³K (0,564 kWh/m³K)

Current vSGP value: 1.07 W/mK

Minimum (arid/ unsaturated): 0.83 W/mK

Maximum (humid/ unsaturated): 1.07 W/mK

vSGP (very Shallow Geothermal Potential - Test Area legend): Medium low conductivity

Conclusion: This site is probably suitable for installing a GSHP system without limitations.

5.3.10 Location

The location of the Geothermal system needs to be as close as possible to the final loads, the K2 building, to avoid energy losses. In [Figure 51](#) the location for the Underground Thermal Energy Storage Systems (UTES) is presented illustrating in blue the boreholes storing cold and in red the ones storing heat. It has been decided to place the cooling storage closer to the building instead of the heating as there is greater demand of the first type of thermal energy than the second, so there will be less energy losses.



Figure 51: Location of BHE systems

5.3.11 Borehole heat exchanger

The demand of heating and cooling energy to be supplied by the Combined System was calculated. The next step is make an initial design to establish the different characteristics of this type of system.

The fundamentals and materials used for obtaining the energy will be chosen and described, such as the type, number and configuration of boreholes, the heat pump size and capacity, as well as the material and extension of the thermal solar collectors.

There are 3 main types of borehole heat exchangers: Simple Coaxial, Single U-pipe and Double U-pipe. The effectiveness of the BHEs is described by the Borehole Thermal Resistance (R_b): the lower R_b , the better heat transfer.

The choice for the ground source extraction will be Single U-pipe. The reason is because, even though the R_b flow resistance is higher compared with the double U-pipe, the single U-pipe is much cheaper and easier to install, and in this specific case, the focus is not so on the energy extraction but storage, to optimise cost-efficiency. The simple Coaxial type has advantages as the low thermal short circuiting, the low R_b and the suitability for deep boreholes. However, it has important drawbacks, like high production costs, difficulty to handle and especially, that is very complicated to perform the so called co-axial pipe in the real construction.

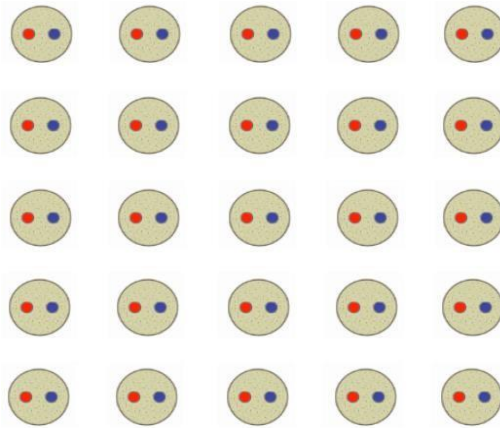


Figure 52: Chosen configuration for BHEs

Within all design options, separate boreholes in the configuration of the distribution have been chosen as shown in the scheme of **Figure 52** having a square 5x5 configuration .

5.3.12 Underground Thermal Energy Storage

The term Underground Thermal Energy Storage (UTES) implies storing of excess heat from solar collectors and cooling from the Absorption Heat Pump, and utilizing during the time needed. A shunt valve directs the heat from the solar collector either to the ground via a ground heat exchanger, to heat pump or directly to the space heating circuit.

The Borehole Heat Exchanger will work mainly as a seasonal heat storage element: on the one hand, extracting heat during the winter period while introducing cooling; on the other hand, in the summer period, heat will be injected into the ground and cooling energy will be extracted.

In this system, the solar collector does not contribute directly to space heating and heating coils and unless the temperature needed matches with the one in the collector, the heat pump covers this base load. Stored heat from the solar collector in the ground contributes to space heating as the ground is the heat pump's heat source.

A control system is needed to direct where the heat from the solar collector is being transferred. Hot water temperature can be a reference point for where the solar heat is used. Then, all the excess heat can be dumped to the boreholes.

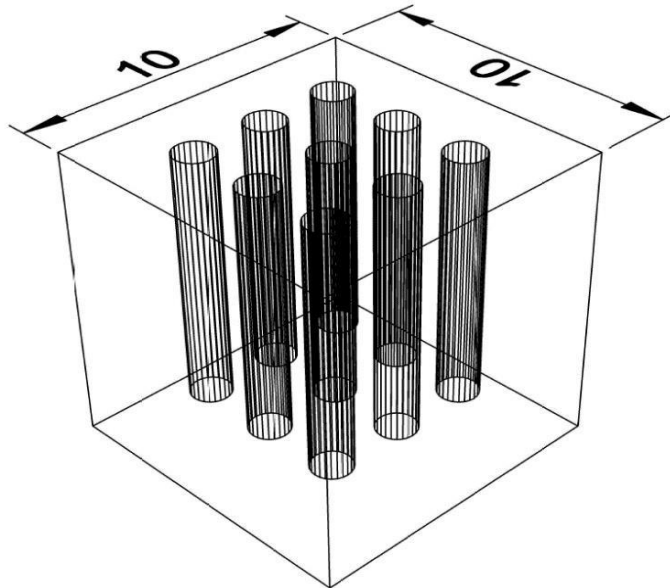


Figure 53: Ideal volume for UTES

As analysed before, the ground heat capacity in the location being studied is $2.03 \text{ MJ/m}^3\text{K}$ ($0,564 \text{ kWh/m}^3\text{K}$). Knowing that the heating and cooling consumption is around $82,000 \text{ kWh}$ per year a rough estimate of $10,000 \text{ kWh/month}$ is assumed. A ground storage capacity for covering the needs of heating 2 days in the worst-case scenario, for the months of January or December is calculated. This capacity would be about 500 kWh , assuming some heat losses. To achieve this, a theoretic cube of 10 meter each side is required.

5.3.13 Heat production

For calculating the heat production of the ground source heating, GeoT*SOL is used, to model a combined system of geothermal boreholes and solar thermal collectors.

The location of the system is selected, (in this case Chania) so that the program can update the climate data for the calculations. After that, the configuration of the system is inserted in the program. The chosen configuration is “*HP system with combination tank and solar thermal support*”, as the one more closely related to the case being studied, for the part of heating production (Figure 54).

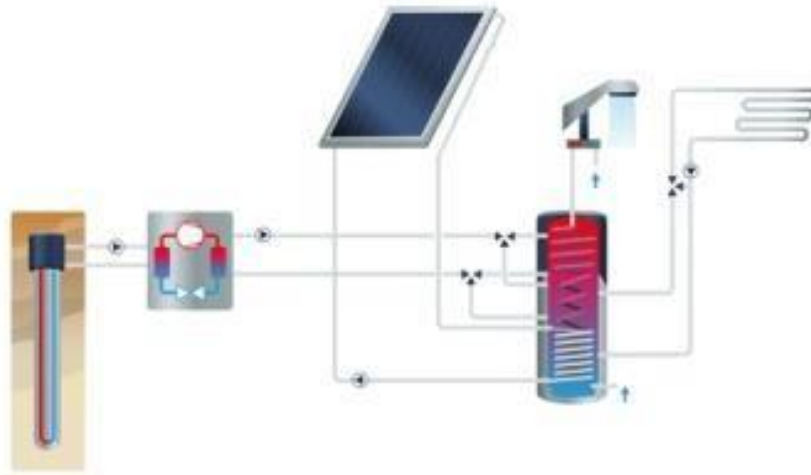


Figure 54: GeoT*SOL system selection

Then, the data regarding the monthly heat consumption of the building needs to be introduced, in order to dimension the energy sources. Once the consumption is set, the parameters of the solar collectors, BHE and heat pump are also included, for the program to calculate the heat production and other specifications.

The Heat Pump chosen for simulating the system in the program is Opthaet OH 55e, from CTA AG, with a nominal heating power of 64.7 kW.

Heat pump system

Heat pump	
Manufacturer:	CTA AG
Product:	Optiheat OH 55e
Nominal heating power:	54.7 kW
Construction type:	Brine/Water
	<input type="button" value="Select"/> <input type="button" value="Properties"/>

Mode of operation	Auxiliary heating
<input checked="" type="radio"/> Monovalent <input type="radio"/> Monoenergetic, parallel <input type="radio"/> Monoenergetic, alternative <input type="radio"/> Monoenergetic, partially parallel	Heating element power: <input type="text" value="75.0"/> kW Heating element out of service above: <input type="text" value="-10.0"/> °C Heat pump out of service below: <input type="text" value="-15.0"/> °C

Figure 55: Heat Pump parameters

The Borehole Heat Exchangers are set to be 25 units at 16.75 meters deep each, as the required heat probe length is 419 meters in total for covering the consumption. The infill will be simple grouting and the type of BHE is single U-pipe, as mentioned before. The pipe diameter is 100 mm, with a flow rate of 8,042 l/h.

Heat source

Heat pump Power input on the cold side: 41.9 kW	Geothermal probe Borehole diameter: 100 mm Construction type: Single U-Pipe Infill: Simple grouting
Brine Nominal output of brine pump: 80.0 W Flow rate: 8,042 l/h Glycol: 30 %	Length of the borehole heat exchanger Spec. extraction rate: 100.0 W/m Maximum drilling depth: 17 m Required heat probe length: 419 m <input type="button" value="Calculate size"/> Number of wells: 25 at 16.7 m
Soil Undisturbed ground temperature: 10.0 °C	

Figure 56: Borehole Heat Exchangers parameters

The ground source heat pump, is designed without considering the contribution of the solar collector, as the energy provided will be redirected to the UTES. In this way, the dimensioning of the BHE has been made with the aim of covering the entire heat demand. Using this energy source alone would cool down the ground very fast, that is why the solar collector are for, apart from providing heat to the system, also to maintain the ground temperature above certain limit values.

5.3.14 Geo-Solar system design

In **Figure 57** it is presented the design of the system intended to cover the heating and cooling needs of the building K2 in the Technical University of Crete. In red is shown the hot water circulation, in yellow the medium temperature water and in blue the chilled water. The following sketch is the conceptual representation of the system, so the dimensions and quantities are not the ones calculated for the real design.

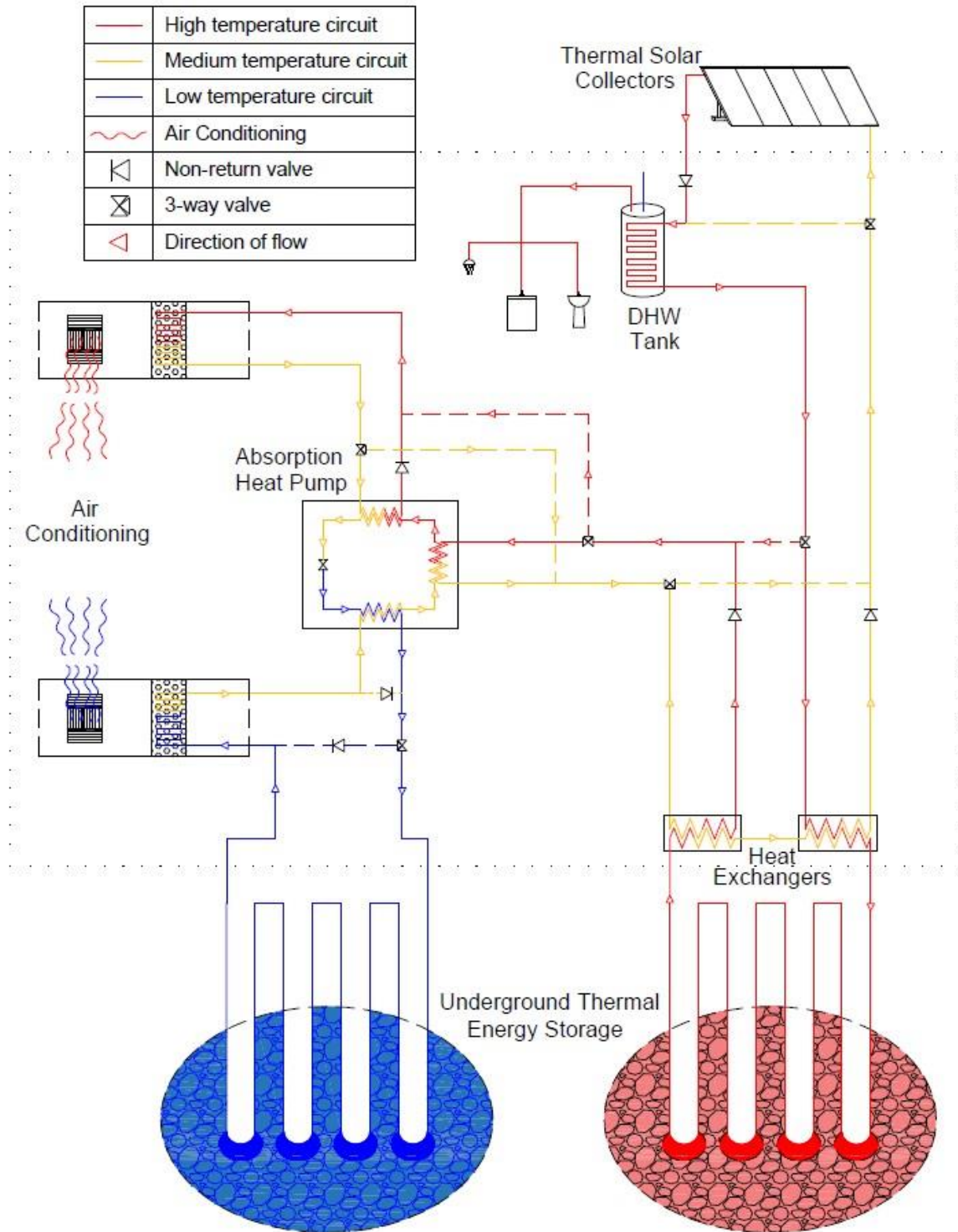


Figure 57: Design of the Geo-Solar system

The system is composed of 4 main elements: Solar Thermal Collectors, two arrangements of Borehole Heat Exchangers that form the Underground Thermal Energy Storage (UTES) for heating and cooling, Absorption Heat Pump and the Air Conditioning system.

The solar collectors convert irradiance from the sun and heat up the water going through their inner circuit. This warm water flows inside the Domestic Hot Water (DHW) tank and releases part of its heat. The DHW tank is filled with cold water from the grid, heated up by the Solar circuit and then supplied to the DHW circuit of the building. After releasing part of the heat in the tank, the solar circuit continues until the Underground Thermal Energy Storage for heating, transferring the rest of the heat to the Borehole by means of a Heat Exchanger, and going back to the Collectors to be heated up again and restart the loop.

The energy transferred to the Borehole Heat Exchangers is either stored or used for air conditioning. For the second purpose, another Heat Exchanger releases heat to the intermediary circuit between the UTES and the Absorption Heat Pump. As explained before, this type of Heat Pump is able to provide heating and cooling with the same equipment. The heat coming from the UTES warms up the fluid-pair in the Generator, evaporating the refrigerant and separating the mixture. The warm evaporated refrigerant arrives to the Condenser at high pressure, where it releases the heat to the Hot Air Conditioning circuit and thereby, the refrigerant condenses. After that, the liquid pressure is reduced in an expansion valve. The refrigerant now at lower temperature, absorbs the heat in the Evaporator from the Cool Air Conditioning circuit, what makes it evaporate and flow back again to the Generator, where it gets mixed with the solution and becomes liquid to restart the loop. The heat absorbed in the Evaporator lowers the temperature of the circuit connected to it, which goes through the second Underground Thermal Energy Storage, intended for cooling. Similarly with heating storage, this second arrangement of boreholes stores and supplies cooling, depending on the needs, to the cooling circuit of air conditioning.

If there is no simultaneous demand of heating and cooling at the same time, there will be always one type of thermal energy being used and another being stored (or both being stored in the case of no consumption). In this way the energy availability and the reliability of supply is secured.

In the schematic the hot and cool air conditioning in different circuits is shown to make the representation easier to understand, but in the real case it consists of one circuit for both, providing hot or chilled air depending on the needs.

The process explained would be the standard operation of the system. However, depending on the climate conditions and specific demands along the year, the circuits can be recirculated through different paths inside the same circuit, to achieve better

results. The additional paths according to which the circuit can be recirculated are represented in dashed lines in **Figure 57**. All together a closed loop system with different circuits is formed, with fluids never making contact with the environment or other fluids, eliminating health and safety issues.

6. References

1. Colak I, Sagiroglu S, Fulli G, Yesilbudak M, Covrig C-F. A survey on the critical issues in smart grid technologies. *Renewable and Sustainable Energy Reviews*. 2016;54:396-405.
2. Meng L, Sanseverino ER, Luna A, Dragicevic T, Vasquez JC, Guerrero JM. Microgrid supervisory controllers and energy management systems: A literature review. *Renewable and Sustainable Energy Reviews*. 2016;60:1263-73.
3. Pan X, Niu X, Yang X, Jacquet B, Zheng D. Microgrid energy management optimization using model predictive control: a case study in China. *IFAC-PapersOnLine*. 2015;48(30):306-11
4. Mahmood A, Javaid N, Razzaq S. A review of wireless communications for smart grid. *Renewable and Sustainable Energy Reviews*. 2015;41:248-60.
5. Kolokotsa D, Gobakis K, Papantoniou S, Georgatou C, Kampelis N, Kalaitzakis K, et al. Development of a web based energy management system for University Campuses: The CAMP-IT platform. *Energy and Buildings*. 2016;123:119-35.
6. Khan AR, Mahmood A, Safdar A, Khan ZA, Khan NA. Load forecasting, dynamic pricing and DSM in smart grid: A review. *Renewable and Sustainable Energy Reviews*. 2016;54:1311-22.
7. Gaurav S, Birla C, Lamba A, Umashankar S, Ganesan S. Energy Management of PV – Battery Based Microgrid System. *Procedia Technology*. 2015;21:103-11.
8. Wenbo S, Eun-Kyu L, Daoyuan Y, Rui H, Chi-Cheng C, Rajit G. Evaluating Microgrid Management and Control with an Implementable Energy Management System Smart Grid Communications (SmartGridComm), 2014 IEEE International Conference; Venice, Italy 2014.
9. Raza MQ, Khosravi A. A review on artificial intelligence based load demand forecasting techniques for smart grid and buildings. *Renewable and Sustainable Energy Reviews*. 2015;50:1352-72.
10. Provata E, Kolokotsa D, Papantoniou S, Pietrini M, Giovannelli A, Romiti G. Development of optimization algorithms for the Leaf Community microgrid. *Renewable Energy*. 2015;74:782-95.
11. Sepasi S, Reihani E, Howlader AM, Roose LR, Matsuura MM. Very short term load forecasting of a distribution system with high PV penetration. *Renewable Energy*. 2017;106:142-8.
12. Beccali M, Cellura M, Lo Brano V, Marvuglia A. Forecasting daily urban electric load profiles using artificial neural networks. *Energy Conversion and Management*. 2004;45(18–19):2879-900.
13. Raza MQ, Nadarajah M, Hung DQ, Baharudin Z. An intelligent hybrid short-term load forecasting model for smart power grids. *Sustainable Cities and Society*.
14. Mellit A, Pavan AM. A 24-h forecast of solar irradiance using artificial neural network: Application for performance prediction of a grid-connected PV plant at Trieste, Italy. *Solar Energy*. 2010;84(5):807-21.
15. Morbitzer CA. "Towards the Integration of Simulation into the Building Design Process". Thesis; University of Strathclyde, Energy System Research Unit, Department of Mechanical Engineering; 2003.
16. Lam KP, Huang YC, Zhai C. "Energy modeling tools assessment for early design phase. Center for Building Performance and Diagnostics", School of Architecture Carnegie Mellon University; 2004.
17. Rizos I. "Next generation energy simulation tools: Coupling 3D sketching with energy simulation tools". Thesis; University of Strathclyde, Energy System.
18. De Wit S, Augenbroe G. Analysis of uncertainty in building design evaluations and its implications. *Energy Build* 2002;34:951e8.
19. Burhenne S, Jacob D, Henze GP. "Uncertainty analysis in building simulation with Monte Carlo techniques. In: Fourth national conference of IBPSA-USA; 2010. New York, NY.
20. Sanguinetti P, Eastman C, Augenbroe G. "Courthouse energy evaluation: BIM and simulation model interoperability in concept design". In: Proceedings of the 11th international IBPSA conference; Glasgow, Scotland, 2009.
21. Struck C, Hensen J, Kotek P. "On the application of uncertainty and sensitivity analysis with abstract building performance simulation tools". *J Build Phys*. vol. 33, pp.5-27, 2009.
22. Rabl A, Rialhe A. "Energy signature models for commercial buildings: test with measured data and interpretation", *Energy and Buildings*, ,vol. 19(2), pp.143-154, ISSN 0378-7788, [http://dx.doi.org/10.1016/0378-7788\(92\)90008-5](http://dx.doi.org/10.1016/0378-7788(92)90008-5), 1992.

23. Massoud S, Wollenberg BF. "Toward a Smart Grid", IEEE P&E Magazine, vol. 3(5), 2005
24. Kephart JO, Chess DM. "The Vision of Autonomic Computing", Computer, vol. 36(1), IEEE, 2003]
25. Hitchin R, Knight I. "Daily energy consumption signatures and control charts for air-conditioned buildings", Energy and Buildings, vol. 112, pp.101-109, ISSN 0378-7788, <https://doi.org/10.1016/j.enbuild.2015.11.059>, Jan.2016.
26. Crawley DB, Lawrie LK, Pedersen CO, Liesen RJ, Fisher DE, Strand RD et al. EnergyPlus: a new-generation building energy simulation program. Available at:http://simulationresearch.lbl.gov/EP/ep_paper.html; 1999 [accessed 06.03.10]
27. Fan RE, Chang KW, Hsieh CJ; Wang XR; Lin CJ. "LIBLINEAR: A library for large linear classification". Journal of Machine Learning Research. 9: 1871–1874, 2008.
28. Naiyang G, Dacheng T, Zhiqiang L, Bo Y. "Online nonnegative matrix factorization with robust stochastic approximation". IEEE Trans. Neural Networks and Learning Systems, vol. 23 (7), pp. 1087–1099, 2012.
29. Gilkey T, "New Air Heating Methods", New methods of heating buildings: a research correlation conference conducted by the Building Research Institute, Division of Engineering and Industrial Research, as one of the programs of the BRI fall conferences, Washington: National Research Council (U.S.). Building Research Institute, p. 60, OCLC 184031, November, 1959.
30. Levenberg K. "A Method for the Solution of Certain Non-linear problems in Least Squares". Quarterly of Applied Mathematics, vol. 2(2), pp.164–168, Jul. 1944.
31. Madsen K, Nielsen HB, Tingleff O. "Methods for Non-Linear Least Squares Problems". Technical University of Denmark, Lecture notes, available at <http://www.imm.dtu.dk/courses/02611/nllsq.pdf>, 2004.
32. Liu QJ, Shi ZH, Fang NF, De Zhu H, Ai L. "Modeling the daily suspended sediment concentration in a hyperconcentrated river on the Loess Plateau", China, using the Wavelet–ANN approach", Geomorphology, vol. 186, pp. 181-190, ISSN 0169-555X, <http://dx.doi.org/10.1016/j.geomorph.2013.01.012>, 2013.
33. Zhang D, Qian Y, Akula N. "Accuracy of CNV detection from GWAS data". PLoS One, vol6(1):e14511, 2011
34. Webber JJR, Gupta YP, " A closed-loop cross-correlation method for detecting model mismatch in MIMO model-based controllers". ISA Transactions vol. 47, pp. 395–400, 2008.
35. Haberl J, Komor P. "Improving commercial building energy audits: how annual and monthly consumption can help", ASHRAE J., vol. 26 Aug1990).
36. Burch J, Subbarao K, Lekov A, Warren M, Norford L. "Short term energy monitoring in a large commercial building in ASHRAE Transactions", vol. 90, pp. 1459-1477.
37. Hyndman RJ, "ARIMAX" Available at <https://robjhyndman.com/hyndsight/arimax/>.
38. Kolokotsa D, Gobakis K, Papantoniou S, Georgatou C, Kampelis N, Kalaitzakis K, Vasilakopoulou K, Santamouris M. "Development of a web based energy management system for University Campuses: The CAMP-IT platform" (2016):
39. Elman JL. "Finding structure in time." Cognitive Science, 14, pp. 179-211, 1990.
40. DOE GLOBAL ENERGY. "Reliability, Office of Electricity Delivery & Energy".
41. Agency, Renewable Energy. "Energy Storage in the UK-An Overview. 2015/2016".
42. Carbon Trust, Imperial College London. "Can storage help reduce the cost of a future UK electricity system?" London : Carbon Trust, February 2016.
43. KPMG. EFR tender results. 2016.
44. Tsakiris FR. "Energy Development in the Non-Connected Islands of the Aegean Sea".
45. Anagnostou C, Papamastoraki-Augoustaki D, Vagiona D. "Moving Towards to Energy Self-Sufficiency: The Case Study of Chania (Crete - Greece)".
46. D3.2 Deliverable "Guidelines for smart buildings and smart grids. Report on the operational phase". Smart Gems project.
47. <http://www.cyi.ac.cy/index.php/cyi/general-information/locations.html>
48. http://trnsys.de/docs/trnsys3d/trnsys3d_uebersicht_en.htm
49. http://scikit-learn.org/stable/modules/generated/sklearn.linear_model.RidgeCV.html
50. http://scikit-learn.org/stable/modules/linear_model.html#ridge-regression

51. http://scikit-learn.org/stable/modules/model_evaluation.html
52. https://en.wikipedia.org/wiki/System_integration
53. https://en.wikipedia.org/wiki/Test_set
54. https://en.wikipedia.org/wiki/Regression_analysis
55. http://scikit-learn.org/stable/modules/model_evaluation.html#scoring-parameter.
56. <http://mnemstudio.org/neural-networks-elman.htm>
57. <https://github.com/josephmisiti/awesome-machine-learning>
58. https://en.wikipedia.org/wiki/Tikhonov_regularization
59. <http://www2.nationalgrid.com/Enhanced-Frequency-Response.aspx>
60. <https://www.energystorageexchange.org/>
61. <https://www.python.org/P>
62. <https://www.r-project.org/>
63. <https://petolau.github.io/Forecast-electricity-consumption-with-similar-day-approach-in-R/>
64. <https://www.otexts.org/fpp/7>
65. <http://www.igme.gr/geoportal/?lang=en> (for Greece)
66. <https://www.ecointeligencia.com/2011/03/la-apuesta-202020-para-2020/>
67. <http://geoweb2.sbg.ac.at/thermomap/index.html?calc=true&lang=en>
68. <http://reregions.blogspot.gr/2010/03/crete-island.html>

9. Annexes

Annex A – PVGIS climate information

Monthly Solar Irradiation

PVGIS Estimates of long-term monthly averages

Location: 35°31'58" North, 24°4'8" East, Elevation: 139 m a.s.l.,

Solar radiation database used: PVGIS-CMSAF

Optimal inclination angle is: 29 degrees

Annual irradiation deficit due to shadowing (horizontal): 0.0 %

Month	H_h	H_{opt}	$H(90)$	DNI	I_{opt}	T_L	D/G	T_D	T_{24h}	N_{DD}
Jan	2400	3630	3620	3380	59	1.9	0.44	12.2	10.4	210
Feb	3170	4290	3720	3890	51	1.9	0.42	13.1	11.2	192
Mar	5000	6000	4190	5510	39	2.2	0.38	14.9	12.8	146
Apr	6270	6630	3320	6720	25	2.4	0.32	18.0	15.8	35
May	7390	7090	2510	7780	10	3.1	0.28	21.7	19.8	3
Jun	8420	7650	2040	9720	0	2.9	0.20	25.1	23.4	2
Jul	8340	7750	2230	9910	4	3.0	0.18	27.8	26.1	1
Aug	7600	7750	3190	9150	17	3.1	0.20	28.0	26.2	2
Sep	5880	6810	4200	7050	34	2.8	0.28	25.8	23.8	4
Oct	4130	5410	4400	5080	48	2.2	0.37	21.2	19.3	24
Nov	2810	4170	4050	3990	58	2.2	0.40	17.6	15.8	89
Dec	2040	3150	3250	2950	61	2.0	0.46	14.1	12.4	171
Year	5300	5870	3390	6270	29	2.5	0.29	20.0	18.1	879

H_h : Irradiation on horizontal plane (Wh/m²/day)

H_{opt} : Irradiation on optimally inclined plane (Wh/m²/day)

$H(90)$: Irradiation on plane at angle: 90deg. (Wh/m²/day)

DNI : Direct normal irradiation (Wh/m²/day)

I_{opt} : Optimal inclination (deg.)

T_L : Linke turbidity (-)

D/G : Ratio of diffuse to global irradiation (-)

T_D : Average daytime temperature (°C)

T_{24h} : 24 hour average of temperature (°C)

N_{DD} : Number of heating degree-days (-)

Annex B – Solar Thermal Collector data sheet

ARCON Solar Collector

Type HT-HEATstore 35/10

Datasheet page 1/2

The highest efficiency in the World for a competitive price

- ARCONs HT-HEATstore collector has the highest efficiency in the world for a flat panel collector. Due to the outstanding performance of the HEATstore collector we recommend it especially for solar thermal installations with a need for higher temperatures, i.e. in the process industry or for seasonal storage.
- Reliability, life time and efficiency is well proven through more than 200.000 installed square meters.
- ARCON HT-HEATstore exist in different variants, i.e. with different absorber tube dimensions, making it possible to optimize flow conditions in challenging solar field layouts.
- ARCON has many years of well proven experience in optimizing yield from large collector fields, for the benefit of the costumer.



Figure 1: HT-HEATstore placed on concrete blocks. Other easy adaptable mounting systems are available on request. Refer to our installation manual.

Data

Outer dimensions: 2,27 x 5,96 x 0,14 m
 Gross area: 13,57 m²
 Aperture area: 12,60 m²
 Weight, without liquid: 251 kg
 Fluid content: 10,6 liter

Efficiency

$$\eta = \eta_0 - \frac{a_1 \cdot (T_m - T_a)}{G} - \frac{a_2 \cdot (T_m - T_a)^2}{G}$$

where:

T_a = Ambient temperature [°C]
 T_m = Mean fluid temperature [°C]
 G = Irradiance [W/m²]

Efficiency factors:

η₀ = 0,827
 a₁ = 1,18 [W/(m²K)]
 a₂ = 0,032 [W/(m²K²)]

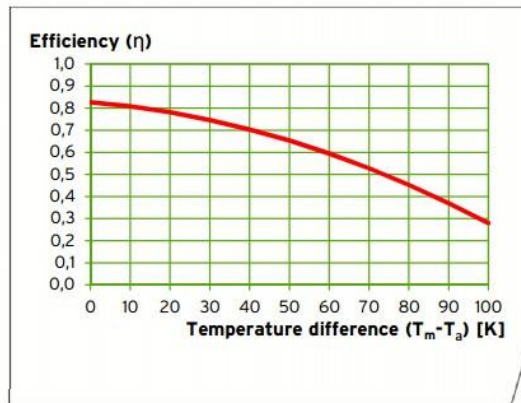


Figure 2: Efficiency curve (G = 800 W/m²). Tested in accordance with EN12975-2:2006. Issued by an accredited testing laboratory. Test report reference no. 3P01664-C.

Temperatur difference [K] T _m - T _a	Collector output [W]		
	Solar irradiance [W/m ²]		
	400	700	1000
10	3979	7105	10231
30	3359	6485	9611
50	2417	5543	8669
70	1152	4278	7404

Figure 3: Collector output at different irradiance

HT-HEATstore 35-10 ENG REV003



ARCON Solar A/S / Skørping Nord 3 / DK-9520 Skørping / Tel. +45 98 39 14 77 / arcon@arcon.dk / www.arcon.dk

ARCON Solar Collector

Type HT-HEATstore 35/10

Datasheet page 2/2

Casing features

Welded aluminum frame and back plate
 Air vents to reduce moist accumulation

Absorber

Type: Selektive - Tinox
 Absorption/Emission: $\alpha > 0,95/\epsilon < 0,05$
 Material: Copper pipes/aluminum plates
 Pipe System: 18xØ10 parallel pipes and 2xØ35 distribution pipes
 Absorber plate thickness: 0,5 mm

Insulation

Back side: 75 mm mineral wool
 Side: 30 mm mineral wool

Cover

Numbers: 2
 Material: Anti reflex glass (AR) + FEP foil
 Thickness: 3,2 mm + 0,025 mm

Connections

Stainless steel flex hose with compression fittings:
 2 x 35 mm

Pressure rating

Max working pressure: 10 bar
 Test pressure: 14,3 bar
 Recommended flow: 0,2-5 m³/h

Collector inclination angle

Recommended: 25-60°

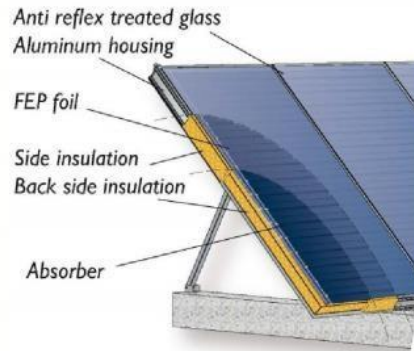


Figure 4: Sectional cut of the HT-HEATstore collector



Figure 5: Stainless steel flex hose mounted on collectors

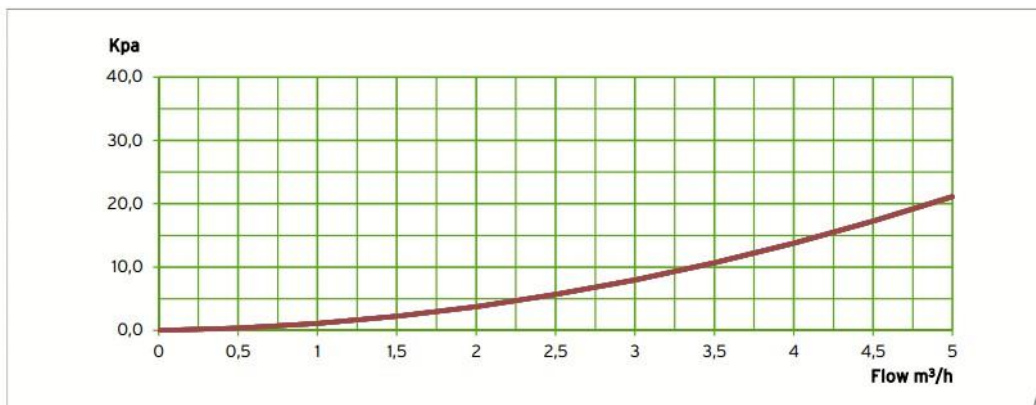


Figure 5: Pressure loss curve incl one hose

HT-HEATstore_35-10 rev002.eng



ARCON Solar A/S / Skørping Nord 3 / DK-9520 Skørping / Tel. +45 98 39 14 77 / arcon@arcon.dk / www.arcon.dk

Annex C – ThermoMap geological information

2017-5-22

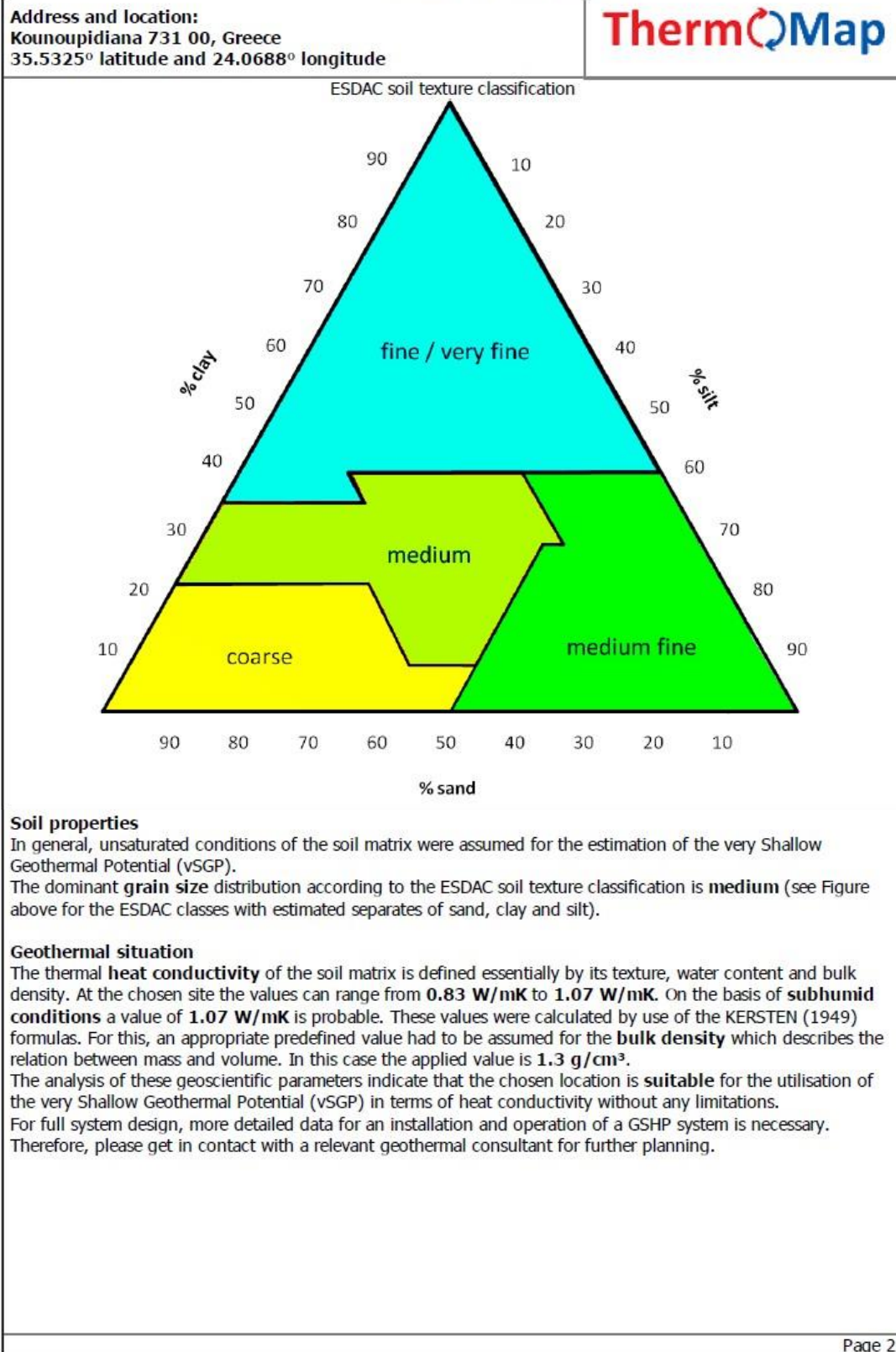
Report European Outline Map 20170522

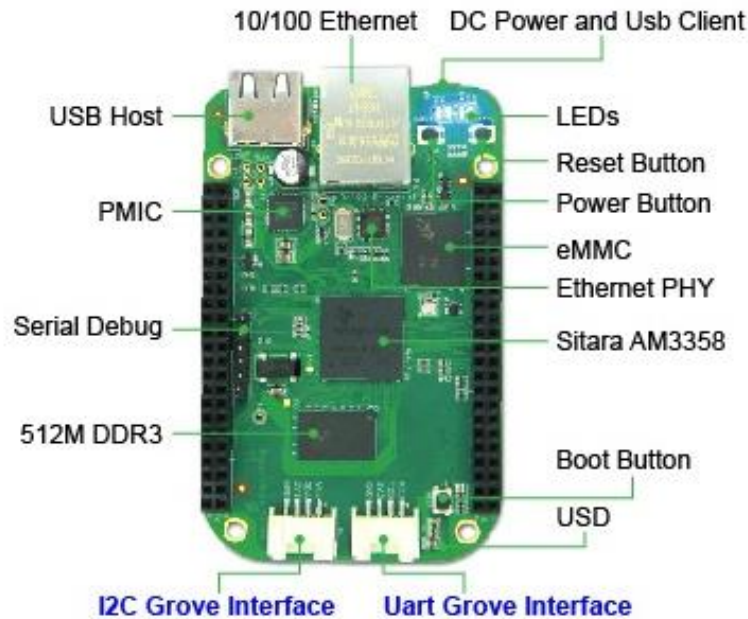
EU project ThermoMap - European Outline Map
 Location Information Sheet for the very Shallow Geothermal Potential from 22/05/2017

<p>Address and location: Kounoupidiana 731 00, Greece 35.5325° latitude and 24.0688° longitude</p>	
	<p>Heat conductivity</p> <ul style="list-style-type: none"> ■ > 1.2 W/mK ■ 1.1 – 1.2 W/mK ■ 1.0 – 1.1 W/mK ■ 0.9 – 1.0 W/mK ■ < 0.9 W/mK no estimation limited usage  <p>Map data ©2017 Google, Mapa GISrael, ORION-ME</p>
<p>Overview maps of the chosen location</p>	
<p>Disclaimer The sole responsibility for the content lies with the authors. It does not necessarily reflect the opinion of the European Commission which doesn't accept responsibility for any use of the information contained herein. The data sources and processings are the ThermoMap partner's responsibility: PLUS: Paris-Lodron Universität Salzburg.</p>	
<p>Introduction The values presented within this Report are generally based on the outcomes of the EU co-funded project ThermoMap (Project number CIP ICT PSP 250446, Website: http://www.thermomap-project.eu/). The key aim of the ThermoMap project was to develop an efficient estimation system for the creation of pan-European superficial geothermal potential maps as a supportive and informative planning tool for installing (very) shallow vertical and horizontal geothermal installations. For this purpose it has made use solely of existing geoscientific datasets and information which do not necessarily reflect the real on-site conditions with regard to all available parameters.</p>	
<p>Possible limitations of usage Based on the available data it can be stated that the chosen site is not located in a protection zone. The topographical analysis revealed a slope, which is less than 15°. Therefore, when installing a (very) shallow geothermal system, no issues with the venting and installation procedure should occur. The determined dominant soil type according to the acknowledged WRB classification system is here Cambisol. With this type of soil in principle no restrictions regarding a sustainable and efficient installation and operation of a (very) shallow geothermal system are known.</p>	
<p>Climatic conditions The climate data, averaged over several years, results in a mean annual air temperature of 18.75 °C whereas the minimum annual air temperature is 9.00 °C. The amount of the annual precipitation is 665 mm. The maximum monthly precipitation of 120 mm occurs in the month(s) of January, December. This implies subhumid conditions for the chosen area.</p>	
<p>Page 1</p>	

2017-5-22

Report European Outline Map 20170522



Annex D – Custom Data Collection System – Hardware overview

- **USB Host** - USB Host
- **DC Power and USB Client** - Power the board and act as client
- **LEDs**
 - **D2** is configured at boot to blink in a heartbeat pattern
 - **D3** is configured at boot to light during microSD card accesses
 - **D4** is configured at boot to light during CPU activity
 - **D5** is configured at boot to light during eMMC accesses
- **Boot button**
 - When there's a SD card insert, the system will boot from SD card first, if you want to boot from eMMC, press this button and then power on.
 - Use as a normal button after boot, connect to **GPIO_72**
- **I2C Grove Interface** - Connected to **I2C2**
- **Uart Grove Interface** - Connected to **UART2**
- **Serial Debug** - Connect to **UART0**, PIN1~PIN6: GND, NC, NC, RX, TX, NC, note that pin1 is near to the USB.

Annex E – PIN Map

Each digital I/O pin has 8 different modes that can be selected, including GPIO.

Note: In GPIO mode, each digital I/O can produce interrupts.

65 POSSIBLE DIGITAL I/Os							
P9				P8			
DGND	1	2	DGND	DGND	1	2	DGND
VDD_3_3	3	4	VDD_3V3	GPIO_38	3	4	GPIO_39
VDD_5V	5	6	VDD_5V	GPIO_34	5	6	GPIO_35
SYS_5V	7	8	SYS_5V	GPIO_66	7	8	GPIO_67
PWR_BUT	9	10	SYS_RESETN	GPIO_69	9	10	GPIO_68
GPIO_30	11	12	GPIO_60	GPIO_45	11	12	GPIO_44
GPIO_31	13	14	GPIO_50	GPIO_23	13	14	GPIO_26
GPIO_48	15	16	GPIO_51	GPIO_47	15	16	GPIO_46
GPIO_5	17	18	GPIO_4	GPIO_27	17	18	GPIO_65
I2C2_CAL	19	20	I2C2_SDA	GPIO_22	19	20	GPIO_63
GPIO_3	21	22	GPIO_2	GPIO_62	21	22	GPIO_37
GPIO_49	23	24	GPIO_15	GPIO_36	23	24	GPIO_33
GPIO_117	25	26	GPIO_14	GPIO_32	25	26	GPIO_61
GPIO_115	27	28	GPIO_123	GPIO_86	27	28	GPIO_88
GPIO_121	29	30	GPIO_122	GPIO_87	29	30	GPIO_89
GPIO_120	31	32	VDD_ADC	GPIO_10	31	32	GPIO_11
AIN4	33	34	GNDA_ADC	GPIO_9	33	34	GPIO_81
AIN6	35	36	AIN5	GPIO_8	35	36	GPIO_80
AIN2	37	38	AIN3	GPIO_78	37	38	GPIO_79
AIN0	39	40	AIN1	GPIO_76	39	40	GPIO_77
GPIO_20	41	42	GPIO_7	GPIO_74	41	42	GPIO_75
DGND	43	44	DGND	GPIO_72	43	44	GPIO_73
DGND	45	46	DGND	GPIO_70	45	46	GPIO_71

Annex F – PWMs and Timers

Up to 8 digital I/O pins can be configured with pulse-width modulators (PWM) to produce signals to control motors or create pseudo analog voltage levels, without taking up any extra CPU cycles.

PWMs and Timers							
P9				P8			
DGND	1	2	DGND	DGND	1	2	DGND
VDD_3_3	3	4	VDD_3V3	GPIO_38	3	4	GPIO_39
VDD_5V	5	6	VDD_5V	GPIO_34	5	6	GPIO_35
SYS_5V	7	8	SYS_5V	TIMER4	7	8	TIMER7
PWR_BUT	9	10	SYS_RESETN	TIMER5	9	10	TIMER6
GPIO_30	11	12	GPIO_60	GPIO_45	11	12	GPIO_44
GPIO_31	13	14	EHRPWM1A	EHRPWM2B	13	14	GPIO_26
GPIO_48	15	16	EHRPWM1B	GPIO_47	15	16	GPIO_46
GPIO_5	17	18	GPIO_4	GPIO_27	17	18	GPIO_65
I2C2_CAL	19	20	I2C2_SDA	EHRPWM2A	19	20	GPIO_63
EHRPWM0B	21	22	EHRPWM0A	GPIO_62	21	22	GPIO_37
GPIO_49	23	24	GPIO_15	GPIO_36	23	24	GPIO_33
GPIO_117	25	26	GPIO_14	GPIO_32	25	26	GPIO_61
GPIO_115	27	28	ECAPPWM2	GPIO_86	27	28	GPIO_88
EHRPWM0B	29	30	GPIO_122	GPIO_87	29	30	GPIO_89
EHRPWM0A	31	32	VDD_ADC	GPIO_10	31	32	GPIO_11
AIN4	33	34	GND_A_ADC	GPIO_9	33	34	EHRPWM1B
AIN6	35	36	AIN5	GPIO_8	35	36	EHRPWM1A
AIN2	37	38	AIN3	GPIO_78	37	38	GPIO_79
AIN0	39	40	AIN1	GPIO_76	39	40	GPIO_77
GPIO_20	41	42	GPIO_7	GPIO_74	41	42	GPIO_75
DGND	43	44	DGND	GPIO_72	43	44	GPIO_73
DGND	45	46	DGND	EHRPWM2A	45	46	EHRPWM2B

Annex G – Analog Inputs

Make sure you don't input more than 1.8V to the analog input pins. This is a single 12-bit analog-to-digital converter with 8 channels, 7 of which are made available on the headers.

Analog Inputs							
P9			P8				
DGND	1	2	DGND	DGND	1	2	DGND
VDD_3_3	3	4	VDD_3V3	GPIO_38	3	4	GPIO_39
VDD_5V	5	6	VDD_5V	GPIO_34	5	6	GPIO_35
SYS_5V	7	8	SYS_5V	GPIO_66	7	8	GPIO_67
PWR_BUT	9	10	SYS_RESETN	GPIO_69	9	10	GPIO_68
GPIO_30	11	12	GPIO_60	GPIO_45	11	12	GPIO_44
GPIO_31	13	14	GPIO_50	GPIO_23	13	14	GPIO_26
GPIO_48	15	16	GPIO_51	GPIO_47	15	16	GPIO_46
GPIO_5	17	18	GPIO_4	GPIO_27	17	18	GPIO_65
I2C2_CAL	19	20	I2C2_SDA	GPIO_22	19	20	GPIO_63
GPIO_3	21	22	GPIO_2	GPIO_62	21	22	GPIO_37
GPIO_49	23	24	GPIO_15	GPIO_36	23	24	GPIO_33
GPIO_117	25	26	GPIO_14	GPIO_32	25	26	GPIO_61
GPIO_115	27	28	GPIO_123	GPIO_86	27	28	GPIO_88
GPIO_121	29	30	GPIO_122	GPIO_87	29	30	GPIO_89
GPIO_120	31	32	VDD_ADC	GPIO_10	31	32	GPIO_11
AIN4	33	34	GNDA_ADC	GPIO_9	33	34	GPIO_81
AIN6	35	36	AIN5	GPIO_8	35	36	GPIO_80
AIN2	37	38	AIN3	GPIO_78	37	38	GPIO_79
AIN0	39	40	AIN1	GPIO_76	39	40	GPIO_77
GPIO_20	41	42	GPIO_7	GPIO_74	41	42	GPIO_75
DGND	43	44	DGND	GPIO_72	43	44	GPIO_73
DGND	45	46	DGND	GPIO_70	45	46	GPIO_71

Annex H – UART

There is a dedicated header for getting to the UART0 pins and connecting a debug cable. Five additional serial ports are brought to the expansion headers, but one of them only has a single direction brought to the headers.

UART							
P9				P8			
DGND	1	2	DGND	DGND	1	2	DGND
VDD_3_3	3	4	VDD_3V3	GPIO_38	3	4	GPIO_39
VDD_5V	5	6	VDD_5V	GPIO_34	5	6	GPIO_35
SYS_5V	7	8	SYS_5V	GPIO_66	7	8	GPIO_67
PWR_BUT	9	10	SYS_RESETN	GPIO_69	9	10	GPIO_68
UART4_RXD	11	12	GPIO_60	GPIO_45	11	12	GPIO_44
UART4_TXD	13	14	GPIO_50	GPIO_23	13	14	GPIO_26
GPIO_48	15	16	GPIO_51	GPIO_47	15	16	GPIO_46
GPIO_5	17	18	GPIO_4	GPIO_27	17	18	GPIO_65
UART1_RTSN	19	20	UART1_CTSN	GPIO_22	19	20	GPIO_63
UART2_TXD	21	22	UART2_RXD	GPIO_62	21	22	GPIO_37
GPIO_49	23	24	UART1_TXD	GPIO_36	23	24	GPIO_33
GPIO_117	25	26	UART1_RXD	GPIO_32	25	26	GPIO_61
GPIO_115	27	28	GPIO_123	GPIO_86	27	28	GPIO_88
GPIO_121	29	30	GPIO_122	GPIO_87	29	30	GPIO_89
GPIO_120	31	32	VDD_ADC	UART5_CTSN+	31	32	UART5_RTSN
AIN4	33	34	GND_A_ADC	UART4_RTSN	33	34	UART3_RTSN
AIN6	35	36	AIN5	UART_4_CTSN	35	36	UART3_CTSN
AIN2	37	38	AIN3	UART5_TXD+	37	38	UART5_RXD+
AIN0	39	40	AIN1	GPIO_76	39	40	GPIO_77
GPIO_20	41	42	GPIO_7	GPIO_74	41	42	GPIO_75
DGND	43	44	DGND	GPIO_72	43	44	GPIO_73
DGND	45	46	DGND	GPIO_70	45	46	GPIO_71

Annex I – I2C

The first I2C bus is utilized for reading EEPROMS on cape add-on boards and can't be used for other digital I/O operations without interfering with that function, but you can still use it to add other I2C devices at available addresses. The second I2C bus is available for you to configure and use.

I2C				P9				P8			
DGND	1	2	DGND	DGND	1	2	DGND				
VDD_3_3	3	4	VDD_3V3	GPIO_38	3	4	GPIO_39				
VDD_5V	5	6	VDD_5V	GPIO_34	5	6	GPIO_35				
SYS_5V	7	8	SYS_5V	GPIO_66	7	8	GPIO_67				
PWR_BUT	9	10	SYS_RESETN	GPIO_69	9	10	GPIO_68				
GPIO_30	11	12	GPIO_60	GPIO_45	11	12	GPIO_44				
GPIO_31	13	14	GPIO_50	GPIO_23	13	14	GPIO_26				
GPIO_48	15	16	GPIO_51	GPIO_47	15	16	GPIO_46				
I2C1_SCL	17	18	I2C1_SDA	GPIO_27	17	18	GPIO_65				
I2C2_SCL	19	20	I2C2_SDA	GPIO_22	19	20	GPIO_63				
I2C2_SCL	21	22	I2C2_SDA	GPIO_62	21	22	GPIO_37				
GPIO_49	23	24	I2C1_SCL	GPIO_36	23	24	GPIO_33				
GPIO_117	25	26	I2C1_SDA	GPIO_32	25	26	GPIO_61				
GPIO_115	27	28	GPIO_123	GPIO_86	27	28	GPIO_88				
GPIO_121	29	30	GPIO_122	GPIO_87	29	30	GPIO_89				
GPIO_120	31	32	VDD_ADC	GPIO_10	31	32	GPIO_11				
AIN4	33	34	GNDA_ADC	GPIO_9	33	34	GPIO_81				
AIN6	35	36	AIN5	GPIO_8	35	36	GPIO_80				
AIN2	37	38	AIN3	GPIO_78	37	38	GPIO_79				
AIN0	39	40	AIN1	GPIO_76	39	40	GPIO_77				
GPIO_20	41	42	GPIO_7	GPIO_74	41	42	GPIO_75				
DGND	43	44	DGND	GPIO_72	43	44	GPIO_73				
DGND	45	46	DGND	GPIO_70	45	46	GPIO_71				

Annex J – SPI

For shifting out data fast, you might consider using one of the SPI ports.

SPI							
P9			P8				
DGND	1	2	DGND	DGND	1	2	DGND
VDD_3_3	3	4	VDD_3V3	GPIO_38	3	4	GPIO_39
VDD_5V	5	6	VDD_5V	GPIO_34	5	6	GPIO_35
SYS_5V	7	8	SYS_5V	GPIO_66	7	8	GPIO_67
PWR_BUT	9	10	SYS_RESETN	GPIO_69	9	10	GPIO_68
GPIO_30	11	12	GPIO_60	GPIO_45	11	12	GPIO_44
GPIO_31	13	14	GPIO_50	GPIO_23	13	14	GPIO_26
GPIO_48	15	16	GPIO_51	GPIO_47	15	16	GPIO_46
SPI0_CS0	17	18	SPI0_D1	GPIO_27	17	18	GPIO_65
SPI1_CS1	19	20	SPI1_CS0	GPIO_22	19	20	GPIO_63
SPI0_D0	21	22	SPI0_SCLK	GPIO_62	21	22	GPIO_37
GPIO_49	23	24	GPIO_15	GPIO_36	23	24	GPIO_33
GPIO_117	25	26	GPIO_14	GPIO_32	25	26	GPIO_61
GPIO_115	27	28	SPI1_CS0	GPIO_86	27	28	GPIO_88
SPI1_D0	29	30	SPI1_D1	GPIO_87	29	30	GPIO_89
SPI1_SCLK	31	32	VDD_ADC	GPIO_10	31	32	GPIO_11
AIN4	33	34	GNDA_ADC	GPIO_9	33	34	GPIO_81
AIN6	35	36	AIN5	GPIO_8	35	36	GPIO_80
AIN2	37	38	AIN3	GPIO_78	37	38	GPIO_79
AIN0	39	40	AIN1	GPIO_76	39	40	GPIO_77
GPIO_20	41	42	SPI1_CS1	GPIO_74	41	42	GPIO_75
DGND	43	44	DGND	GPIO_72	43	44	GPIO_73
DGND	45	46	DGND	GPIO_70	45	46	GPIO_71

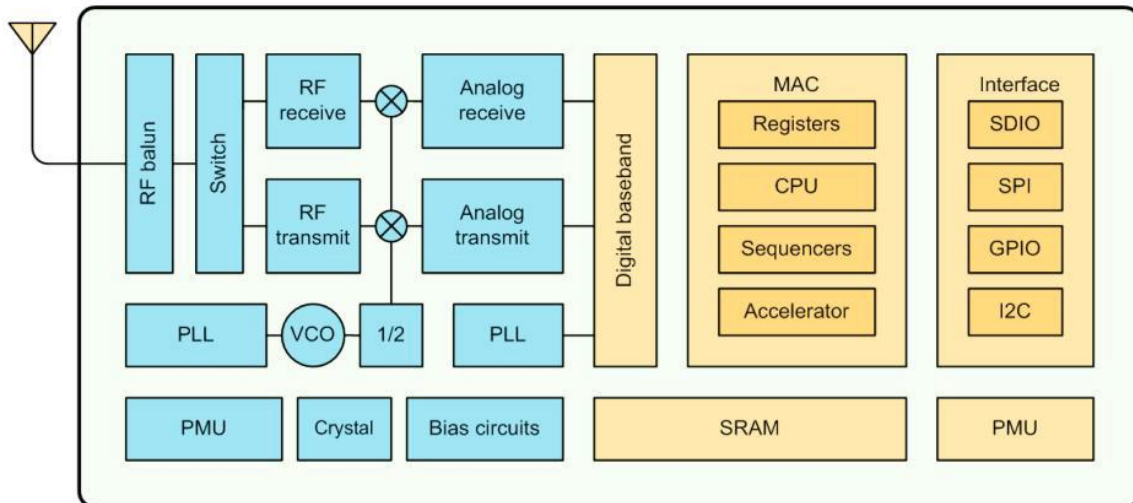
Annex K - ESP8266 general features and ESP-12F Board

ESP8266 is a chip with complete and self-contained Wi-Fi networking capabilities, ESP8266 can perform either as a standalone application or as the slave to a host MCU. When ESP8266EX hosts the application, it promptly boots up from the flash. The integrated high-speed cache helps to increase the system performance and optimize the system memory.

Moreover, ESP8266 can be applied to any micro-controller design as a Wi-Fi adaptor through SPI / SDIO or I2C / UART interfaces.

ESP8266 – Main specs

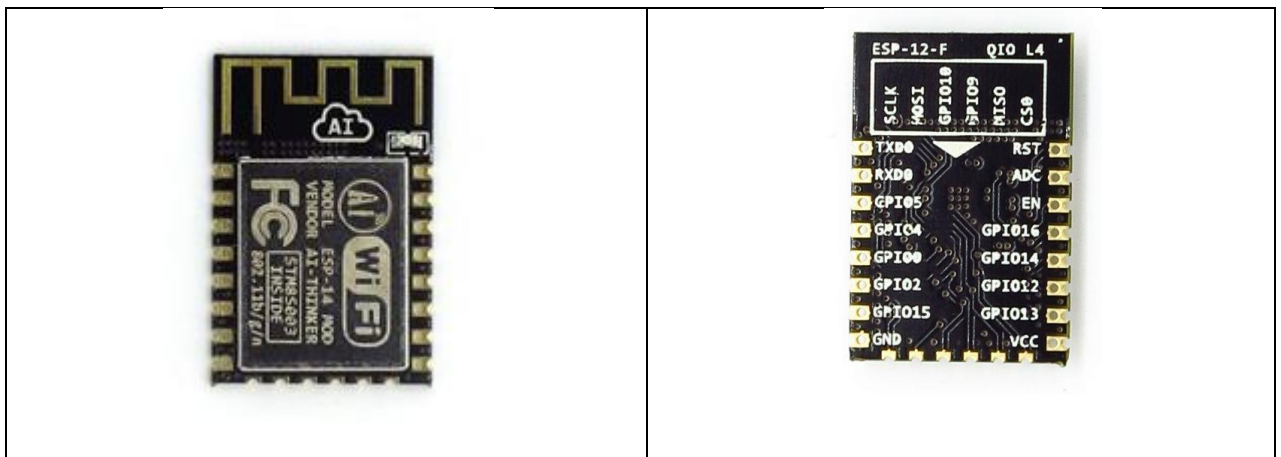
- Low power 32-bit RISC CPU: Tensilica Xtensa L106 running at 80 MHz
- 64 KiB of instruction RAM, 96 KiB of data RAM
- External QSPI flash: 4 MiB
- 802.11 b/g/n
- Integrated 10-bit ADC
- Integrated TCP/IP protocol stack
- Integrated TR switch, balun, LNA, power amplifier and matching network
- Integrated PLL, regulators, and power management units
- Supports antenna diversity
- Wi-Fi 2.4 GHz, support WEP, WPA/WPA2 or Open
- Support STA/AP/STA+AP operation modes
- Support Smart Link Function for both Android and iOS devices
- SDIO 2.0, (H) SPI, UART, I2C, I2S, IRDA, PWM, GPIO (16)
- STBC, 1x1 MIMO, 2x1 MIMO
- A-MPDU & A-MSDU aggregation and 0.4s guard interval
- Deep sleep power <10uA (More than 2 years with a con battery CR2032) , Power down leakage current < 5uA
- Wake up and transmit packets in < 2ms
- Standby power consumption of < 1.0mW (DTIM3)
- +20dBm output power in 802.11b mode
- Operating temperature range -40C ~ 125C
- FCC, CE, and ROSH certified

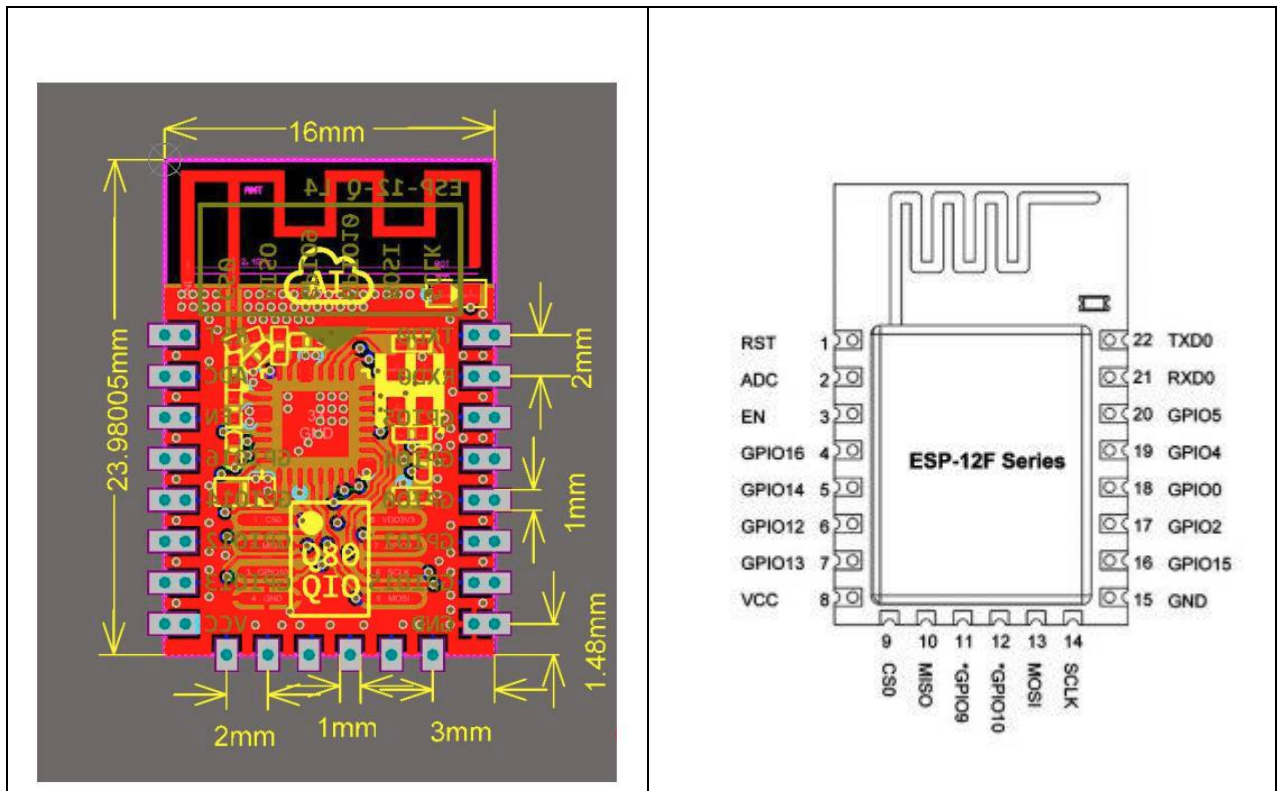


ESP8266 Functional Block Diagram

As board we have chosen an **ESP-12F** as peripheral smart devices for reading sensors; this board mount the ESP8266 chip and provides

- 20 available PINS
- PCB trace as antenna,
- mm 24.0 × 16.0,
- FCC and CE approved
- 4 MiB Flash





Open source SDKs, for the chosen board, include:

- NodeMCU — A Lua-based firmware.
- Arduino — A C++ based firmware. This core enables the ESP8266 CPU and its Wi-Fi components to be programmed like any other Arduino device. The ESP8266 Arduino Core is available through GitHub.
- MicroPython — A port of MicroPython (an implementation of Python for embedded devices) to the ESP8266 platform.
- ESP8266 BASIC — An open source basic interpreter specifically tailored for the internet of things. Self hosting browser based development environment.
- Zbasic for ESP8266 — A subset of Microsoft's widely used Visual Basic 6 which has been adapted as a control language for the ZX microcontroller family and the ESP8266.
- Espruino — An actively maintained JavaScript SDK and firmware, closely emulating Node.js. Supports a few MCUs, including the ESP8266.
- Mongoose Firmware — An open source firmware with complimentary cloud service.[11]
- ESP-Open-SDK — Free and open (as much as possible) integrated SDK for ESP8266/ESP8285 chips.
- ESP-Open-RTOS — Open source FreeRTOS-based ESP8266 software framework.

Annex L – C++ Elman network testing Example

```
// Description:           Elman Network Example.

#include <iostream>
#include <iomanip>
#include <cmath>
#include <string>
#include <ctime>
#include <cstdlib>

using namespace std;

const int maxTests = 10000;
const int maxSamples = 4;

const int inputNeurons = 6;
const int hiddenNeurons = 3;
const int outputNeurons = 6;
const int contextNeurons = 3;

const double learnRate = 0.2;    //Rho.
const int trainingReps = 2000;

//beVector is the symbol used to start or end a sequence.
double beVector[inputNeurons] = {1.0, 0.0, 0.0, 0.0, 0.0, 0.0};

double sampleInput[3][inputNeurons] = {
    // 0  1  2  3  4  5
    {0.0, 0.0, 0.0, 1.0, 0.0, 0.0},
    {0.0, 0.0, 0.0, 0.0, 0.0, 1.0},
    {0.0, 0.0, 1.0, 0.0, 0.0, 0.0}};

//Input to Hidden weights (with biases).
double wih[inputNeurons + 1][hiddenNeurons];

//Context to Hidden weights (with biases).
double wch[contextNeurons + 1][hiddenNeurons];

//Hidden to Output weights (with biases).
double who[hiddenNeurons + 1][outputNeurons];

//Hidden to Context weights (no biases).
double whc[outputNeurons + 1][contextNeurons];

//Activations.
double inputs[inputNeurons];
double hidden[hiddenNeurons];
double target[outputNeurons];
double actual[outputNeurons];
double context[contextNeurons];

//Unit errors.
double erro[outputNeurons];
double errh[hiddenNeurons];

void ElmanNetwork();
void testNetwork();
void feedForward();
void backPropagate();
void assignRandomWeights();
int getRandomNumber();
double sigmoid(double val);
double sigmoidDerivative(double val);

int main() {

    cout << fixed << setprecision(3) << endl;           //Format all the output.
    srand((unsigned)time(0));    //Seed random number generator with system time.
    ElmanNetwork();
    testNetwork();

    return 0;
}
```



```

void ElmanNetwork(){
    double err;
    int sample = 0;
    int iterations = 0;
    bool stopLoop = false;

    assignRandomWeights();

    //Train the network.
    do {

        if(sample == 0){
            for(int i = 0; i <= (inputNeurons - 1); i++){
                inputs[i] = beVector[i];
            } // i
        } else {
            for(int i = 0; i <= (inputNeurons - 1); i++){
                inputs[i] = sampleInput[sample - 1][i];
            } // i
        }

        //After the samples are entered into the input units, the sample are
        //then offset by one and entered into target-output units for
        //later comparison.
        if(sample == maxSamples - 1){
            for(int i = 0; i <= (inputNeurons - 1); i++){
                target[i] = beVector[i];
            } // i
        } else {
            for(int i = 0; i <= (inputNeurons - 1); i++){
                target[i] = sampleInput[sample][i];
            } // i
        }

        feedForward();

        err = 0.0;
        for(int i = 0; i <= (outputNeurons - 1); i++){
            err += sqrt(target[i] - actual[i]);
        } // i
        err = 0.5 * err;

        if(iterations > trainingReps){
            stopLoop = true;
        }
        iterations += 1;

        backPropagate();

        sample += 1;
        if(sample == maxSamples){
            sample = 0;
        }
    } while(stopLoop == false);

    cout << "Iterations = " << iterations << endl;
}

void testNetwork(){
    int index;
    int randomNumber, predicted;
    bool stopTest, stopSample, successful;

    //Test the network with random input patterns.
    stopTest = false;
    for(int test = 0; test <= maxTests; test++){

        //Enter Beginning string.
        inputs[0] = 1.0;
        inputs[1] = 0.0;
        inputs[2] = 0.0;
        inputs[3] = 0.0;
        inputs[4] = 0.0;
        inputs[5] = 0.0;
        cout << "(0) ";
    }
}

```



```

feedForward();

stopSample = false;
successful = false;
index = 0;
randomNumber = 0;
predicted = 0;

do {

    for(int i = 0; i <= 5; i++){
        cout << actual[i] << " ";
        if(actual[i] >= 0.3){
            //The output unit with the highest value (usually over 3.0)
            //is the network's predicted unit that it expects to appear
            //in the next input vector.
            //For example, if the 3rd output unit has the highest value,
            //the network expects the 3rd unit in the next input to
            //be 1.0
            //If the actual value isn't what it expected, the random
            //sequence has failed, and a new test sequence begins.
            predicted = i;
        }
    } // i
    cout << "\n";

    randomNumber = getRandomNumber(); //Enter a random letter.

    index += 1; //Increment to the next position.
    if(index == 5){
        stopSample = true;
    } else {
        cout << "(" << randomNumber << ") ";
    }

    for(int i = 0; i <= 5; i++){
        if(i == randomNumber){
            inputs[i] = 1.0;
            if(i == predicted){
                successful = true;
            } else {
                //Failure. Stop this sample and try a new sample.
                stopSample = true;
            }
        } else {
            inputs[i] = 0.0;
        }
    } // i

    feedForward();

} while(stopSample == false); //Enter another letter into this sample sequence.

if((index > 4) && (successful == true)){
    //If the random sequence happens to be in the correct order,
    //the network reports success.
    cout << "Success." << endl;
    cout << "Completed " << test << " tests." << endl;
    stopTest = true;
    break;
} else {
    cout << "Failed." << endl;
    if(test > maxTests){
        stopTest = true;
        cout << "Completed " << test << " tests with no success." << endl;
        break;
    }
}
} // Test
}

void feedForward(){
    double sum;

    //Calculate input and context connections to hidden layer.
    for(int hid = 0; hid <= (hiddenNeurons - 1); hid++){

```



```

    sum = 0.0;
    //from input to hidden...
    for(int inp = 0; inp <= (inputNeurons - 1); inp++){
        sum += inputs[inp] * wih[inp][hid];
    } // inp
    //from context to hidden...
    for(int con = 0; con <= (contextNeurons - 1); con++){
        sum += context[con] * wch[con][hid];
    } // con
    //Add in bias.
    sum += wih[inputNeurons][hid];
    sum += wch[contextNeurons][hid];
    hidden[hid] = sigmoid(sum);
} // hid

//Calculate the hidden to output layer.
for(int out = 0; out <= (outputNeurons - 1); out++){
    sum = 0.0;
    for(int hid = 0; hid <= (hiddenNeurons - 1); hid++){
        sum += hidden[hid] * who[hid][out];
    } // hid

    //Add in bias.
    sum += who[hiddenNeurons][out];
    actual[out] = sigmoid(sum);
} // out

//Copy outputs of the hidden to context layer.
for(int con = 0; con <= (contextNeurons - 1); con++){
    context[con] = hidden[con];
} // con
}

void backPropagate(){

    //Calculate the output layer error (step 3 for output cell).
    for(int out = 0; out <= (outputNeurons - 1); out++){
        erro[out] = (target[out] - actual[out]) * sigmoidDerivative(actual[out]);
    } // out

    //Calculate the hidden layer error (step 3 for hidden cell).
    for(int hid = 0; hid <= (hiddenNeurons - 1); hid++){
        errh[hid] = 0.0;
        for(int out = 0; out <= (outputNeurons - 1); out++){
            errh[hid] += erro[out] * who[hid][out];
        } // out
        errh[hid] *= sigmoidDerivative(hidden[hid]);
    } // hid

    //Update the weights for the output layer (step 4).
    for(int out = 0; out <= (outputNeurons - 1); out++){
        for(int hid = 0; hid <= (hiddenNeurons - 1); hid++){
            who[hid][out] += (learnRate * erro[out] * hidden[hid]);
        } // hid
        //Update the bias.
        who[hiddenNeurons][out] += (learnRate * erro[out]);
    } // out

    //Update the weights for the hidden layer (step 4).
    for(int hid = 0; hid <= (hiddenNeurons - 1); hid++){
        for(int inp = 0; inp <= (inputNeurons - 1); inp++){
            wih[inp][hid] += (learnRate * errh[hid] * inputs[inp]);
        } // inp
        //Update the bias.
        wih[inputNeurons][hid] += (learnRate * errh[hid]);
    } // hid
}

void assignRandomWeights(){

    for(int inp = 0; inp <= inputNeurons; inp++){
        for(int hid = 0; hid <= (hiddenNeurons - 1); hid++){
            //Assign a random weight value between -0.5 and 0.5
            wih[inp][hid] = -0.5 + double(rand()/(RAND_MAX + 1.0));
        }
    }
}

```



```

    } // hid
} // inp

for(int con = 0; con <= contextNeurons; con++){
    for(int hid = 0; hid <= (hiddenNeurons - 1); hid++){
        //Assign a random weight value between -0.5 and 0.5
        wch[con][hid] = -0.5 + double(rand()/(RAND_MAX + 1.0));
    } // hid
} // con

for(int hid = 0; hid <= hiddenNeurons; hid++){
    for(int out = 0; out <= (outputNeurons - 1); out++){
        //Assign a random weight value between -0.5 and 0.5
        who[hid][out] = -0.5 + double(rand()/(RAND_MAX + 1.0));
    } // out
} // hid

for(int out = 0; out <= outputNeurons; out++){
    for(int con = 0; con <= (contextNeurons - 1); con++){
        //These are all fixed weights set to 0.5
        whc[out][con] = 0.5;
    } // con
} // out

}

int getRandomNumber(){
    //Generate random value between 0 and 6.
    return int(6*rand()/(RAND_MAX + 1.0));
}

double sigmoid(double val){
    return (1.0 / (1.0 + exp(-val)));
}

double sigmoidDerivative(double val){
    return (val * (1.0 - val));
}

```